Naval Research Laboratory

Stennis Space Center, MS 39529-5004

NRL/MR/7320--16-9495

Validation of Delft3D as a Coastal Surge and Inundation Prediction System

JAY VEERAMONY

Ocean Dynamics and Prediction Branch
Oceanography Division

ANDREW CONDON

American Society for Engineering Education
Stennis Space Center, Mississippi

ROBERT LINZELL
KIM WATSON

Vencore Services and Solutions, Inc.
Stennis Space Center, Mississippi

April 7, 2016

REPORT DOCUMENTATION PAGE

Form Approved
OMB No. 0704-0188

1. REPORT DATE *(DD-MM-YYYY)*	**2. REPORT TYPE**	**3. DATES COVERED** *(From - To)*
07-04-2016	Memorandum Report	

4. TITLE AND SUBTITLE

Validation of Delft3D as a Coastal Surge and Inundation Prediction System

5a. CONTRACT NUMBER

5b. GRANT NUMBER

5c. PROGRAM ELEMENT NUMBER
0602435N

6. AUTHOR(S)

Jay Veeramony, Andrew Condon,[1] Robert Linzell,[2] and Kim Watson[2]

5d. PROJECT NUMBER

5e. TASK NUMBER

5f. WORK UNIT NUMBER
73-4546-03-5

7. PERFORMING ORGANIZATION NAME(S) AND ADDRESS(ES)

Naval Research Laboratory
Oceanography Division
Stennis Space Center, MS 39529-5004

8. PERFORMING ORGANIZATION REPORT NUMBER

NRL/MR/7320--16-9495

9. SPONSORING / MONITORING AGENCY NAME(S) AND ADDRESS(ES)

Office of Naval Research
One Liberty Center
875 North Randolph Street, Suite 1425
Arlington, VA 22203-1995

10. SPONSOR / MONITOR'S ACRONYM(S)

ONR

11. SPONSOR / MONITOR'S REPORT NUMBER(S)

12. DISTRIBUTION / AVAILABILITY STATEMENT

Approved for public release; distribution is unlimited.

13. SUPPLEMENTARY NOTES

[1]American Society for Engineering Education, Stennis Space Center, MS
[2]Vencore Services and Solutions, Inc., Stennis Space Center, MS

14. ABSTRACT

Coastal regions are vital to naval operations and have rapidly growing populations making them increasingly vulnerable to storm surge and inundation. The US Navy currently uses the Delft3D modeling suite (Stelling, 1996) for predicting nearshore circulation when inundation is not the primary concern, and PCTides for surge modeling. This report will detail the validation of the new Coastal Surge and Inundation Prediction System (CSIPS) based on Delft3D for operational use by the US Navy. Baseline studies using re-analysis winds during Hurricanes Ike and Irene as well as some sensitivity studies are presented. We also compare the results from Delft3D and PCTides in an "operational scenario" to available data.

15. SUBJECT TERMS
Coastal inundation
Surge modeling

16. SECURITY CLASSIFICATION OF:			**17. LIMITATION OF ABSTRACT**	**18. NUMBER OF PAGES**	**19a. NAME OF RESPONSIBLE PERSON**
					Jay Veeramony
a. REPORT	**b. ABSTRACT**	**c. THIS PAGE**	Unclassified Unlimited	124	**19b. TELEPHONE NUMBER** *(include area code)*
Unclassified Unlimited	Unclassified Unlimited	Unclassified Unlimited			(228) 688-4835

Standard Form 298 (Rev. 8-98)
Prescribed by ANSI Std. Z39.18

CONTENTS

LIST OF FIGURES

LIST OF TABLES

1 INTRODUCTION

Coastal regions are vital to naval operations and have rapidly growing populations making them increasingly vulnerable to storm surge and inundation. It is estimated that 10% of the world population lives in the 2% of the total landmass of the earth that comprises the low elevation coastal zone (LECZ), which is the land area contiguous with the coast that is 10 m or less in elevation (Oliver-Smith, 2009)). Nearly two-thirds of coastal megacities (populations greater than 5 million) are located in the LECZ (Oliver-Smith, 2009) and population densities within 100 km of the coast are three times higher than the global average density (Small and Nichols, 2003). Many military facilities including most US naval bases are situated within the LECZ as well. These low-lying regions are at most risk from storm surge and coastal inundation as demonstrated by recent natural disasters such as Hurricanes Katrina (2005), Ike (2008), and Irene (2011) along the US Gulf and East Coasts, Cyclone Nargis (2008) along the coast of Myanmar, and the strong storm in December 2008 that affected Papua New Guinea, Wake Island and Kwajalein Atoll. Not only are many of these coastal regions key to naval operations, but the Navy's humanitarian assistance and disaster response teams play an important role in bringing aid to these affected areas (Ingram and Greenfield 2011), making it critical to provide accurate and timely forecasts of coastal inundation.

The US Navy currently uses the Delft3D modeling suite (Stelling, 1996) for predicting nearshore circulation when inundation is not the primary concern, and uses PC-Tides (Posey et al. 2008) for worldwide coastal surge and inundation. However, PC-Tides does not include waves or other global ocean circulation and is also limited to a maximum resolution of approximately 1km, which is insufficient for inundation predictions (Hope et al. 2013). While the omission of the global ocean circulation is likely to have minor impact on the surge and inundation levels, the omission of waves has a significant effect on the water levels (Hope et al. 2013). The Delft3D modeling system (Delft3D –FLOW and Delft3D-WAVE) uses multiple nests to capture large, basin-scale circulation as well as coastal circulation and tightly couples waves and circulation at all scales. A number of storm surge modeling systems exist with similar features such as: ADCIRC (Westerink et al. 1992, Leuttich et al. 1992), CH3D-SSMS (Sheng et al. 2010a,b), CMEPS (Xie et al. 2004, 2008), ELCIRC (Zhang et al. 2004, Wang et al. 2005), FVCOM (Weisberg and Zheng 2008) and POM (Peng et al. 2004). However each of these systems has the weakness of requiring knowledgeable or specifically trained individuals who possess a thorough understanding of storm surge and inundation physics, to perform the model set-up and data/file management manually. In using Delft3D, the Delft Dashboard (DDB), a graphical user interface (GUI) product, can be used to simplify the set-up of Delft3D features such as the grid, elevation data, boundary forcing, and nesting. In this way fewer man-hours and training will be needed to perform inundation forecasts without any loss in accuracy that may accompany more simplified modeling systems.

This report will detail the validation of the new Coastal Surge and Inundation Prediction System (CSIPS) for operational use by the US Navy. The remainder of this chapter will describe the models and test cases. In the second chapter we introduce the user interface. The third chapter details the baseline studies with the test cases as well as some sensitivity studies using Delft3D. In chapter four, we compare the results in an "operational scenario" to the data. In the fifth

Manuscript approved February 4, 2016.

chapter, we compare the results from Delft3D to that of PCTides, and we end with conclusions in chapter 6.

1.1 Project Description

Recent natural disasters reveal that the Navy's humanitarian assistance and disaster response planners need reasonable estimates of the extent of inundation due to significant oceanic and meteorological events. Preparation, staging, and resource planning efforts would benefit from such products. The US Pacific Command (USPACOM) has requested Joint Staff assistance to initiate ocean surge forecast products for prioritized areas. To meet this request, we have developed an operational workflow for event-based forecasting using the coastal modeling system Delft3D that includes surge and inundation prediction. We have developed a GUI based on the Delft DashBoard tool that helps process global/regional data sets for topography, bathymetry and land cover/use for initialization of surge and inundation models, as well as utilize Joint Typhoon Warning Center (JTWC) forecast information in wind forecasts to drive the model. We have integrated meteorological forcing into Delft3D that represents cyclone activity. This report details the validation studies performed using two Hurricanes Ike and Irene that impacted the United States of America and for which data was collected at numerous locations. In addition we have applied the GUI to setup and run surge and inundation for one USPACOM area (Guam) which was impacted by Typhoon Pongsona, but for which we have limited data. We also compare the forecast capabilities of the Delft3D system to the PCTides model that is currently being used by the US Naval Oceanographic Office (NAVOCEANO) for storm surge and inundation predictions.

1.2 Delft3d modeling suite

The Delft3D suite of models is a fully integrated software suite for 2-dimensional (2D) and 3-dimensional (3D) computations for coastal, river and estuarine areas. The suite is composed of several modules that can simulate hydrodynamic flows (Delft3d-FLOW), waves (Delft3d-WAVE), sediment transport (Delft3d-SED), and water quality (Delft3d-WAQ). The Navy uses coupled Delft3d-FLOW (henceforth FLOW) and Delft3D-WAVE (henceforth WAVE) for simulation of ocean conditions in coastal regions. The coupled system has been validated rigorously for the nearshore region (Hsu et al. 2006, 2008).

FLOW is a multidimensional hydrodynamic simulation program that calculates non-steady hydrodynamic flow that result from external forcings such as wind, tides, and waves on a rectilinear or curvilinear boundary fitted grid. In our applications for simulation of storm surge and inundation, we use this model in 2D mode only, since tests have indicated that the increased computational effort for 3D simulations yield little to no additional information for this phenomenon. This is primarily due to the well mixed upper ocean boundary layer that can extend down upto 100m on the continental shelf during the passage of tropical systems (Hope et al. 2013, Sullivan et al. 2012). FLOW solves the Navier Stokes equations for an incompressible fluid under shallow water and Boussinesq assumptions. In 2D mode, the depth-averaged continuity equation is solved along with the momentum equations in the horizontal directions.

Hydrostatic pressure is assumed and vertical accelerations due to buoyancy and sudden changes in bottom topography are not taken into account.

WAVE is a wrapper that enables the coupling of the third-generation SWAN model (Holthuijsen et al. 1993, Booij et al. 1999, Ris et al. 1999) to the other modules of the Delft3D suite. SWAN is a phased-averaged wave model that is used to simulate the evolution of random, short-crested wind waves. It is based on the discrete spectral action balance equation and accounts for refraction due to currents and bottom topography, dissipation due to whitecapping, depth-limited wave breaking, and bottom friction, and non-linear wave-wave interactions. When FLOW and WAVE are run in coupled mode, the user specifies how often the modules "talk" to each other. They are linked dynamically where the FLOW module passes to WAVE the currents, the water levels, wind and any changes in topography (if the Delft3D-SED is included in the coupling), and WAVE passes to FLOW the wave orbital velocity as well as forces based on the energy dissipation rate or the radiation stresses.

1.3 PCTides model

PCTides (Posey et al. 2008) is a stand-alone global tide-forecasting system, based on the shallow water equations, which can be set up rapidly for any user-specified location(s) to predict the water-level elevation and depth-averaged ocean currents. In addition, PCTides can model the effects of wind and pressure, via the wind stress and surface pressure gradients, in water-level prediction. This is the model that is currently used at NAVOCEANO for predictions of coastal surge and inundation due to tropical or extra-tropical storm systems. PCTides includes all of the necessary global databases for bathymetry, tidal data for open boundaries and utilizes the tide station data from the International Hydrographic Office (IHO) to improve the model results. PCTides is very efficient in terms of computational effort, but is limited to coarse resolution grids, which leads to inaccuracies in predicted water levels by not representing accurately enough the changes in the bathymetry or topography. Also the effects of waves are not included in the water level or current predictions, which leads to substantial underestimation of the water levels as will be shown in the validation test cases.

1.4 Hurricanes Studied

1.4.1 Hurricane Ike

Ike was named as a tropical storm on September 1, 2008 just west of the Cape Verde Islands (NHC 2010). Late on September 3, it reached hurricane strength and by 0600 September 4, Ike was a major category four hurricane (track depicted in Figure 2.1-1). Ike's strength would fluctuate over the following days as Ike interacted with the southernmost portion of the Bahamas and the Turks and Caicos Islands on September 7 as a category three storm and Cuba on September 8-9 as a category four storm. Ike emerged from the Cuban coast as a category one hurricane. In the Gulf of Mexico Ike strengthened into a category two storm of enormous size. The storm finally made landfall on September 13 at 0700 along the northern portion of Galveston Island on the Texas coast as a 95 kt, strong category two hurricane. As Ike moved inland it weakened and was downgraded to a tropical storm with a center well inland by 1800 on the 13th.

Ike provides an ideal test case for CSIPS due to the large storm surge and inundation produced along the Texas and Louisiana coastlines and wealth of data collected. In addition to the surge at

landfall, there was a large forerunner surge along the Louisiana-Texas coast 12-24 hours prior to landfall (Kennedy et al., 2011a) that was significantly larger at some locations than the surge at landfall. A number of National Ocean Services (NOS) tide stations, located throughout the northwestern Gulf of Mexico, captured the surge event with time series of water level and wind. Surge in excess of 1.5 meters was found along the central Louisiana coast increasing to over 3 meters along the southwestern Louisiana coast. The highest NOS gauge recorded surge was at Sabine Pass North, Texas near the Louisiana border (4.07 m above mean sea level (MSL)). Water levels reached even higher across the Bolivar Peninsula where United States Geological Survey (USGS) sensors (East et al. 2008) and post-storm high water mark analysis from the Federal Emergency Management Agency (FEMA 2009) showed inundation reaching around 4.5 m above MSL. Along with the abundance of water level data, Ike passed by a number of National Data Buoy Center (NDBC) Coastal-Marine Automated Network (CMAN) buoys which recorded wave and wind data. Due to this large collection of data and the destructive nature of the storm, Ike also has been a well-studied storm (East et al. 2008; FEMA 2009; Rego and Li 2010; Kennedy et al. 2011a, b; Bender et al. 2013; Kerr et al. 2013) providing high resolution data sets and analysis techniques for our study.

1.4.2 Hurricane Irene

Irene moved across the Bahamas and up the US east coast in late August 2011 (track depicted in Figure 2.2-1). Irene is noted for making multiple landfalls and causing widespread inland flooding due to rainfall in parts of the northeast US (NHC 2011). Irene also produced coastal flooding and inundation due to its storm surge up the east coast from North Carolina through southern New England. Irene was first named just before 0000 UTC on August 21, 2011 while located east of Martinique. The storm moved on a west-northwest course over the northwestern Caribbean Sea with official landfalls in St. Croix, U.S. Virgin Islands (USVI) and Punta Santiago, Puerto Rico (PR) before strengthening and approaching the Bahamas. Irene impacted Acklins/Crooked Island of the Bahamas as a category 3 hurricane with winds of 100 kt on August 24 at 1600 coordinated universal time (UTC). The hurricane slowly weakened while impacting Long Island, Eleuthera, and Abacos Bahamas over the next day. Over the next day and a half Irene slowly weakened as it approached the US mainland on a northward course. At 1200 UTC on August 27 Irene made landfall near Cape Lookout, North Carolina (NC) as a category 1 hurricane with 75 kt winds which were primarily contained to the east of the circulation. Irene's next landfall came at 0935 UTC on August 28 near Atlantic City, New Jersey (NJ). By this time Irene had weakened as it moved north-northeastward just offshore of the Delmarva Peninsula and approached NJ. The 60 kt winds that approached Atlantic City were again mainly to the east of the storm center and offshore. The final landfall occurred at Coney Island in Brooklyn NY at 1300 UTC on the 28th. Irene had weakened to 55 kt winds but still brought a strong surge into the New York City area.

Irene contrasts with Ike in that the storm affected a much larger area in a different basin. Irene was a weaker storm, with a much lower resulting surge, that ran nearly parallel to the US east coast, causing flooding and inundation from North Carolina through Connecticut. Having two contrasting test cases helped assess the model capability over a range of conditions and to develop confidence in CSIPS. Similar to Ike, a wealth of observational data for Irene is available. This data includes time series of water levels and winds from National Ocean Services (NOS, available online: http://tidesandcurrents.noaa.gov/) tide stations along the east coast, significant wave height, period, direction, and wind speed and direction from NDBC (available online:

http://www.ndbc.noaa.gov/) stations throughout the Atlantic and coastal regions, and a series of storm tide and high water mark recordings from the USGS (2012). From these observations surge in excess of 2 meters was recorded and the high water marks suggest surge upwards of 3 m occurred within parts of Pamlico Sound, NC. Values in the New York City region averaged between 1 – 1.5 m. The NDBC buoy located 150 n. mi east of Cape Hatteras, NC recorded maximum wave heights just under 10 m as did the buoy offshore of Cape Canaveral, Florida (FL). By all accounts Irene was a destructive storm which produced breaches along the Outer Banks (Clinch et al. 2012), damaged residential structures along North Carolina (Lester 2012), and brought up questions about the vulnerability of New York City to storm surge (Coch 2012; Aerts 2012). This report uses the data collected from Irene to validate CSIPS.

1.4.3 Super Typhoon Pongsona

The third test case selected was Typhoon Pongsona that impacted Guam in 2002. Guam has a typical island bathymetry – the water depth is very large and becomes shallow over a small distance. Thus the gradients in bathymetry are large and waves will be dominant. Pongsona was named a tropical storm at 1200 UTC on December 3, 2002, south-southeast of Ujelang Atoll. Per JTWC, the storm subsequently began to track westward on the 4th while slowly strengthening, reaching typhoon intensity on December 5 at 0600 UTC. Pongsona continued to move westward at 9-10 kts, that changed to west-northwest, then into a northwesterly heading by December 7, 0000 UTC. Wind speeds had reached 95 kts by this time. On December 8 at 0000 UTC, Pongsona began a period of rapid intensification, and was still moving to the northwest as it began to bear down on Guam, centered only 75 nm to the southeast. Six hours later, mean surface winds (MSW) reached 130-kt super typhoon intensity. The eyewall made landfall on northeastern Guam on December 8 at approximately 0500 UTC. The mean surface wind (MSW) on Guam was estimated at 102 kts with peak gusts of 130 kts. The lowest pressure reported from the National Weather Office was 940.4 mb. Its course began to change to a north-northwesterly heading. Special Sensor Microwave/Imager (SSM/I) imagery depicted a well-developed eyewall and a 32-nm symmetric eye on December 8at 2030 UTC. Gales covered an area between 300 and 350 nm in diameter, and storm-force winds extended outward an estimated 70 nm from the centre over water. By December 9, 0000 UTC, the strength of the typhoon began to wane as the MSW dropped to 125 kts, just below super typhoon strength. The intensity had fallen further to 110 kts by 1800 UTC, and by December 10, 0000 UTC Pongsona was accelerating northwards at 21 kts. By December 11, 0000 UTC, Pongsona had transitioned to an extratropical cyclone.

2 DELFT3D CASE STUDIES

2.1 Hurricane Ike

2.1.1 Model Domains

For Hurricane Ike studies a total of 5 domains were used (Figure 2.1-1). The large scale domain covered the Gulf of Mexico (GoM) with a resolution of 0.1°(approximately 10 km). This large scale domain consisted of 22,784 (178 x 128) grid cells. Nested within the GoM domain was a nearshore domain which covered much of the northern Gulf (NG) from the Texas coast to the mouth of the Mississippi River with a resolution of 0.02° (approximately 2 km) and consisting of 138,761 cells (461 x 301). Within the nearshore domain were three coastal domains with a resolution of 0.004° (approximately 400 m). These coastal domains covered Galveston Bay (GB), the Port Arthur area along the Texas Louisiana border (PA), and Vermillion Bay area of Louisiana (VB). The GB domain features 84,581 cells (301 x 281), the PA domain features 75,551 cells (301 x 251), and the VB domain has 81,826 cells (326 x 251). The simulation period for the GoM domain begins on September 5, 2008 at 12:15 UTC and ends on September 14, 2008 at 23:15 UTC. The conditions along open boundaries in inner nests are specified as Riemann time-series, where the Riemann variables are calculated using the water levels and currents from the immediate outer nest. These simulations start on September 9, 2008 at 00:00 UTC and run through September 14, 2008 23:15 UTC. The simulations cover the same time period as those in the NG domain. For all domains an initial water level of 0.11 m was imposed. This value was derived by examining seasonal sea level trends throughout the Gulf of Mexico for the month of September where steric effects commonly elevate sea levels throughout the region.

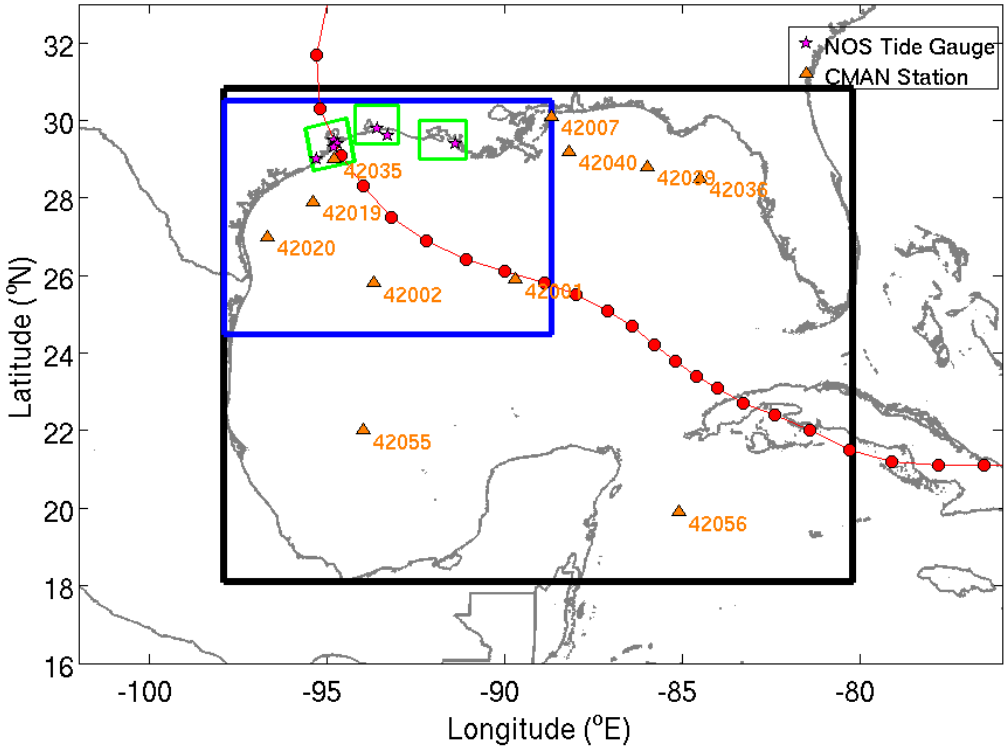

Figure 2.1-1: Domains used for Hurricane Ike studies. The black box outlines the 0.1° domain, the blue box the 0.02° domain, and the green boxes the three 0.004° domains.

To validate the system, the model results are compared to the large collection of observational data detailed above. Although the GoM and NG domains contain a larger selection of NOS stations, only those that are contained in all three resolutions of domains are included. This means that seven NOS stations are used and are listed in Table 2.1-1. However, for the wave comparisons only one buoy was located in a region with coverage from all three domain resolutions, since most of the buoy locations tend to be further offshore than the extent of the high resolution coastal domains. Therefore, all buoys with available data during the period within the GoM domain are considered and listed in Table 2.1-2. To examine the atmospheric forcing a combination of offshore buoys and coastal stations were used. The same NOS stations listed in Table 2.1-1 were used in the wind comparison. Likewise the same buoys used for the wave comparison (Table 2.1-2) are used for the wind comparison.

Table 2.1-1: NOS tide stations used in comparison of hydrographics for Hurricane Ike.

Station ID	Location	Latitude (°N)	Longitude (°E)	Domains
8764227	Armeda Pass, LA	29.450	-91.338	GoM, NG, VB
8768094	Calcasieu Pass, LA	29.768	-93.343	GoM, NG, PA
8770570	Sabine Pass North, TX	29.730	-93.870	GoM, NG, PA
8771013	Eagle Point, TX	29.480	-94.918	GoM, NG, GB
8771341*	Galveston Bay North Jetty, TX	29.357	-94.723	GoM, NG, GB
8771510	Galveston Pleasure Pier, TX	29.285	-94.788	GoM, NG, GB
8772447	USCG Freeport, TX	28.943	-95.303	GoM, NG, GB

* Station stopped recording September 13, 2008 at 01:30 UTC

Table 2.1-2: NDBC stations used in wave comparison for Hurricane Ike.

Station ID	Latitude (°N)	Longitude (°E)
42001	25.9000	-89.6670
42002	25.7900	-93.6660
42007	30.0900	-88.7690
42019	27.9130	-95.3600
42020	26.9660	-96.6950
42035	29.2320	-94.4130
42036	28.5000	-84.5170
42039	28.7910	-86.0080
42040	29.2050	88.2050
42055	22.0170	-94.0460
42056	19.8740	-85.0590

CSIPS will be compared to the observation data to show the accuracy of the simulation results as well as the sensitivity of those results to different input parameters. Specifically the sensitivity of the results to the bathymetry and topography dataset, the inclusion of wave effects, the bottom roughness parameterization, and the forecast winds and track of the storm will be examined.

These sensitivities will be analyzed across all three domain resolutions and compared to the observations as well as a best available or baseline simulation.

2.1.2 Baseline

The baseline simulations for Hurricane Ike consist of 3 sets of simulations; the large scale simulation in the GoM domain, followed by the nearshore simulation in the NG domain, and finally the three high resolution simulations in the coastal domains. The elevation dataset used consisted primarily of bathymetry and topography gathered and made available by the Southeastern Universities Research Association (SURA) Inundation Testbed. This is a high resolution (~30 m) dataset available for much of the northern Gulf of Mexico. In areas where the SURA data is not available the National Geophysical Data Center (NGDC) Coastal Relief Model, Shuttle Radar Topography Mission (SRTM), and General Bathymetric Chart of the Oceans (GEBCO) data were used to fill in (Figure 2.1-2). The baseline simulation was dynamically coupled to the wave module so that wave effects are accounted for. The wave simulations are much more computationally expensive than is the hydrodynamic component. With this in mind the wave grid mirrored the hydrodynamic grid but with half the resolution for all domains (0.2°, 0.04°, 0.008° for the GoM, NG, and GB/PA/VB domains respectively). The wave model was run in non-stationary mode with a 6 minute timestep and communicated with the hydrodynamic model every hour of simulation. Within the hydrodynamic model the bottom roughness was calculated using the Manning formulation. To determine the values for the spatially varying Manning's N coefficient, land use data was obtained from National Land Cover Database (NLCD) and converted to a corresponding Manning's N value based on the tables in Mattocks and Forbes (2008). For offshore areas where land use data is non-existent, a constant value of 0.02 $s/m^{1/3}$ was used (Figure 2.1-3). The values around the coast are generally small but increase inland and in urban areas. The GoM simulation was performed with a 30 second timestep, the NG domain with a 60 second timestep, and the coastal domains with a 15 second timestep after experimentation addressing the stability of the simulations with the amount of clock time to complete. The GoM domain required smaller timesteps because of the large gradients in bathymetry near the island of Cuba. The open boundary conditions for the GoM domain were specified in terms of astronomic components, which were obtained from the TPXO 7.2 tidal database (Egbert and Erofeeva, 2002). A total of 13 harmonic constituents were used along with a constant value (zero phase) to account for the initial water level conditions. The open boundaries were Riemann which simulates a weakly reflective boundary which allows outgoing waves to cross the boundary without being reflected back. The atmospheric forcing was provided on an equidistant grid from Oceanweather Inc. (OWI). The fields consists primarily of the NOAA H*wind (Powell et al. 1998) snapshot for the core hurricane characteristics and are then blended to background winds to create a smooth wind field. Both fields were output on a 0.02 domain with a temporal resolution of 15 minutes. The winds were adjusted to account for land effects by employing a directional land-masking (Westerink et al. 2008). The same NLCD land use data was used to obtain the surface roughness length (z_0) values for each grid cell and the wind field was adjusted accordingly based on the wind direction. The air-sea drag

formulation of Holthuijsen et al. (2012) was used to compute the drag coefficient values for the conversion of wind speed to wind stress.

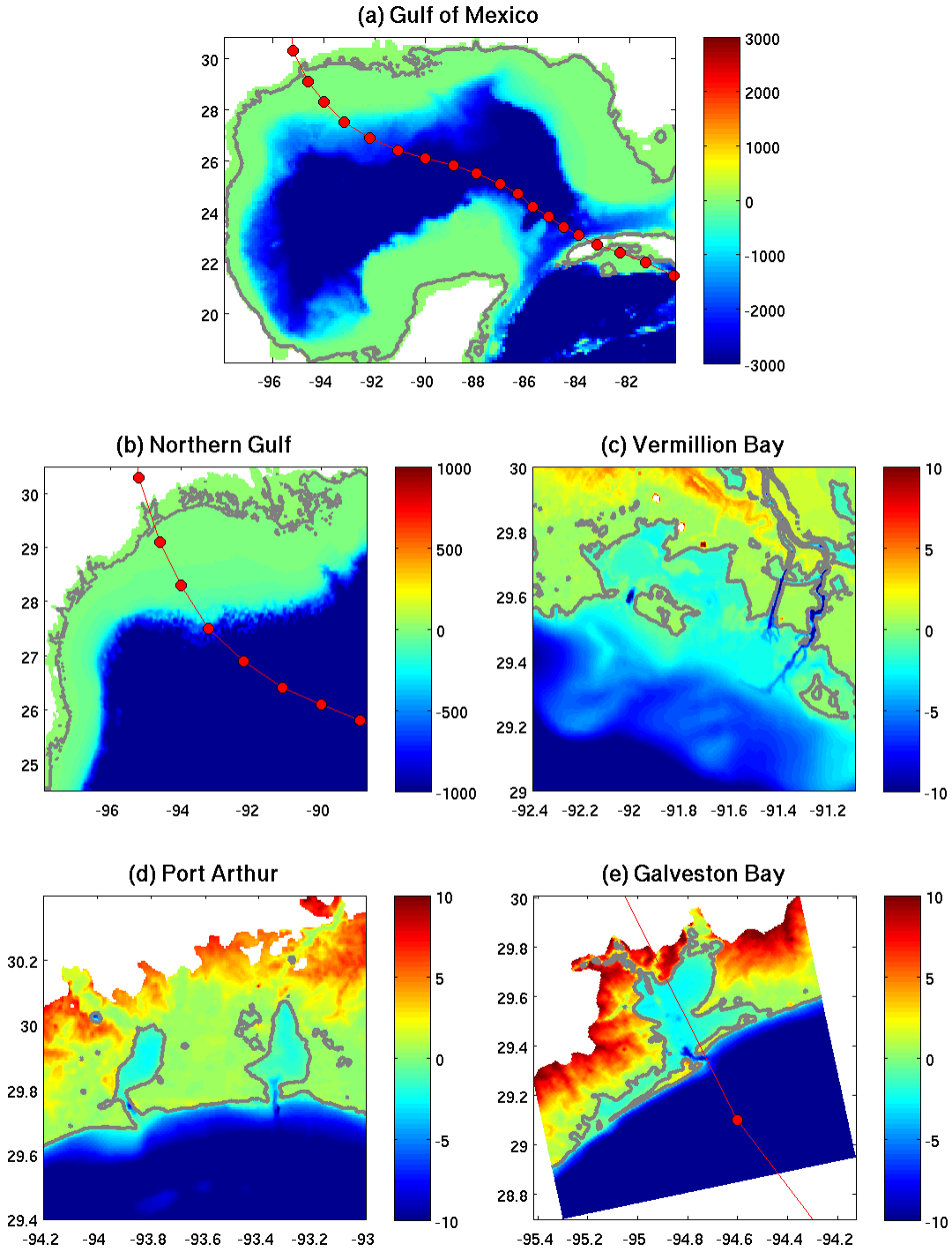

Figure 2.1-2: Bathymetry and topography (m, MSL) for the 5 domains used in the Ike validation studies: (a) GoM domain, (b) NG domain, (d) VB domain, (d) PA domain, and (e) GB domain.

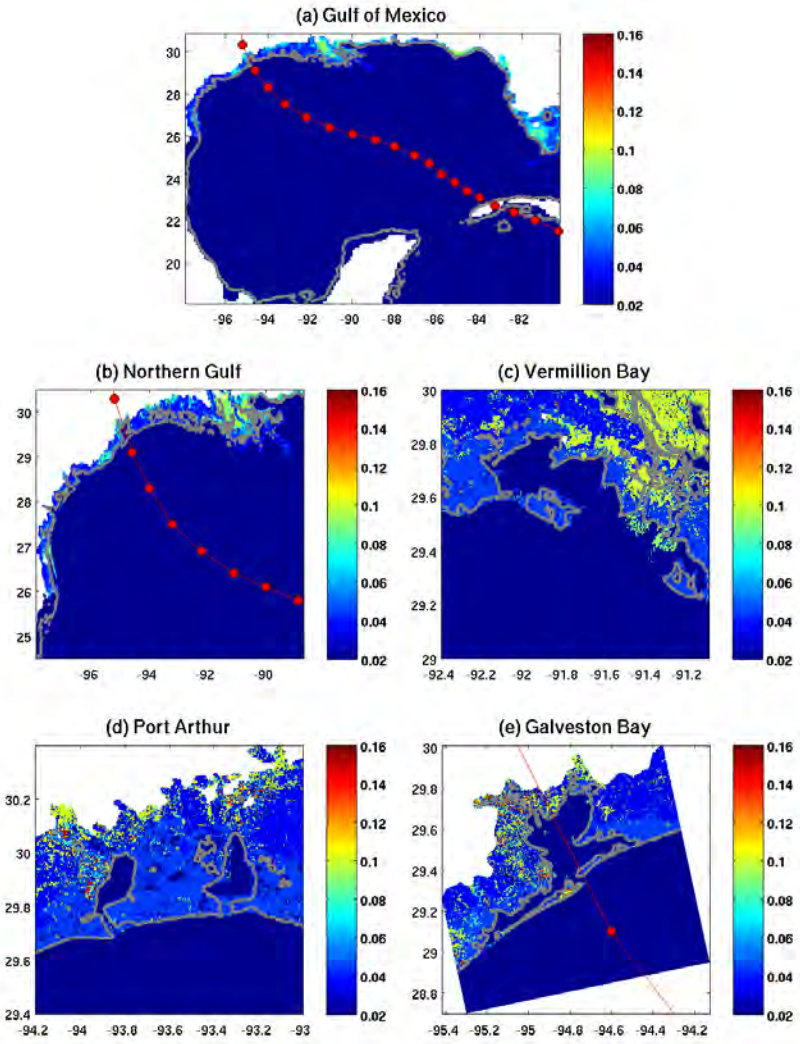

Figure 2.1-3: Variable Manning's N for the 5 domains used in the Ike validation studies (a) GoM domain, (b) NG domain, (c) VB domain, (d) PA domain, and (e) GB domain.

2.1.3 Wind Field Comparison

To validate the modeling system, proper forcing is necessary. In storm surge and inundation modeling the primary forcing comes from the hurricane wind field. The OWI winds used the in baseline simulation represent the best available winds for re-analysis of Hurricane Ike. Figure 2.1-4 shows the comparison between the modeled wind speed and direction and the observed wind speed and direction at the 11 NDBC buoys listed in Table 2.1-2. These offshore buoys are expected to compare well with the simulated results since they are far from the influence of land which acts to reduce the wind speed based on the roughness of the terrain. The figure demonstrates that the simulated and observed winds and speed compare well throughout the Gulf of Mexico. To show a quantitative assessment of the agreement between the simulated and

modeled winds, a number of metrics following the Interagency Performance Evaluation Task Force (IPET) established for their risk assessment of the New Orleans area following Hurricane Katrina (Ebersole et al. 2007) were used. In the following metrics the observed wind speed is denoted *O* and the simulated wind speed denoted *S*. The triangular bracket denotes the arithmetic mean of the data.

$$\bar{O} = \langle O \rangle ; \qquad \bar{S} = \langle S \rangle$$

$$BIAS = \langle S - O \rangle$$

Absolute Error: $Abs.Err = \langle |S - O| \rangle$

Root Mean Square Error (RMSE): $RMSE = \langle (S - O - BIAS)^2 \rangle^{1/2}$

Scatter Index: $SI = 100 * \frac{RMSE}{\bar{S}}$

Correlation Coefficient: $r = \frac{\langle (O - \bar{O})(S - \bar{S}) \rangle}{[\langle (O - \bar{O})^2 \rangle \langle (S - \bar{S})^2 \rangle]^{\frac{1}{2}}}$

Slope and Intercept of Linear Regression: $M = a + b * S$

A secondary linear regression is applied where the intercept *a* is forced to zero and following Ebersole et al. (2007) termed the symmetric *r* value (Symm r). With these descriptions the scatter index represents a percentage with lower values indicating more reliable estimates. In addition to these estimates a root mean square error (RMSE) skill score was developed as

$$RMSESS = 1 - \frac{\sqrt{\sum (S-O)^2}}{\sqrt{\sum O^2}},$$

where a value close to one indicates a good score.

As seen qualitatively in Figure 2.1-4, Table 2.1-3 shows that there is very good agreement between the observed and simulated winds. Throughout the basin the agreement is strong, although there is a small but consistent bias for the simulated winds to slightly overestimate the observed winds. This bias is under 1.75 m/s for all stations. The absolute error is a little bit greater for all stations but below 2.5 m/s for all buoys and the root mean square (RMS) error is generally about 1 m/s indicating that the simulation captures the variability in the observed wind field well. Buoy 42035, located just offshore of Galveston, scores the poorest for a number of indicators. This buoy is located nearly directly in the path of Hurricane Ike and likely

experienced the most variability in the observations due to the chaotic nature of the hurricane. Overall the simulated and observed winds compare very well offshore.

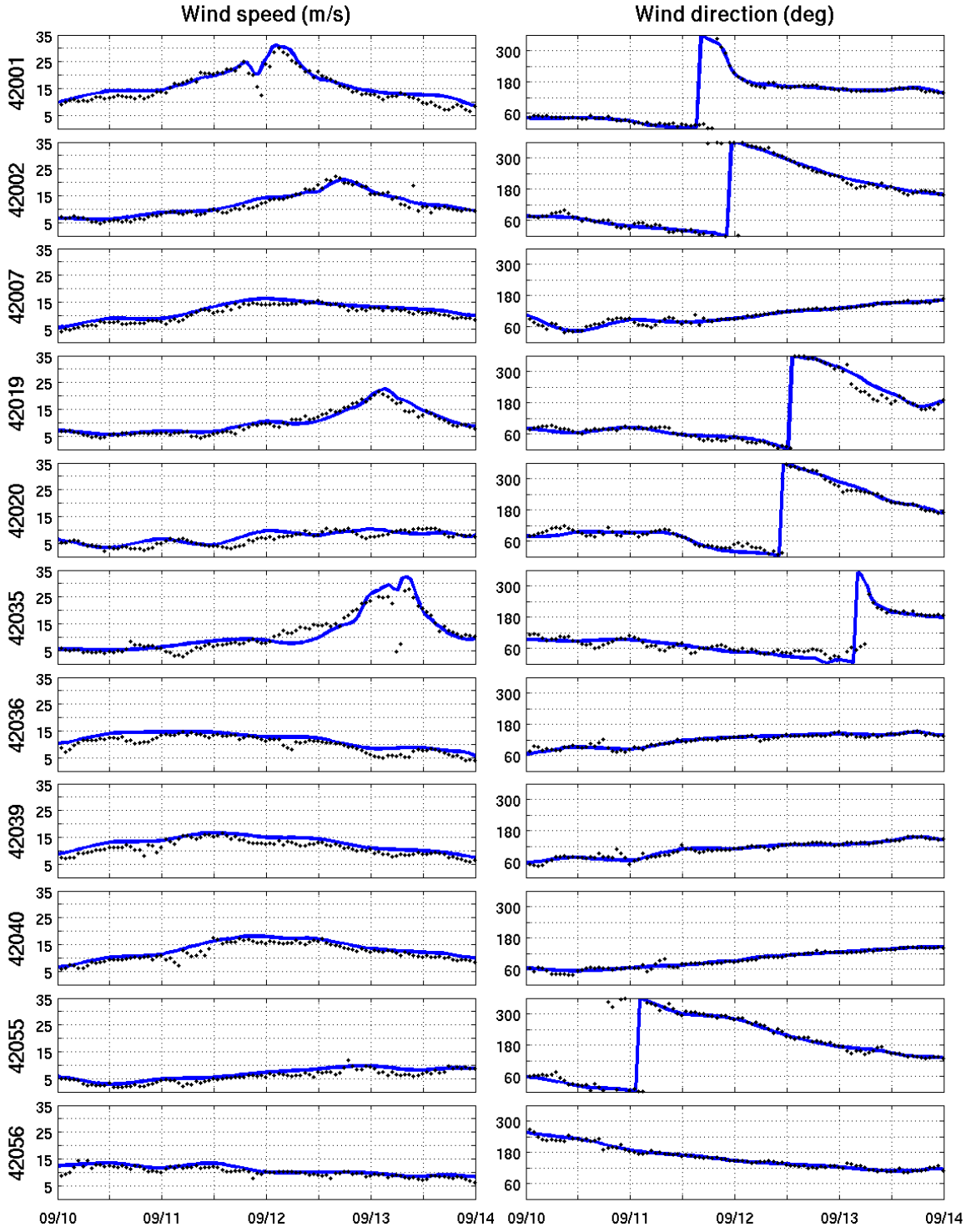

Figure 2.1-4: Comparison between the baseline (Run 000) wind speed and direction and the observed wind speed and direction at 11 NDBC CMAN stations. Black dots are data and blue lines are from the model.

Table 2.1-3: Statistical comparison between observed and simulated winds at NDBC CMAN stations for baseline simulation winds. All speeds in m/s.

Buoy ID	Mean Cond		Bias	Abs. Err	RMS Err	Scat Indx	Linear Regression Estimators				RMSE-SS	No. Obs
	Obs	Sim					Corr (r)	Symm r	Slope (a)	Interc (b)		
42001	15.22	16.53	1.31	1.75	1.83	11.09	0.56	1.06	0.88	3.17	0.91	96
42002	11.27	11.77	0.50	1.06	1.30	11.02	0.65	1.02	0.86	2.08	0.96	96
42007	10.75	11.91	1.16	1.21	0.71	5.97	0.71	1.09	0.92	2.01	0.89	96
42019	9.83	10.33	0.50	1.08	1.23	11.94	0.58	1.03	0.96	0.88	0.95	96
42020	6.65	7.21	0.57	1.31	1.52	21.03	0.75	1.04	0.67	2.77	0.91	96
42035	10.89	11.33	0.44	2.45	4.13	36.45	0.47	1.01	0.92	1.31	0.96	95
42036	10.02	11.70	1.67	1.67	1.09	9.28	0.70	1.14	0.83	3.36	0.83	96
42039	11.11	12.81	1.70	1.72	0.88	6.88	0.70	1.14	0.89	2.89	0.85	96
42040	11.97	13.37	1.40	1.44	0.97	7.26	0.72	1.11	0.96	1.87	0.88	96
42055	5.64	6.73	1.10	1.19	0.84	12.46	0.73	1.15	0.88	1.75	0.81	96
42056	10.04	10.89	0.85	0.97	0.91	8.32	0.70	1.08	0.87	2.20	0.92	96

As Hurricane Ike comes onshore there is a transition from the somewhat smooth and uniform ocean surface to the rough varying friction surface of the topography. In addition as the hurricane comes ashore the cooler and drier land based air is introduced to the hurricane leading to a decrease in the intensity of the storm. To capture the change from the marine exposure winds to the land exposure a directional land masking technique was applied. This technique, based on Westerink et al. (2008), reduces wind speeds to account for the higher surface roughness of the land surface. For each grid cell a representative roughness length is determined based on the NLCD land use data. To account for the wind direction, the directional roughness length is computed based on the land cover types within a fetch of 10 km, in a given 30 degree sector. This means that each grid cell contains 12 directional roughness lengths corresponding to 12 different wind directions that each accounts for the cells in that direction within a 10 km fetch. This computation can change throughout the course of a simulation as areas become flooded and dried and the corresponding land characteristics change. For this study no attempt to capture this process was made. The directional land masking was done prior to the simulation based on the initial land use characteristics.

Figure 2.1-5 and Table 2.1-4 show the comparison between the simulated and observed winds at the 7 NOS stations located within the coastal zone. These stations are right at the transition from marine exposure to land exposure making it difficult to exactly simulate the observed wind speed. The range of the bias is much greater, between -4 and +6.26 m/s. The slight positive bias that exists offshore is no longer present, but now there is a much larger spread. Of note is that the two largest outliers in terms of bias are the stations furthest from the core of the hurricane. In fact most of the stations located close to the hurricane track show very good agreement with the

observations with small biases, low values of absolute error and low values of RMS error. The station at Galveston Pleasure Pier where landfall was made shows a very high RMSE skill score and an extremely low bias indicating good agreement throughout the timeframe.

The wind field evaluation provides confidence that the core of the hurricane is modeled well and that the forcing is very well simulated offshore and near the landfall location on shore. The

further away from the hurricane center, the worse the simulated wind field compares to observations in the very nearshore/coastal NOS stations.

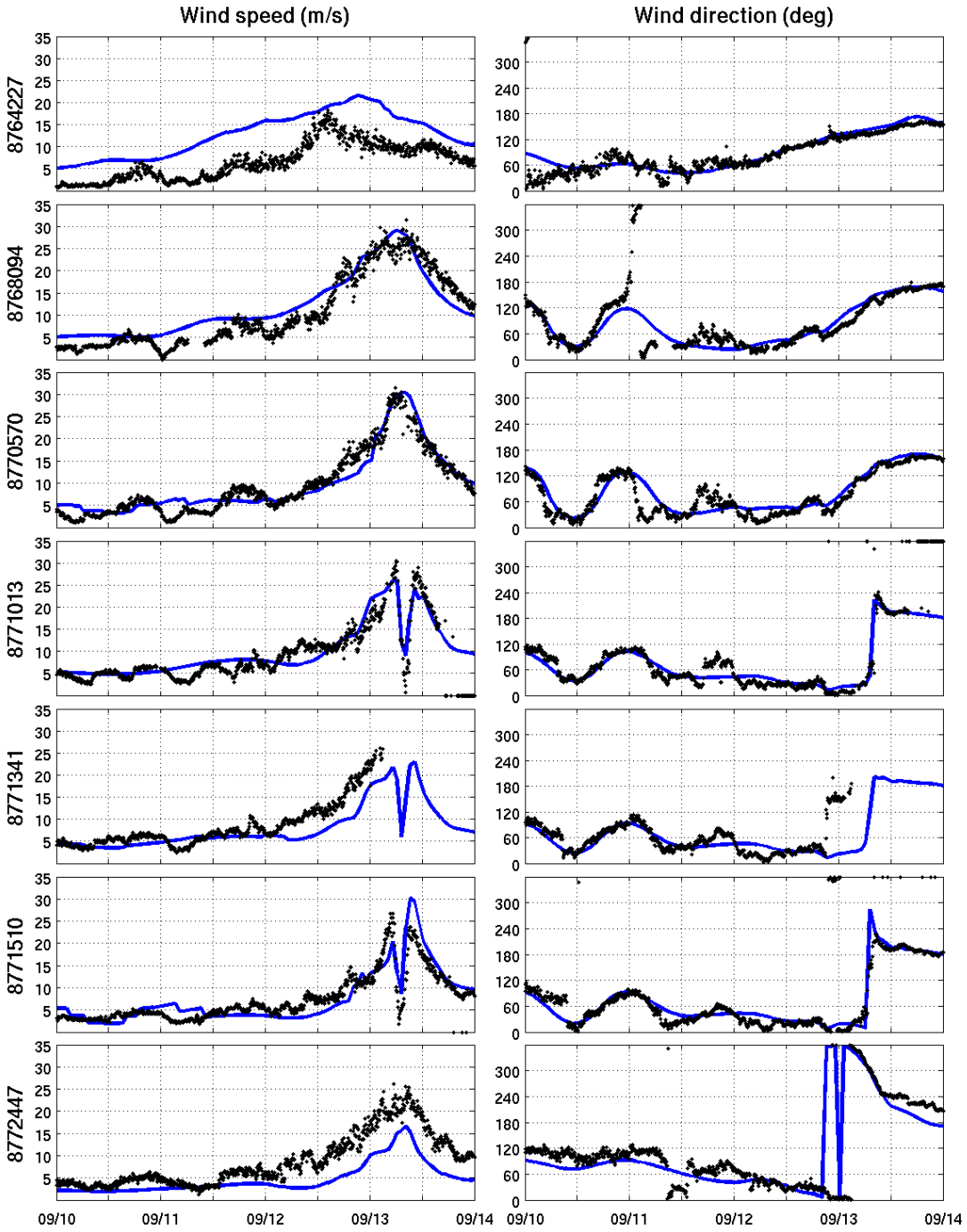

Figure 2.1-5: Comparison between the baseline (Run 000) and wind speed and direction and the observed wind speed and direction at 7 NOS stations. Black dots are data and blue lines are from the model.

Table 2.1-4: Statistical comparison between observed and simulated winds at NOS stations for baseline simulation winds. All speeds in m/s.

NOS ID	Mean Cond		Bias	Abs. Err	RMS Err	Scat Indx	Linear Regression Estimators				RMSE-SS	No. Obs
	Obs	Sim					Corr (r)	Symm r	Slope (a)	Interc (b)		
8764227	6.50	12.76	6.26	6.26	2.45	19.22	0.71	1.69	1.03	6.09	0.04	927
8768094	10.87	12.22	1.35	2.74	2.84	23.25	0.64	1.01	0.82	3.33	0.88	906
8770570	9.38	9.53	0.15	1.84	2.30	24.13	0.48	0.98	0.91	1.00	0.98	947
8771013	8.97	9.69	0.72	2.21	3.01	31.05	0.46	0.98	0.79	2.65	0.92	864
8771341	8.33	6.33	-2.0	2.45	2.49	39.40	0.37	0.71	0.57	1.55	0.76	720
8771510	7.28	7.33	0.05	2.20	2.88	39.27	0.43	1.00	1.00	0.07	0.99	954
8772447	8.70	4.71	-4.0	4.01	2.86	60.66	0.50	0.55	0.56	-0.17	0.54	960

2.1.4 Water Level and Inundation Comparison

The surge during Ike influenced a large area of the Texas and Louisiana coasts. In validation of the storm surge and inundation prediction system there are two different components in terms of surge and flooding. First the model must be able to accurately predict the water level at the NOS stations free of the interactions with land. This is a somewhat simpler task and can be commonly done at rather coarse resolutions. The harder task is to accurately simulate the overland flooding, or inundation that results from the surge. This task is especially difficult due to the large and abrupt changes in topography and flood control structures that may not be simulated. For this reason a very high resolution is needed. In addition, the validation of the inundation is more difficult since there is much greater uncertainty in the accuracy of the observations over land. Prior to landfall, a large number of temporary USGS stations were deployed to collect surge values. To validate inundation, we use data from these USGS stations (Table 2.1-5) as well as high water marks (HWMs. The HWMs are collected post-storm by survey crews and come with a large degree of uncertainty. The marks are commonly taken as water lines or debris lines on structures which are surveyed and reported in a common datum. Wave action can lead to large variations in these marks as can differences in the surveyors. The marks do not provide any details into the temporal nature of the event as well. With these caveats in mind it is stressed that the NOS hydrograph comparisons provide an accurate and reliable measure of the accuracy of the simulation system.

Figure 2.1-6 shows a hydrograph comparison between the observations at the 7 NOS stations that are free of land interactions and the simulated results in each of the three layers of domains (left panel), and also comparisons to a sample of the USGS deployments (right panel) . Overall there is good agreement between the observations and the modeled results. However, there are some differences amongst the different domains for the same stations. Typically, the higher resolution domain gives the more accurate results, with one exception. The forerunner surge is predicted better by the larger, but more coarsely resolved GoM domain. For surge, especially on land, the higher resolution definitely has the advantage. This can be illustrated by examining the peak water levels. Figure 2.1-7 shows the peak water level at all the NOS and USGS stations,

including those near land, versus the simulated peak level (note that station 8771341 stops recording so the simulated peak is the level at the time that the observations stop). Save for one or two outliers, the more resolved the domain, the closer the value to observations. For stations in open water, not influenced by land, Table 2.1-6 shows statistics for the simulated and peak water levels are comparable between the different domains. These are as defined earlier with the addition of the mean absolute percent error (MAPE) which is simply the arithmetic mean of the absolute percent error. From the table and the figure there is a slight underestimate of the peak, although the MAPE is below 15% for all of the resolutions. It is interesting to note that the coarsest resolution actually performs very well in capturing the peak water level at the coastal observing stations. To highlight the peak water level and to give a feel for the magnitude of the errors, Table 2.1-7 shows the observed and peak water levels at each station. In terms of the timing of the peak water level, Table 2.1-8 shows the lag in hours (negative lag indicates the simulated peak occurs prior to the observed peak). The lag varies across stations and domains, but in general the simulated peak occurs slightly after the observed peak; the outlier being Calcasieu Pass, Louisiana (LA) where the simulated peak occurs before the observed. The average absolute error across all stations and domains is just under three hours. Similar to the hydrograph and the wind results the two largest outliers are the two stations furthest from the storm, Armeda Pass, LA and USCG Freeport, Texas (TX) stations.

Table 2.1-5: List of USGS deployments for Hurricane Ike

Station ID	Latitude (°N)	Longitude (°E)
SSS-TX-MAT-010	28.8364	-95.6683
SSS-TX-MAT-009	28.7706	-95.6167
SSS-TX-MAT-008	28.7642	-95.6269
SSS-TX-MAT-007	28.6114	-96.2153
SSS-TX-MAT-006	28.6831	-95.9756
SSS-TX-MAT-005	28.6006	-95.9781
SSS-TX-MAT-004	28.8389	-95.8528
SSS-TX-MAT-003	28.7875	-95.9958
SSS-TX-MAT-002	28.7864	-96.1503
SSS-TX-MAT-001	28.7206	-96.2739
SSS-TX-JEF-009	29.6626	-94.0884
SSS-TX-JEF-008	29.7647	-93.8978
SSS-TX-JEF-007	29.7739	-93.9425
SSS-TX-JEF-006	29.7111	-93.8600
SSS-TX-JEF-005	29.6969	-94.0983
SSS-TX-JEF-004	29.7103	-94.1164
SSS-TX-JEF-002	29.6750	-94.0436
SSS-TX-JEF-001	29.6844	-94.1928
SSS-TX-HAR-004	29.7131	-94.9933
SSS-TX-HAR-003	29.5919	-95.1283
SSS-TX-HAR-002	29.6203	-94.9989
SSS-TX-GAL-022	29.5517	-95.0247
SSS-TX-GAL-021	29.5133	-95.1039
SSS-TX-GAL-020	29.4567	-95.0478

SSS-TX-GAL-019	29.5064	-94.9578
SSS-TX-GAL-018	29.3558	-95.0400
SSS-TX-GAL-016	29.3039	-94.9053
SSS-TX-GAL-015	29.0861	-95.1172
SSS-TX-GAL-011	29.2208	-94.9447
SSS-TX-GAL-010	29.2381	-94.8778
SSS-TX-GAL-008	29.3344	-94.7511
SSS-TX-GAL-005	29.5944	-94.3903
SSS-TX-GAL-002	29.4658	-94.6481
SSS-TX-GAL-001	29.4514	-94.6342
SSS-TX-CHA-004	29.7728	-94.6869
SSS-TX-CHA-003	29.6042	-94.6753
SSS-TX-CAL-005	28.6414	-96.3233
SSS-TX-CAL-004	28.6606	-96.4117
SSS-TX-CAL-003	28.6192	-96.6197
SSS-TX-CAL-002	28.4444	-96.4025
SSS-TX-CAL-001	28.4064	-96.7117
SSS-TX-BRA-011	29.2967	-95.3567
SSS-TX-BRA-010	29.3364	-95.2842
SSS-TX-BRA-009	29.0131	-95.3297
SSS-TX-BRA-008	29.0356	-95.3989
SSS-TX-BRA-007	29.2867	-95.1314
SSS-TX-BRA-006	28.8667	-95.5872
SSS-TX-BRA-005	28.9494	-95.5556
SSS-TX-BRA-004	28.8683	-95.4486
SSS-TX-BRA-002	29.0847	-95.2881
SSS-TX-BRA-001	29.2119	-95.2083

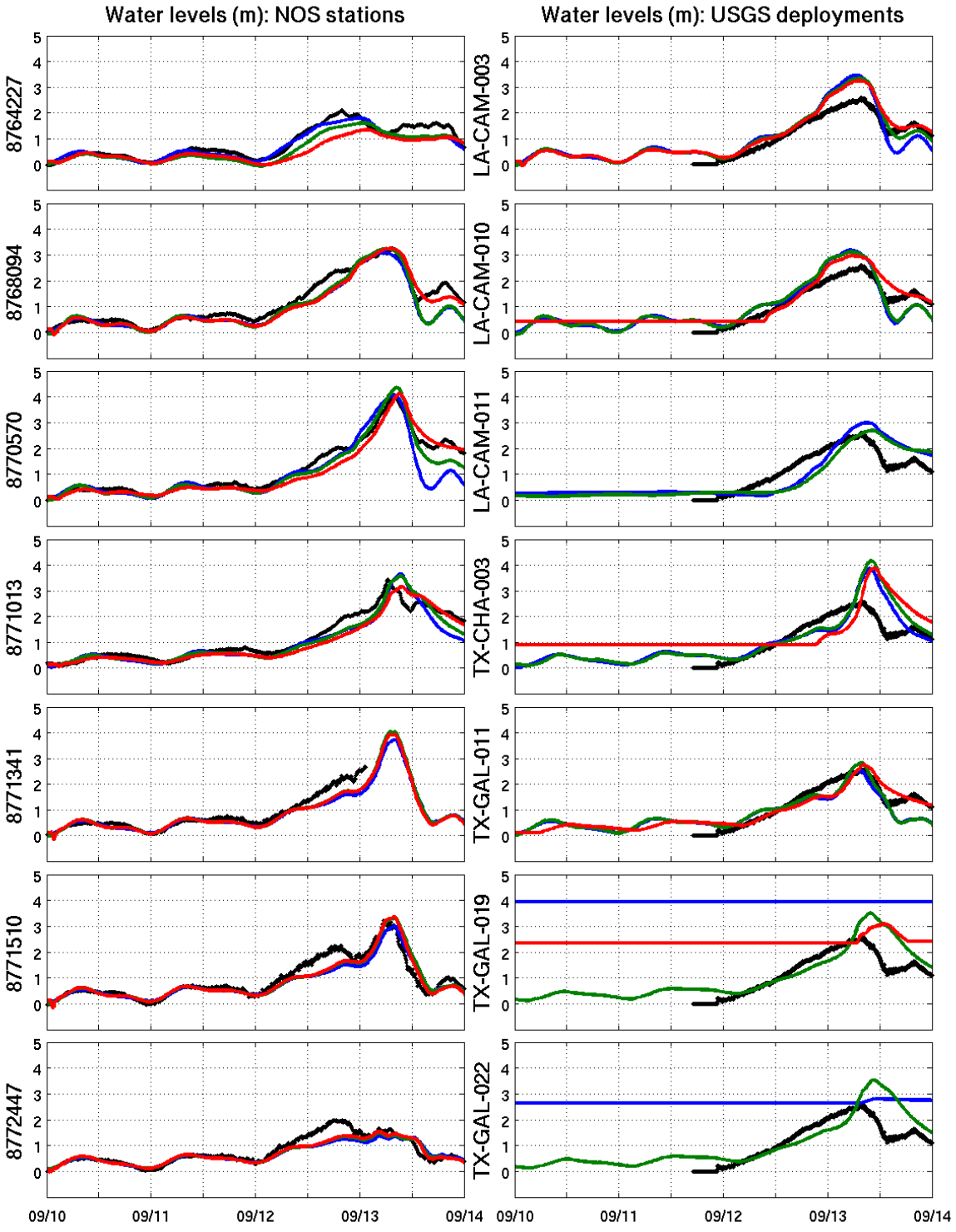

Figure 2.1-6: Hydrograph comparison between NOS stations and baseline simulation runs (left panel) for different domains. The right panel shows comparisons to select USGS temporary deployments for Ike. Black dots are data, blue line is the GoM domain, green line is NG domain and the red line is one of the high res domains.

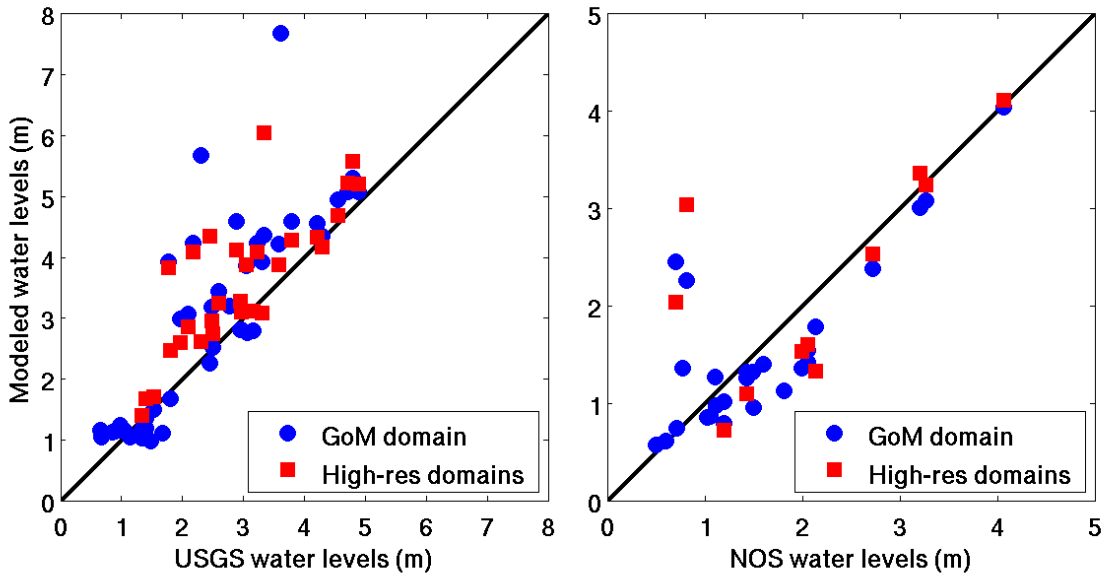

Figure 2.1-7: Simulated versus observed peak water levels at all the USGS deployments and NOS stations for the Gulf of Mexico domain (low-res) and the appropriate high-resolution domains.

Table 2.1-6: Statistics for the peak water level at the 7 NOS stations.

	GoM	NG	VB/PA/GB
Corr r	0.91	0.97	0.95
Bias (m)	-0.15	-0.17	-0.29
RMSE (m)	0.26	0.10	0.21
Scatter Index	9.32	3.52	7.87
MAPE	7.04	12.98	14.36

Table 2.1-7: Peak water levels (m) at the 7 NOS stations as observed and simulated.

	Obs.	GoM	NG	VB/PA/GB
8764227	2.10	2.24	1.60	1.33
8768094	3.26	3.03	3.24	3.25
8770570	4.07	3.55	4.36	4.11
8771013	3.44	3.56	3.57	3.15
8771341*	2.68	2.41	1.97	1.96
8771510	3.21	3.01	3.32	3.36
8772447	1.99	1.93	1.48	1.54

* Peak water level at time station stopped recording, actual simulated peaks are: 3.53, 4.02, 3.93

Table 2.1-8: Mean absolute error of the time lag (in hrs.) between the simulated and observed peak water level (negative lag indicates simulated peak occurs prior to observed).

NOS Stations	GoM	NG	VB/PA/GB	Mean Abs. Error
8764227	6.9	5.0	5.8	5.9
8768094	-2.1	-1.7	-0.4	1.4
8770570	1.5	0.6	1.3	1.1
8771013	0.1	3.0	3.2	2.1
8771341	0.6	0.2	0.2	0.3
8771510	4.4	2.5	2.5	3.1
8772447	2.8	8.3	8.3	6.5
Mean Abs. Error	2.8	3.0	3.1	

Evaluation of the inundation in the region is much more qualitative since there are no quantitative estimates of the extent of the inundation. Figure 2.1-8 shows an estimate of the inundation depth as presented by the Harris County Flood Control District. The inundation extends from Brazoria County TX through Iberia Parish LA with the highest levels in Chambers and Jefferson County TX. Figure 2.1-9 shows an estimate of the inundation depth as computed in the NG domain to present a continuous plot at a higher resolution than the GoM domain (note the units have changed to feet to be consistent with the Harris County Flood District figure). Also with this figure are the envelopes of high water (EOHW) for the GB and PA domains to present a close up on the inundation in these regions. From Figure 2.1-8 and Figure 2.1-9 there is qualitative agreement between the official estimates of the inundation and the results of the simulations. To get a quantitative estimate a high water mark analysis was performed. As

mentioned previously the HWM analysis is done with the knowledge that the error bars on the actual observations can be considerably larger than the water level taken from the NOS stations.

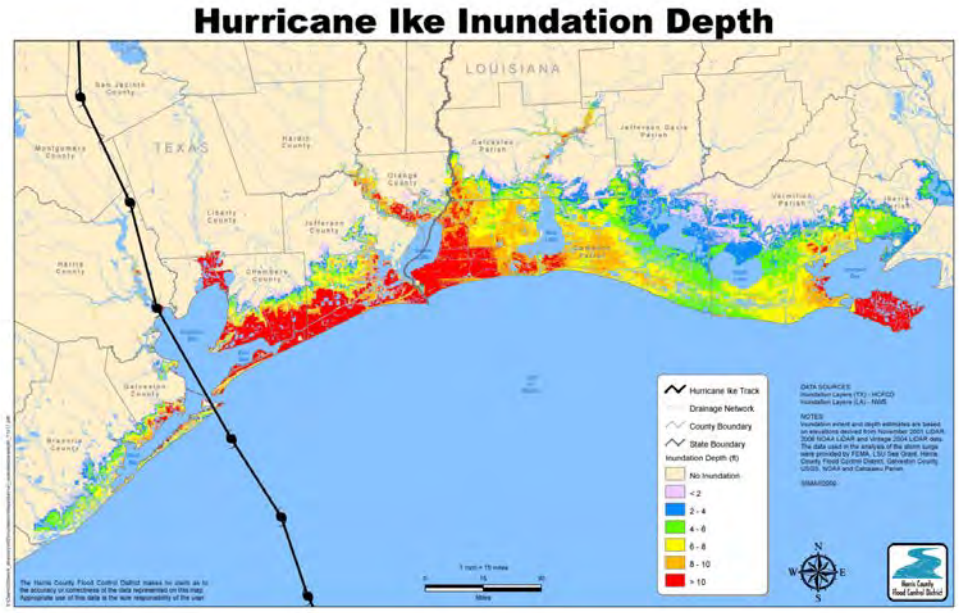

Figure 2.1-8: Hurricane Ike estimated inundation depth (ft.). Image courtesy of Harris County Flood Control District.

(a)

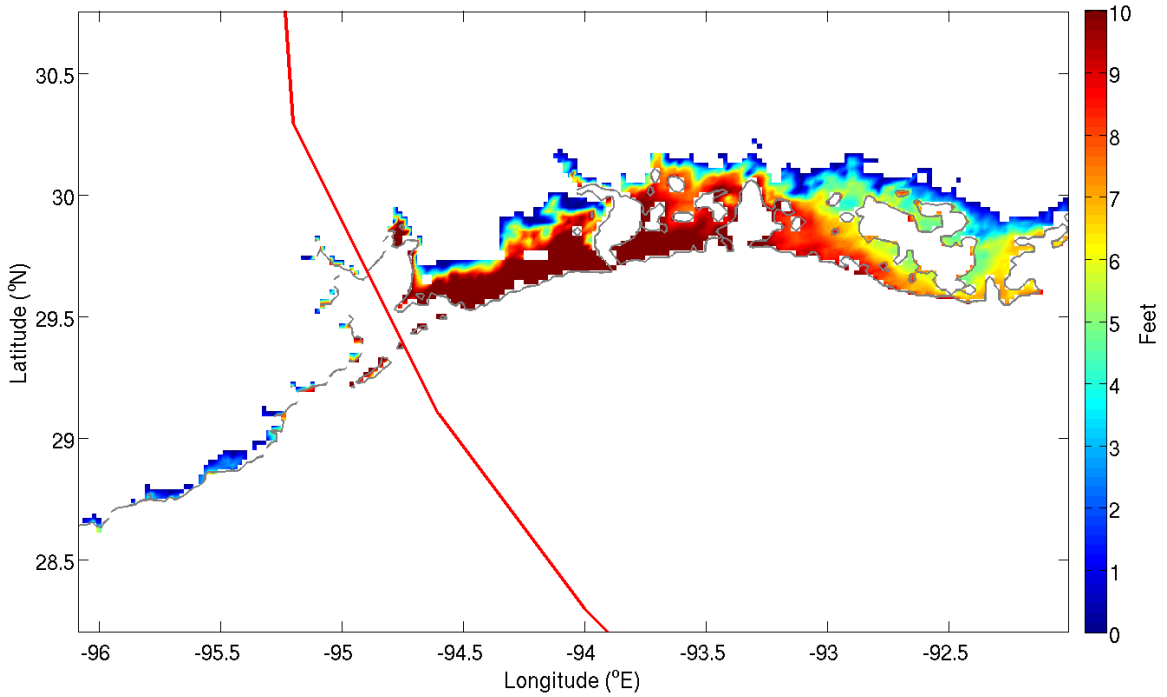

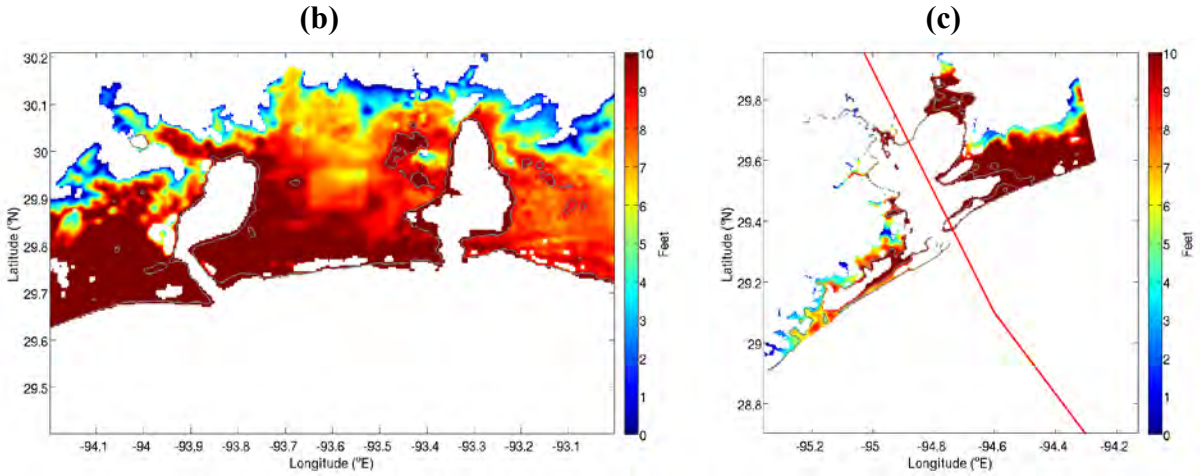

Figure 2.1-9: Simulated envelope of high water for baseline simulations (inundation in feet).

The HWM comparison presented in Figure 2.1-10 along with the statistics in Table 2.1-9 show that the errors in the inundation are larger than those in the water levels at the observation stations. Likewise the magnitude of the inundation is higher than the surge with maximum values around 4.60 m. Similar to the water levels the bias becomes more negative in each level of nesting. Overall there is a slight improvement in the results as the domain resolution becomes finer as demonstrated in the decrease in the MAPE with each nest.

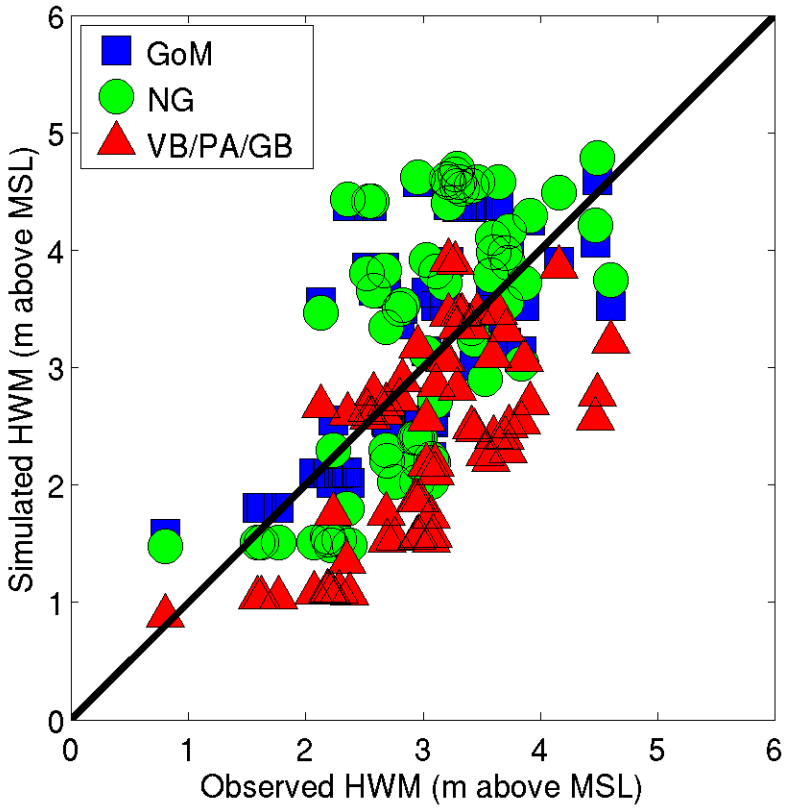

Figure 2.1-10: HWM comparison for baseline simulations of Hurricane Ike.

Table 2.1-9: Statistics from HWM analysis for Hurricane Ike.

	GoM	NG	VB/PA/GB
Corr r	0.51	0.67	0.68
Bias (m)	0.05	-0.08	-0.22
RMSE (m)	0.53	0.42	0.42
Scatter Index	17.10	14.27	14.85
MAPE	16.79	16.05	15.39

Overall the baseline simulation results show that CSIPS is capable of producing water level results with high accuracy in the baseline simulations. The extent of the inundation closely matches the best estimates, the hydrographs produced by the model show that the peak and timing of the peak is modeled well in comparison with the observations. The HWM analysis shows that there is improvement in the inundation results in each layer of nesting. Ideally, given the widely changing nature of the topography, the domain would feature resolution below 100 m to produce inundation estimates. However the 0.004° domain appears adequate to get estimates near 15% error.

2.1.5 Wave Comparison

In addition to water level results, CSIPS provides estimates of the wave height, period, and direction among other things. By dynamically coupling the wave and hydrodynamic simulations the influence of the waves on water levels is passed to the hydrodynamic model for use in water level calculations. The wave forcing on the water column is computed based on the method of Dingemans et al. (1987) where it is shown that the wave-induced currents are driven by the divergence-free part of the wave force and the setup is driven by the rotation-free part of the wave force. This is a much more stable and accurate method compared to using radiation stress method, where low resolutions in computational grids would significantly impact the calculation of the gradients and would lead to erroneous results. The changes in water surface levels is passed to the wave model allowing calculation of waves in areas that would not normally be flooded in a static simulation.

The wave simulation is much more computationally expensive than the hydrodynamic simulation. To save some of this cost the waves are run on grids with half the resolution of the hydrodynamic grid. The wave height, period and direction results of the GoM baseline simulation are shown in Figure 2.1-11 and the statistics for the wave heights in Table 2.1-10 and wave periods in Table 2.1-11. Overall the agreement between the simulated and observed wave heights and periods is very good as indicated in the tables (direction was disregarded since many of the buoys do not have data; however a qualitative analysis of the plots shows very strong agreement). The significant wave height biases, absolute errors and root mean square errors are all less than 1 meter. Considering wave heights peaked at over 9 meters at buoy 42001, these low statistics indicate positive simulation results. In regards to the wave period the simulation results show biases generally less than 1 second, absolute errors under 2 seconds and root mean square errors mainly under 2 seconds as well with a few stations around 2.6s. The observed periods range up to 16.67 seconds showing the large swells produced by Ike. Both the wave height and

period statistics show low scatter index percent and high RMSE skill scores. Overall the wave results from the baseline simulation compare well with the observations.

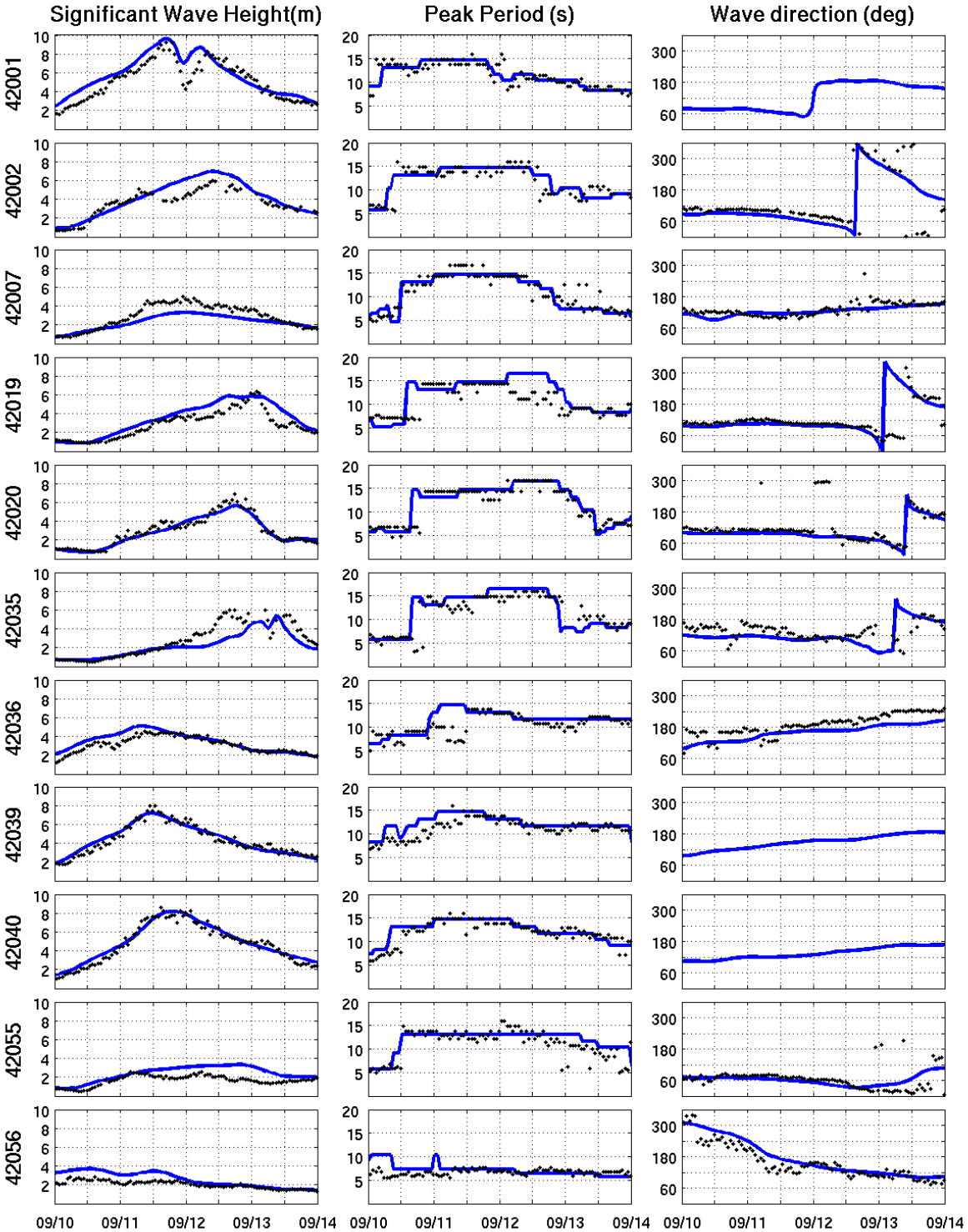

Figure 2.1-11: Wave comparison between Baseline GoM simulation and NDBC CMAN stations. Buoys 42001, 42039 and 42040 did not report wave directions.

Table 2.1-10: Statistical comparison between observed and simulated wave height at NDBC CMAN stations for baseline simulation. All heights in m.

Buoy ID	Mean Cond		Bias	Abs. Err	RMS Err	Scat Indx	Linear Regression Estimators				RMSE -SS	No. Obs
	Obs	Sim					Corr (r)	Symm r	Slope (a)	Interc (b)		
42001	5.14	5.76	0.61	0.87	0.87	15.18	0.70	1.09	0.91	1.08	0.88	96
42002	3.59	4.04	0.45	0.73	0.81	20.10	0.64	1.14	1.20	-0.26	0.87	74
42007	2.90	2.29	-0.61	0.69	0.60	26.29	0.71	0.75	0.55	0.70	0.79	96
42019	2.85	3.45	0.60	0.67	0.58	16.83	0.71	1.19	1.10	0.33	0.79	94
42020	2.98	2.82	-0.16	0.34	0.42	14.81	0.68	0.93	0.89	0.16	0.95	95
42035	2.64	2.04	-0.60	0.76	0.93	45.56	0.70	0.71	0.56	0.57	0.77	88
42036	3.12	3.43	0.31	0.40	0.45	13.04	0.73	1.09	1.02	0.26	0.90	96
42039	4.38	4.43	0.05	0.35	0.42	9.55	0.70	1.00	0.91	0.45	0.99	96
42040	4.76	4.92	0.16	0.40	0.44	9.02	0.73	1.01	0.91	0.59	0.97	96
42055	1.69	2.39	0.71	0.71	0.49	20.42	0.53	1.39	1.12	0.51	0.58	95
42056	2.04	2.56	0.52	0.52	0.45	17.40	0.76	1.28	1.88	-1.28	0.75	96

Table 2.1-11: Statistical comparison between observed and simulated wave period at NCBD CMAN stations for baseline simulation. All periods in s.

Buoy ID	Mean Cond		Bias	Abs. Err	RMS Err	Scat Indx	Linear Regression Estimators				RMSE -SS	No. Obs
	Obs	Sim					Corr (r)	Symm r	Slope (a)	Interc (b)		
42001	11.65	11.60	-0.05	1.02	1.44	12.44	0.71	0.99	0.79	2.44	1.00	96
42002	11.84	12.01	0.17	1.40	1.93	16.04	0.65	1.00	0.74	3.20	0.99	77
42007	11.12	10.88	-0.24	1.17	1.59	14.59	0.81	0.97	0.91	0.79	0.98	96
42019	10.64	11.78	1.14	2.01	2.62	22.23	0.71	1.10	0.94	1.81	0.89	94
42020	11.54	11.91	0.36	1.17	1.83	15.41	0.75	1.02	0.92	1.33	0.97	95
42035	11.42	11.94	0.52	1.61	2.63	22.00	0.68	1.03	0.85	2.27	0.95	88
42036	10.45	11.37	0.92	1.53	2.28	20.05	0.34	1.06	0.47	6.48	0.91	96
42039	11.22	12.20	0.98	1.23	1.31	10.77	0.49	1.07	0.62	5.28	0.91	96
42040	12.00	12.36	0.36	1.00	1.44	11.63	0.54	1.02	0.69	4.09	0.97	96
42055	11.00	11.83	0.83	1.48	1.94	16.38	0.51	1.04	0.55	5.75	0.92	95
42056	6.65	7.14	0.49	1.01	1.40	19.56	-0.15	1.06	-0.40	9.77	0.93	96

2.1.6 Sensitivity Studies

To assess the sensitivity of the system to a variety of inputs a number of tests were conducted. Specifically the importance of the bathymetry, waves, bottom roughness and wind field were examined. To conduct the sensitivity studies only the component being considered was changed with all other parameters being kept the same as the baseline simulation. Due to the large number of simulations and observations available for comparison, only the highest resolution results

(VB/PA/GB domains) will be discussed. These results will be discussed in terms of accuracy in predicting the peak water level at the seven NOS stations as was done in Figure 2.1-7 and Table 2.1-6 with any other interesting features of the wave, wind, inundation, or water levels results pointed out as needed.

2.1.7 Bathymetry

The baseline simulations feature a bathymetry dataset comprised mainly of high resolution data composited by the SURA Inundation Testbed for the Gulf of Mexico. Unfortunately this data is not available worldwide. More than likely the only available datasets will be the GEBCO combined bathymetry and topography dataset and the SRTM topography dataset. There are some significant differences between the datasets as shown in Figure 2.1-12 which depicts the percent change between the baseline dataset and the GEBCO or GEBCO+SRTM datasets. From the figure, the largest changes are in the coastal zone which is of utmost importance in the modeling of storm surge and inundation. Much of the topography shows a positive percent change indicating the new datasets feature higher topography. Much of the nearshore region shows cool shades indicating that the new datasets are shallower in this region than the baseline. These changes in the elevation dataset are evident in Figure 2.1-13 which shows that the Armeda Pass and Eagle Point stations never get inundated and are placed on land cells, not water cells in the GEBCO+SRTM data. Additionally Calcasieu Pass and Sabine Pass North stations are not inundated by the tides, only by the combination of the tides and surge. Due to this, these stations do not compare nearly as well as the results from the baseline simulations. The remaining stations (Galveston North Jetty, Galveston Pleasure Pier, and USCG Freeport) do compare well with the observations. Figure 2.1-14 shows the simulated peak water level versus observations and Table 2.1-12 shows the statistics for the plot. Although the MAPE is around 20 for each

elevation dataset, this is not the most accurate measure since two of the stations are set at an elevation just above the peak water level elevation and never actually get flooded.

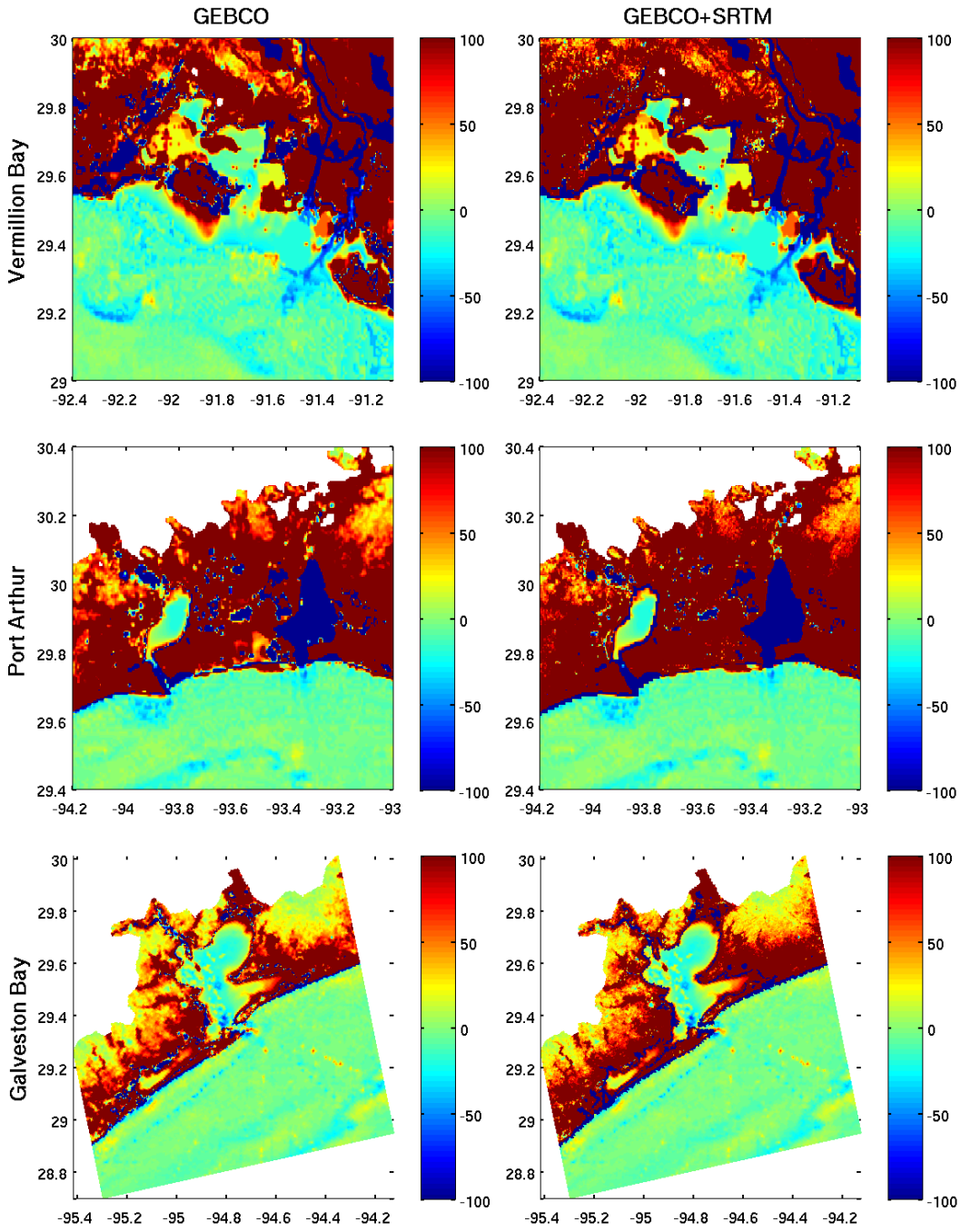

Figure 2.1-12: Percent change in the elevation between the Baseline simulation and GEBCO only (left panel)and GEBCO and SRTM (right panel) for the innermost nests.

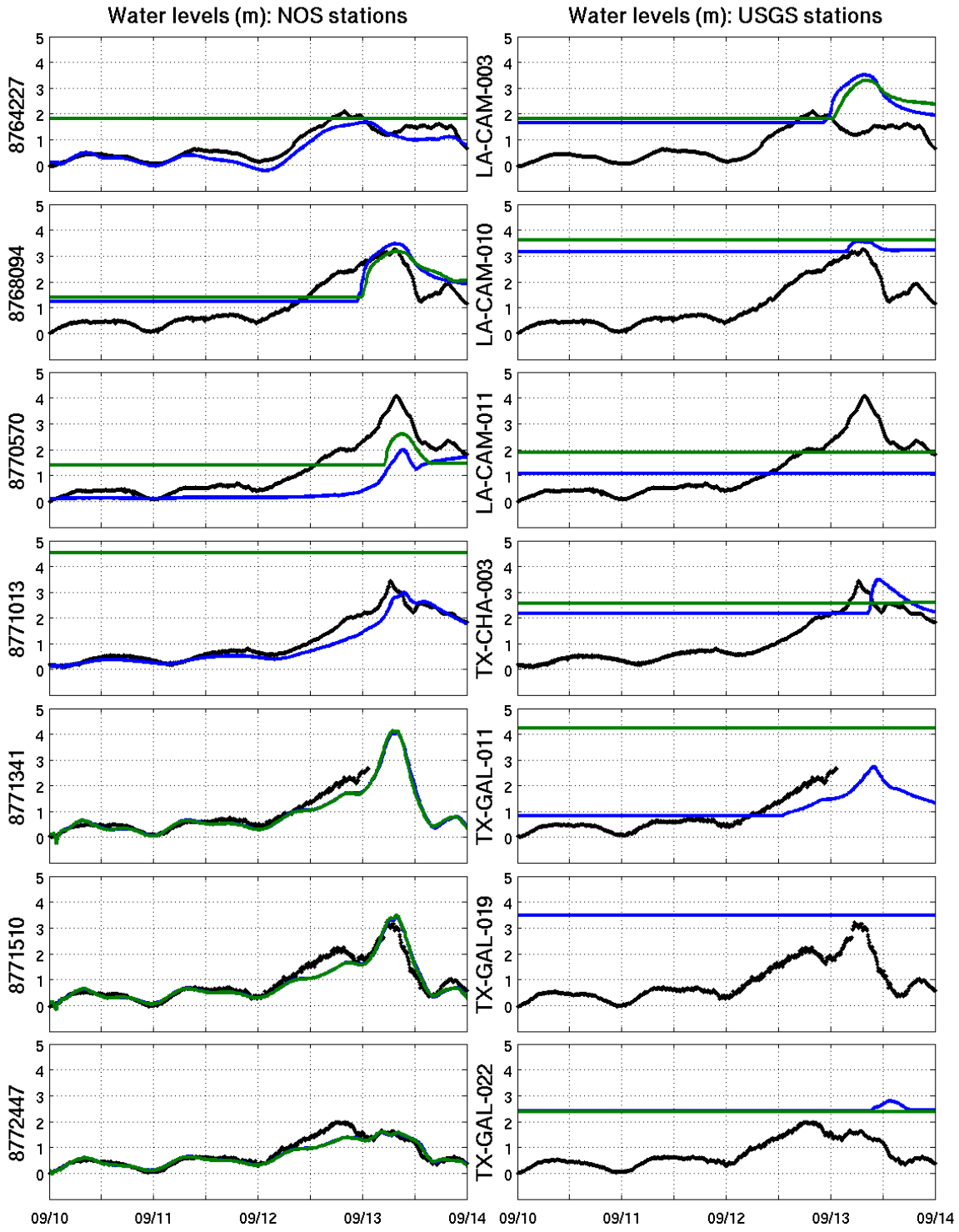

Figure 2.1-13: Hydrographs for 7 NOS Stations and 7 USGS stations for different elevation datasets in the VB/PA/GB domains, with data in black, GEBCO only in blue and GEBCO+SRTM in green

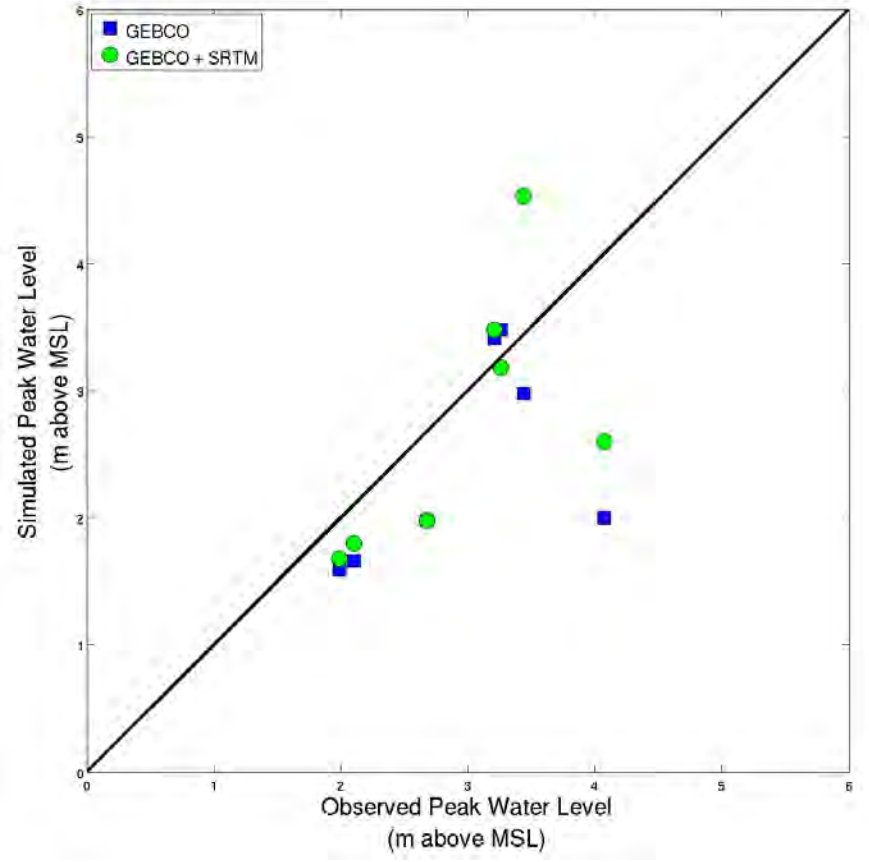

Figure 2.1-14: Simulated versus observed peak water levels at the 7 NOS stations for high resolution simulations with elevation dataset from GEBCO only and GEBCO + SRTM.

Table 2.1-12: Statistics for the peak water level at the NOS stations for the baseline VB/PA/GB domains and runs with GEBCO bathymetry/topography and GEBCO + SRTM bathymetry and topography in same domains.

	GEBCO	GEBCO + SRTM
Corr r	0.28	0.43
Bias (m)	-0.52	-0.21
RMSE (m)	0.49	0.62
Scatter Index	20.22	22.67
MAPE	20.63	19.24

These simulations highlight that high quality bathymetry and topography data is needed to accurately simulate the surge and inundation. Forecasters must check the elevation of their output locations and make sure that the model elevation is what it is expected to be. If this is not the case, the station can be moved to adjacent cells that more accurately represent what the expected conditions are.

2.1.8 Waves

The computation of the wave field is a very time consuming process. To evaluate whether it is a necessary process a series of simulations without waves were run and compared to those with waves. Figure 2.1-15 shows the hydrograph comparison for the baseline simulation with waves

and the sensitivity study simulation without waves. Figure 2.1-16 and Table 2.1-13 show the peak water level comparison and the statistics. From the figures it is obvious that the wave coupling is essential for reducing the error in the simulations. Without the coupling there is a negative bias of over one meter which is about 80 cm greater than the bias in the baseline runs. The hydrographs show the same trends in the baseline and the simulation without waves, suggesting that the wave coupling does not influence the timing of the surge, only the magnitude.

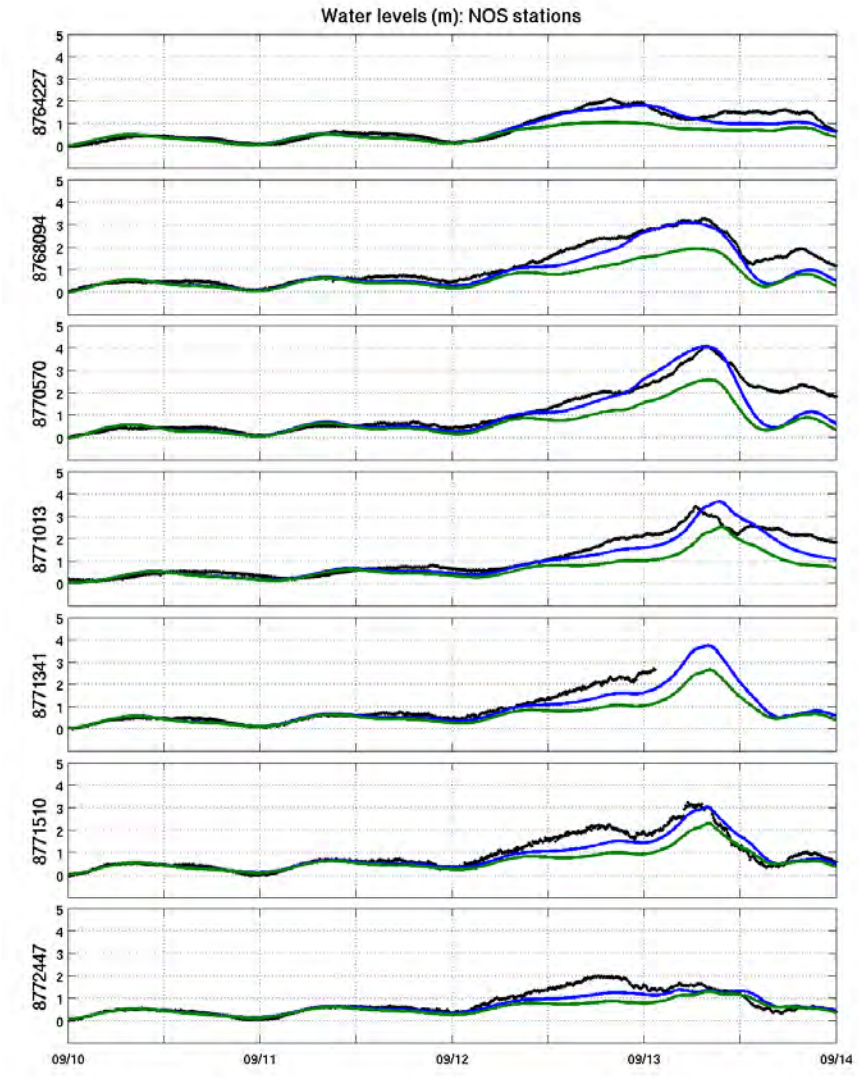

Figure 2.1-15: Hydrograph comparison between data (black), simulations with waves (blue lines) and simulations without waves (green lines) in the VB/PA/GB domains

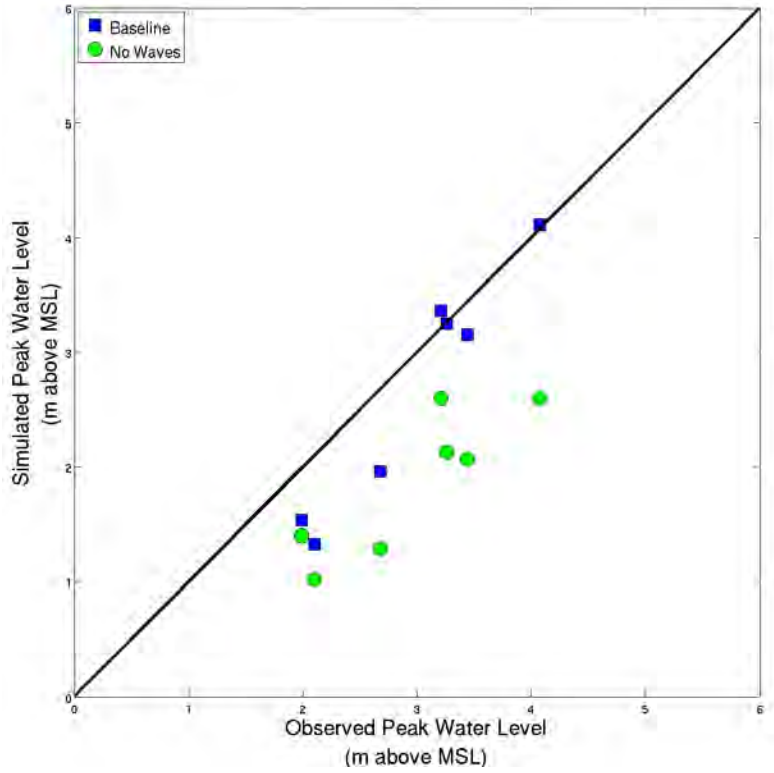

Figure 2.1-16: Simulated versus observed peak water levels at the 7 NOS stations for high resolution simulations of the baseline runs and runs with no waves.

Table 2.1-13: Statistics for the peak water level at the NOS stations for the baseline VB/PA/GB domains and runs with no waves in same domains.

	Baseline	No Waves
Corr r	0.95	0.76
Bias (m)	-0.29	-1.09
RMSE (m)	0.21	0.44
Scatter Index	7.87	23.39
MAPE	14.36	37.51

2.1.9 Bottom Roughness

The frictional effects of the bottom are depicted using the Manning formulation. Categorical descriptions of Manning's N coefficients exist for various land use classes. Based on this information a spatially varying Manning's N file can be used in CSIPS. However the development of this file can be time consuming and the land use data, which are necessary for its development, may not be available worldwide. With that in mind three simulations were conducted with a constant Manning's N value (0.02, 0.025, and 0.03 $s/m^{1/3}$). These cover the values that are commonly used in storm surge studies for open water. The value of 0.02 $s/m^{1/3}$ was used in the spatially varying case to represent the offshore areas. Once over land the roughness value increases based on the land type. Typical values for land range from 0.05-0.1 $s/m^{1/3}$, except for high intensity developed areas where the value is 0.15 $s/m^{1/3}$ (Mattocks and

Forbes, 2008). A fourth simulation with a constant Manning's N value of 0.02 s/m$^{1/3}$ for open water and 0.075 s/m$^{1/3}$ for land was conducted.

Table 2.1-14 shows the statistics for the various values and Figure 2.1-17 show the plot of the peak water level for three cases. Since these stations are located in the nearshore regions where the influence of the increased roughness of the land is not as important, the constant value of 0.02 s/m$^{1/3}$ performs very well. The higher values show a larger decrease in the peak water levels and increasingly poor results with increasing Manning's N values. While that spatially varying Manning's N coefficient does not appear to be essential for accurate prediction of the water levels at the NOS stations, Table 2.1-15 shows the statistics for the HWM comparison. The HWMs are much more sensitive to the bottom roughness since these are locations on land which are initially dry and become flooded during the course of the simulation. With the constant Manning's N value the differences in the land type are not accounted for. The land surface is going to be rougher than the water surface, so the constant value of 0.02 is shown to be too low with a positive bias. Jumping to a constant value of 0.025 shows a negative bias of 0.33 m, which is slightly larger than the baseline simulation. With a higher constant value of 0.03 the bias increases more in the negative direction to -0.65. Along with the changes in the bias, the MAPE is also much higher for all cases than the baseline simulation. Given these results it is concluded that the water level results in the coastal region show very little effect from the spatially varying Manning's N, but the inundation results are very sensitive to this parameter.

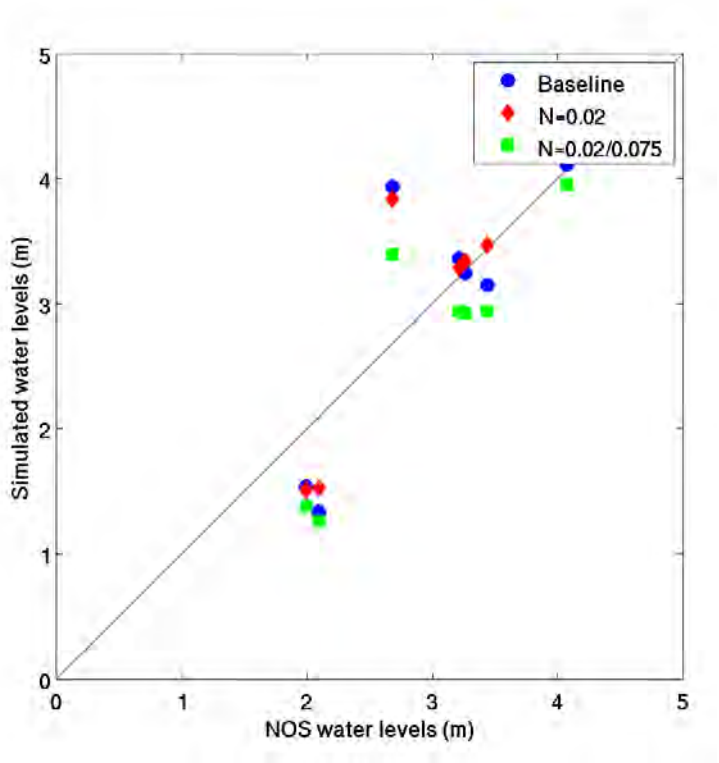

Figure 2.1-17: Simulated versus observed peak water levels at the 7 NOS stations for high resolution simulations of the baseline runs and runs with constant Manning's N coefficients.

Table 2.1-14: Statistics for the peak water level at the NOS stations for the baseline VB/PA/GB

domains and runs with constant Manning's N coefficient of 0.02, 0.025, and 0.03 in same domains.

	Baseline	Manning's N 0.02	Manning's N 0.025	Manning's N 0.03
Corr r	0.95	0.97	0.93	0.89
Bias (m)	-0.29	-0.16	-0.51	-0.74
RMSE (m)	0.21	0.10	0.25	0.30
Scatter Index	7.87	3.65	10.16	13.32
MAPE	14.36	13.62	21.25	28.79

Table 2.1-15: Statistics for the HWM comparison for the baseline VB/PA/GB domains and runs with constant Manning's N coefficient of 0.02, 0.025, and 0.03 in same domains.

	Baseline	Manning's N 0.02	Manning's N 0.025	Manning's N 0.03
Corr r	0.68	0.37	0.42	0.42
Bias (m)	-0.22	0.16	-0.33	-0.65
RMSE (m)	0.42	0.57	0.55	0.55
Scatter Index	14.85	17.89	20.31	23.27
MAPE	15.39	26.25	24.40	25.34

2.1.10 Forecast Wind

The baseline simulation utilizes the best available hindcast winds and pressure fields. In a forecast environment, these winds are not available so an analytic wind model must be used to generate a snapshot of the hurricane wind field based on the forecast information. CSIPS uses the analytic model of Condon and Veeramony (2014) to generate these snapshots on the Delft3D spiderweb grid. This model uses all available forecast information and multivariate interpolation to produce the hurricane wind field. This includes the radial extent of the 64, 50, and 34 knot winds along with the central pressure deficit, maximum wind speed, ambient pressure, radius to maximum winds, radius of the outermost closed isobar, and eye diameter when available. When the radial extent of the winds is not available, the Holland (1980) model is used to fill in. The spiderweb grid provides a moving snapshot of the hurricane wind field. The main advantage is that the file can be read in quickly and the wind field interpolated throughout the computational domain. This is a much quicker process than reading in the entire wind field from the computational mesh or another equidistant grid. Perhaps the largest drawback to using an analytic wind model is that it is designed to accurately represent the hurricane wind field but does not produce the larger scale atmospheric conditions. This results in no wind forcing outside of the immediate hurricane vortex, which can be problematic if large scale atmospheric conditions prior to the storm are anything greater than benign.

The CSIPS system is designed to provide forecasts starting 48 hours prior to landfall and continuing until landfall. Ike made landfall on September 13, around 0700 UTC. Table 2.1-16 shows the forecast times, locations, and intensity of Ike at the time of forecast. The analytic model is used to develop wind fields starting with the 40th forecast of Hurricane Ike (F040). This forecast was issued on September 11, 2008 at 0300 UTC. The storm was located about 500 km

west of Florida Keys in the Gulf of Mexico with sustained winds of 85 knots (44 m/s) and a minimum central pressure of 944 mb. Following this entry the forecasts are issued every 6 hours up until advisory 048 which was the last forecast prior to landfall (issued September 13, 2008 at 0300 UTC) with Ike located less than 100 km from the Texas Coast.

Table 2.1-16: Forecast times and storm position and intensity at time of forecast.

Forecast	Date (2008) / Time (UTC)	Storm Latitude	Storm Longitude	Max. Wind Speed knots (m/s)
040	Sept. 11 / 0300	24.9 N	-86.7 E	85 (44)
041	Sept. 11 / 0900	25.2 N	-86.7 E	85 (44)
042	Sept. 11 / 1500	25.5 N	-88.4 E	85 (44)
043	Sept. 11 / 2100	26.0 N	-89.4 E	85 (44)
044	Sept. 12 / 0300	26.3 N	-90.4 E	85 (44)
045	Sept. 12 / 0900	26.7 N	-91.6 E	90 (46)
046	Sept. 12 / 1500	27.2 N	-92.6 E	90 (46)
047	Sept. 12 / 2100	27.7 N	-93.5 E	90 (46)
048	Sept. 13 / 0300	28.6 N	-94.4 E	95 (49)

In addition to testing the sensitivity of the results to using the analytic forecast wind model, and to different forecasts, the variation in the track is also considered. Figure 2.1-18 shows the forecast track for each advisory along with a track along the left extent of the National Hurricane Center's (NHC) forecast cone (http://www.nhc.noaa.gov/aboutcone.shtml) and a track along the right extent of the cone. One thing of note throughout the forecast period is that the landfall location does not vary much. It remains within the bounds of the forecast cone for the first forecast (F040) and subsequent forecasts feature little variation. In terms of intensity the storm maintained intensity at 44 m/s (85 knots) for the first day, then increased to 46 m/s (90 knots) and 49 m/s (95 knots) just prior to landfall. Ike did not intensify as much as was initially forecast as is evident from Figure 2.1-19. The initial forecasts had Ike as a Category 3 storm prior to

landfall. In subsequent advisories the intensity was adjusted down somewhat, but in many cases the forecast was still slightly stronger than what actually occurred.

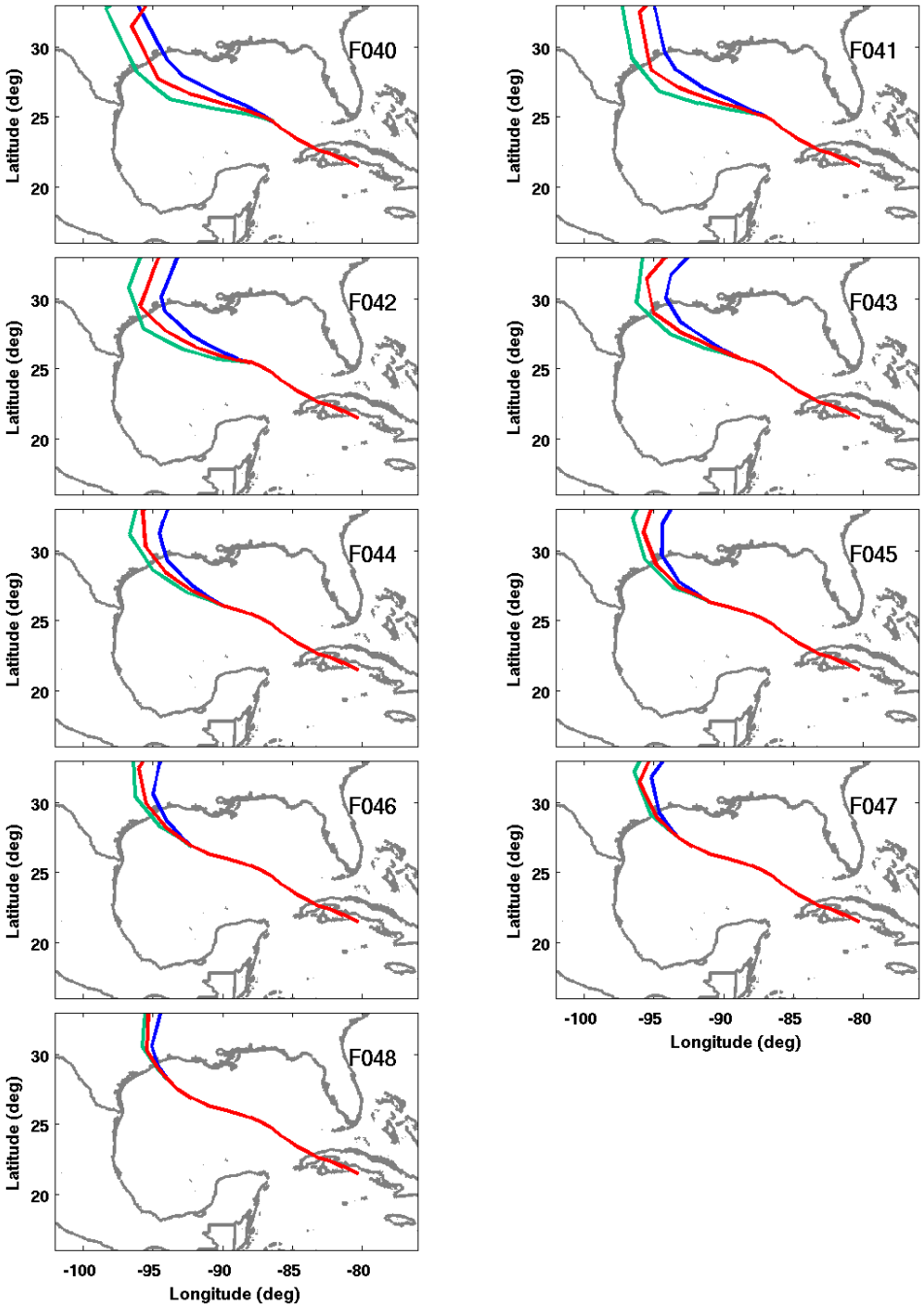

Figure 2.1-18: Forecast tracks for the 040 through 048 forecasts of Hurricane depicting the left side of the NHC cone (green line), right side (blue line) and center (red line).

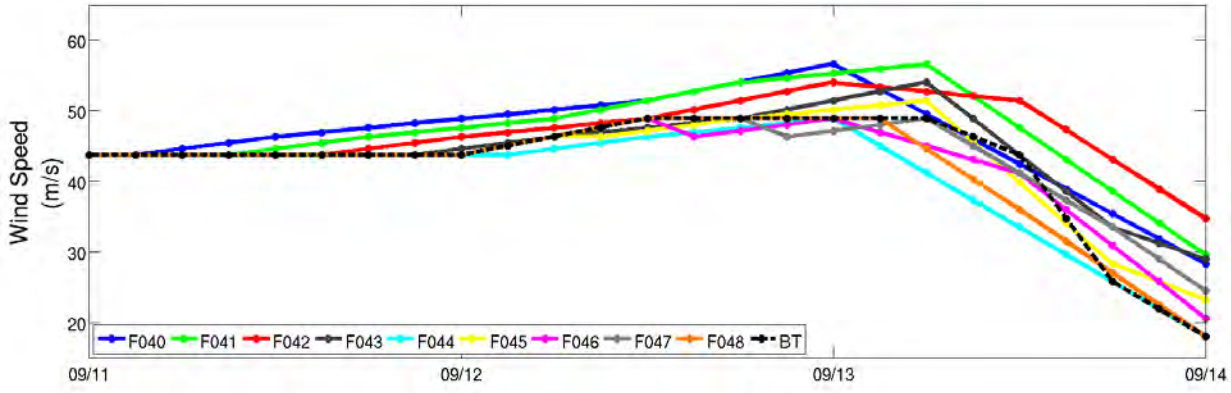

Figure 2.1-19: Changes in the forecast intensity of hurricane Ike for each forecast.

To begin the evaluation Figure 2.1-20 shows the peak water level at the 7 NOS stations for the forecast wind fields following the center of the hurricane cone. These are the actual forecasts as issued by the NHC. The statistics for the comparison are in Table 2.1-17 and show that the correlation increases as the storm approaches the coast. The initial forecasts had little correlation, and large RMSE and MAPE values. As the storm gets closer to the coast and the forecasts become more accurate, the correlation increases and the RMSE and MAPE decrease. The results from the simulations of the final four forecasts show much greater improvement over the first five. Table 2.1-18 and Figure 2.1-21 show the peak water statistics and plots for the winds produced using the best track file. Although the correlation is slightly lower, the rest of the metrics compare very well to the baseline statistics and show a MAPE of just over 10% which is actually a little lower than the baseline. The bias has shifted from about 0.3 m negative to about 0.2 m positive. This slight overestimate is likely due to the slightly stronger wind fields produced with the analytic wind model as compared to the re-analysis winds.

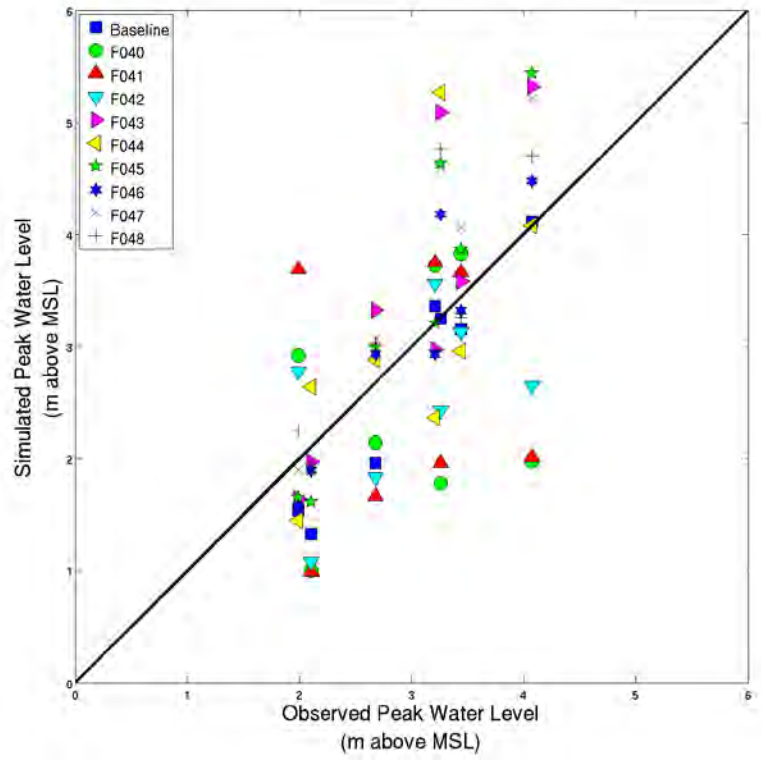

Figure 2.1-20: Peak water level at 7 NOS stations for center forecast runs.

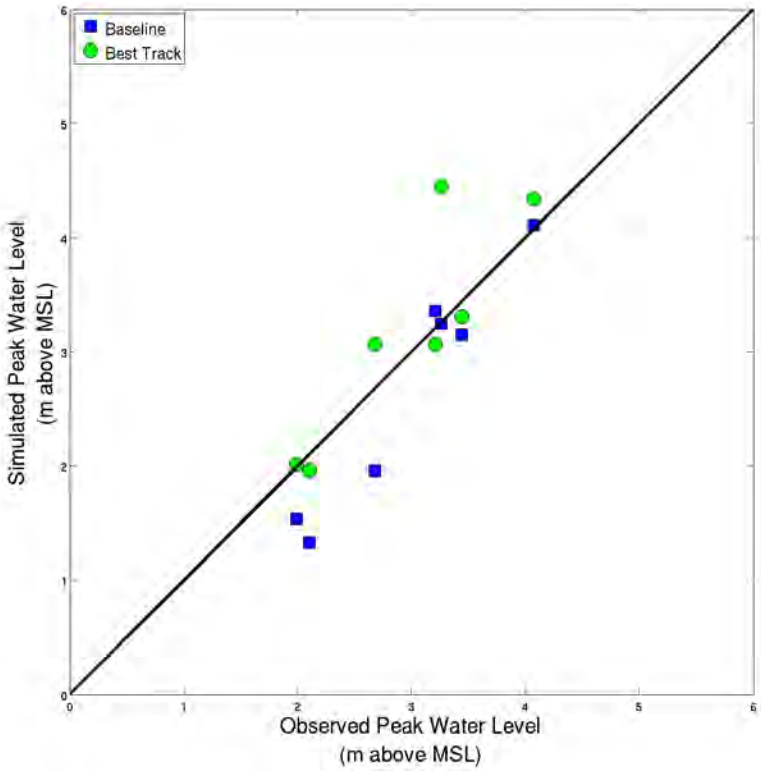

Figure 2.1-21: Peak water level at 7 NOS stations for the baseline simulation and the analytic winds from the best track.

Table 2.1-17: Statistics for the peak water level at the NOS stations for the baseline VB/PA/GB domains and runs with analytic wind model and different forecasts.

	Baseline	F040	F041	F042	F043	F044	F045	F046	F047	F048
Corr r	0.95	0.06	0.01	0.25	0.77	0.41	0.91	0.86	0.93	0.71
Bias (m)	-0.29	-0.45	-0.43	-0.47	0.45	0.13	0.38	0.08	0.48	0.31
RMSE (m)	0.21	0.88	0.91	0.84	0.44	0.71	0.27	0.34	0.22	0.49
Scatter Index	7.87	35.54	35.87	33.69	12.98	22.92	8.13	11.23	6.52	14.96
MAPE	14.36	34.75	41.44	28.55	20.92	23.19	20.02	12.85	17.39	15.23

Table 2.1-18: Statistics for the peak water level at the NOS stations for the baseline VB/PA/GB domains and runs with analytic wind model for best track.

	Baseline	Best Track
Corr r	0.95	0.78
Bias (m)	-0.29	0.21
RMSE (m)	0.21	0.43
Scatter Index	7.87	13.60
MAPE	14.36	10.50

With too many simulations and results to present in a plot, Table 2.1-19 shows the statistics for each forecast advisory run using the track along the center, left, and right of the forecast cone. For the later forecasts there is little variation since the cone is very narrow. However the earlier forecasts show much greater variation. A good indication of the variation is in the bias numbers which are much different for the left and right tracks compared with the center track. For example in forecast advisory 043 following the center of the cone produces a positive bias of 0.45 m, while a landfall along the left side of the cone produces a positive bias of 0.86 m. To contrast this landfall following the track along the right side of the cone produces a negative bias of 1.02 m. An examination of the tracks in Figure 2.1-18(d) shows that following the left side of the cone places the most intense winds right near the recording stations in Galveston Bay and along the Texas and Louisiana border. The track along the right extent of the forecast cone places the strongest winds to the east of the majority of the recording stations producing the large negative bias. The spread in the two tracks is less than 200 km, but the results are dramatically different showing that the system is very sensitive to the input track.

2.1.11 Conclusions

Validation of the CSIPS for hindcast simulations of Hurricane Ike along with sensitivity studies has been presented. The baseline simulations show very good agreement between the simulated and observed peak water levels at the NOAA tide gauges for all three domain resolutions. In fact the coarsest domain does a very good job in capturing the water level at these coastal stations. To

accurately predict the inundation, the higher resolution domains perform better. The wave results compare very well in the coarse domain as well.

In a forecast environment, many of the inputs that are used in the hindcast study will not be available. To determine the importance of these inputs, sensitivity studies examining the influence of the bathymetry, wave coupling, bottom roughness, wind field, and track were conducted. The overall conclusion is that the results are sensitive to each of the components. The bathymetry and topography datasets show a lot of variation from one set to the next. When the recording stations are properly placed, the variation was slight. However, many of the stations that should have been located in wet grid cells were not in the lower resolution elevation datasets. Adjacent cells were wet and the operator would have to adjust the station locations accordingly to get accurate results. The wave coupling was found to be essential to accurately capturing the peak of the storm surge. The bottom roughness had little influence on the coastal water levels, but did have a large influence on the inundation results. The spatially varying Manning's N coefficient used in the baseline simulation varied only over land. As a result the use of a constant Manning's N coefficient produced similar results in the nearshore water levels, but very different results in the inundation. For this test a constant value of 0.02 performed the best but that is likely subject to the land-use characteristics of the location. Like the other variables the results are sensitive to the forecast wind field. As the forecast evolves the results get better as expected. The later forecasts that more closely resemble the best track do a nice job of capturing the peak water levels. By adjusting the track of the storm left or right of the actual forecast, the simulated water levels can change dramatically illustrating how sensitive storm surge is to the hurricane track.

Table 2.1-19: Statistics for the peak water level at the NOS stations for the baseline VB/PA/GB domains and runs with analytic wind model for each forecast and the corresponding Center, Left, and Right track.

F040	Center	Left	Right	F041	Center	Left	Right
Corr r	0.06	0.05	0.27	Corr r	0.01	0.07	0.21
Bias (m)	-0.48	-1.17	-1.41	Bias (m)	-0.43	-1.11	-1.53
RMSE (m)	0.88	0.89	0.77	RMSE (m)	0.91	0.88	0.80
Scatter Index	35.54	49.44	49.36	Scatter Index	35.87	47.27	55.49
MAPE	34.75	46.73	49.64	MAPE	41.44	46.54	51.97
F042	Center	Left	Right	F043	Center	Left	Right
Corr r	0.25	0.02	0.29	Corr r	0.77	0.63	0.02
Bias (m)	-0.47	-0.91	-1.24	Bias (m)	0.45	0.86	-1.02
RMSE (m)	0.84	0.90	0.76	RMSE (m)	0.44	0.56	0.90
Scatter Index	33.69	43.88	43.97	Scatter Index	12.98	14.57	46.27
MAPE	28.55	39.91	42.37	MAPE	20.92	34.72	55.19
F044	Center	Left	Right	F045	Center	Left	Right

Corr r	0.41	0.75	0.00	Corr r	0.91	0.62	0.27
Bias (m)	0.13	0.77	-1.01	Bias (m)	0.38	0.388	-0.55
RMSE (m)	0.71	0.45	0.90	RMSE (m)	0.27	0.57	0.78
Scatter Index	22.92	12.08	45.90	Scatter Index	8.13	14.81	32.29
MAPE	23.19	24.09	47.39	MAPE	20.02	34.75	36.06
F046	Center	Left	Right	F047	Center	Left	Right
Corr r	0.86	0.79	0.39	Corr r	0.93	0.92	0.71
Bias (m)	0.08	0.55	-0.31	Bias (m)	0.48	0.63	0.28
RMSE (m)	0.34	0.42	0.71	RMSE (m)	0.22	0.26	0.49
Scatter Index	11.23	11.98	26.61	Scatter Index	6.52	7.16	15.14
MAPE	12.85	20.51	25.79	MAPE	17.39	21.91	20.28
F048	Center	Left	Right				
Corr r	0.71	0.70	0.68				
Bias (m)	0.31	0.34	0.24				
RMSE (m)	0.49	0.50	0.52				
Scatter Index	14.96	15.08	16.35				
MAPE	15.23	16.13	14.10				

2.2 Hurricane Irene

2.2.1 Model Domains

Similar to the validation done with Hurricane Ike, for Irene three series of domains were used (Figure 2.2-1). The large scale domain featured coarse resolution (0.1°) and covered most of the United States east coast (EC). This domain features 58,996 cells (196 x 301) and stretches from the northern Caribbean to northeast Canada including all of the US. Atlantic coast. Nested within the EC domain is a medium resolution nearshore domain covering the mid-atlantic (MA). This domain features 130,626 cells (246 x 531) with a 0.02° resolution. Within the MA domain are five high resolution (0.004°) coastal domains (b). These domains include some of the heavily influenced by the storm. They are the New York City domain (NY), the Delaware Bay (DB) domain, the Chesapeake Bay (CB) domain, the Outer Banks (OB) domain, and the Wilmington/Jacksonville (WJ) domain. These domains are all various sizes with the NY domain containing 68,541 cells (341 x 201), the DB domain containing 91,113 cells (251 x 363), the CB domain containing 321,074 cells (466 x 689), the OB domain has 253,011 cells (451 x 561) and the WJ domain features 135,751 cells (301 x 451). The simulation period in the EC domain begins on August 18, 2011 at 0000 UTC and runs for 12.75 days until 1800 on August 30. The MA domain simulations begin 4 days later on August 22 and run through the same period. The simulations in the high resolution domains begin 5.25 days after those in the EC domain and run through 1200 UTC on August 29. As was done in Ike, the water level along the open boundaries of the MA domain is forced by the simulated results in the EC domain and the water levels in the coastal domains are forced by the water level results in the MA domain. Due to the size and varying nature of the water level in the EC domain no initial water level was specified. However in the MA domain an initial water level of 0.07 m was used based on an average of seasonal sea level trends in the region. For the coastal domains the initial water level was taken as 0.06, 0.06, 0.072, 0.065, and 0.00 m for the NY, DB, CB, OB, and WJ domains respectively.

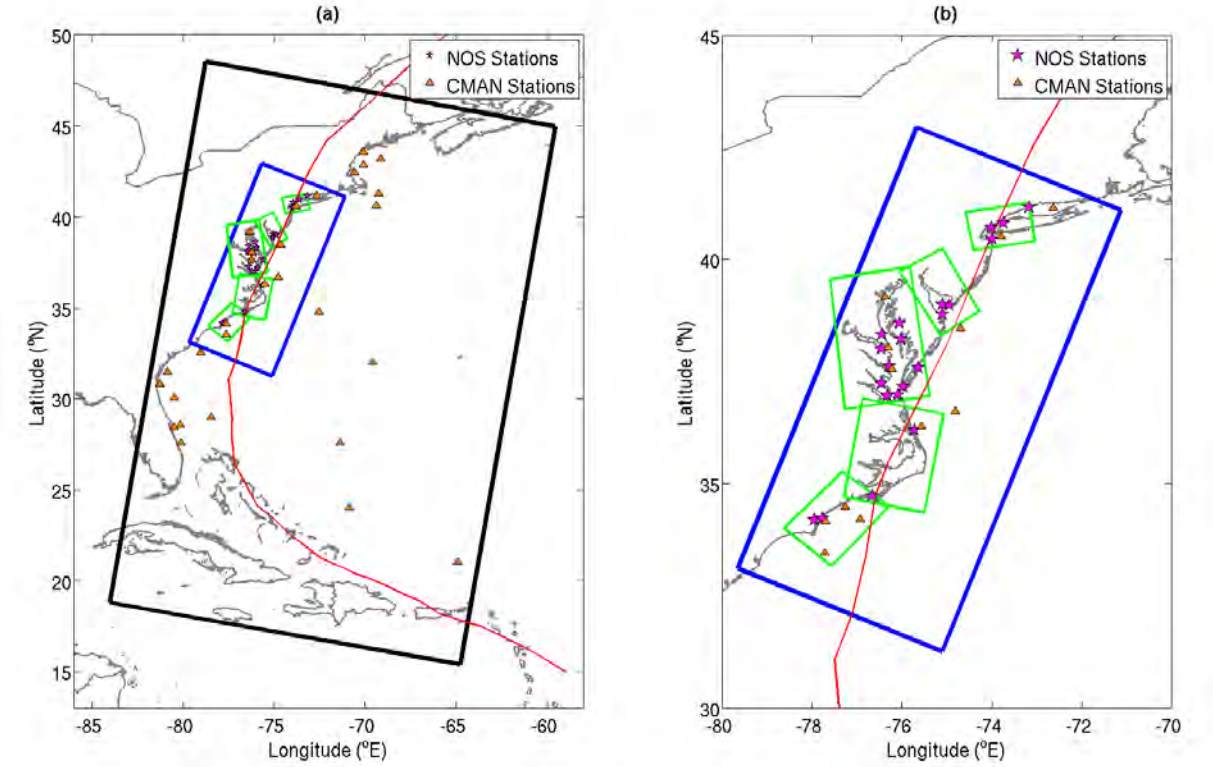

Figure 2.2-1: Domains used for Hurricane Irene studies. The black box outlines the 0.1° domain, the blue box the 0.02° domain, and the green boxes the three 0.004° domains in (a) and a close up of the MA and NY, DB, CB, OB, and WJ domains in (b).

To validate the system the model results are compared to the large collection of observational data detailed below. Although the EC and MA domains contain a larger selection of NOS stations, only those that are contained in all three resolutions of domains are included to facilitate comparisons across grid resolutions (see Table 2.2-1 and Figure 2.2-2). This means that twenty-one NOS stations listed in Table 2.2-1 are used. These vary from stations within the estuaries of the Chesapeake and Delaware Bays, to those along the open coast. As noted in Table 2.2-1 three of these stations recorded water levels but did not have corresponding meteorological observations. For the wave comparisons thirty buoys were available for comparison in the EC domain (Table 2.1-2). Eleven of these buoys were also within the MA domain, and eight of those were within a coastal domain. Six of these buoys did not record meteorological data along with wave data. To examine the atmospheric forcing a combination of offshore buoys and coastal stations with data available were used. The same 18 NOS stations listed in Table 2.2-1 and 24 buoys used for the wave comparison in Table 2.1-2 are used for the wind comparison. In addition, prior to landfall, the USGS deployed 198 stations, of which 92 stations fall within the high-resolution domains in our simulations. Table 2.2-3 lists the 92 USGS stations, with the station IDs and their locations.

Table 2.2-1: 21 NOS tide stations used in comparison of hydrographs for Hurricane Irene.

Station ID	Location	Latitude (°N)	Longitude (°E)	Domains
8467150	Bridgeport, CT	41.173	-73.182	EC, MA, NY
8516945	Kings Point, NY	40.810	-73.765	EC, MA, NY
8518750*	The Battery, NY	40.701	-74.014	EC, MA, NY
8531680	Sandy Hook, NJ	40.467	-74.009	EC, MA, NY
8536110	Cape May, NJ	38.968	-74.960	EC, MA, DB
8555889	Brandywine Shoal Light, DE	38.987	-75.113	EC, MA, DB
8557380	Lewes, DE	38.782	-75.120	EC, MA, DB
8571421	Bishops Head, MD	38.220	-76.038	EC, MA, CB
8571892	Cambridge, MD	38.573	-76.068	EC, MA, CB
8577330	Solomons Island, MD	38.317	-76.452	EC, MA, CB
8631044	Wachapreague, VA	37.607	-75.685	EC, MA, CB
8632200	Kiptopeke, VA	37.165	-75.988	EC, MA, CB
8635750	Lewisetta, VA	37.996	-76.464	EC, MA, CB
8636580	Windmill Point, VA	37.616	-76.290	EC, MA, CB
8637689	Yorktown, VA	37.227	-76.478	EC, MA, CB
8638610*	Sewells Point, VA	36.947	-76.330	EC, MA, CB
8638863	Chesapeake Bay Bridge Tunnel, VA	36.967	-76.113	EC, MA, CB
8651370	Duck Pier, NC	36.183	-75.747	EC, MA, OB
8656483	Beaufort, NC	34.720	-76.670	EC, MA, OB
8658120*	Wilmington, NC	34.227	-77.953	EC, MA, WJ
8658163	Wrightsville Beach, NC	34.213	-77.787	EC, MA, WJ

Indicates stations without wind data

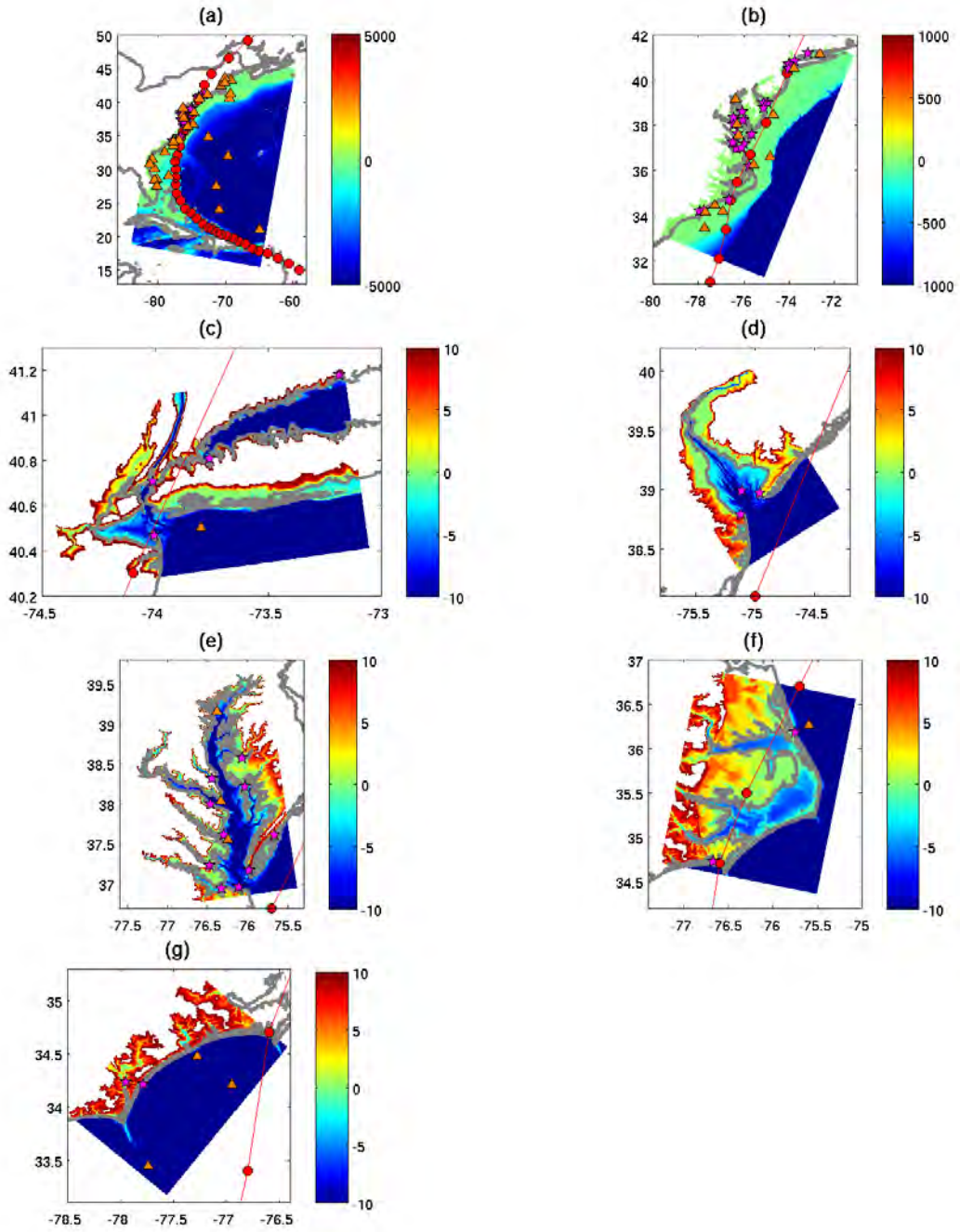

Figure 2.2-2: Bathymetry and topography (m, MSL) for the 7 domains used in the Irene validation studies (a) East Coast (EC) domain, (b) Mid-Atlantic (MA) domain, (c) New York (NY) domain, (d)Delaware Bay (DB) domain, (e) Chesapeake Bay (CB) domain, (f) Outer Banks (OB) domain, and (g) Wilmington/Jacksonville (WJ) domain. x-axis is longitude (deg), and y-axis is latitude (deg), with the triangle representing the locations of the CMAN stations and stars representing NOS stations.

Table 2.2-2: NDBC CMAN stations used in wave comparison for Hurricane Irene.

Station ID	Latitude (°N)	Longitude (°E)	Station ID	Latitude (°N)	Longitude (°E)
41001	34.561	-72.631	44007	43.531	-70.144
41004	32.501	-79.099	44008	40.502	-69.247
41008	31.400	-80.868	44009	38.461	-74.703
41009	28.523	-80.184	44013	42.346	-70.651
41010	28.906	-78.471	44014	36.611	-74.842
41012	30.042	-80.534	44018	42.126	-69.630
41013	33.436	-77.743	44039	41.138	-72.655
41036	34.207	-76.949	44042	38.033	-76.336
41043	21.061	-64.966	44043	39.152	-76.391
41046	23.838	-68.333	44058	37.552	-76.251
41047	27.469	-71.491	44060	41.263	-72.067
41048	31.950	-69.497	44065	40.369	-73.703
44005	43.204	-69.128			

Table 2.2-3: USGS stations used for water level comparisons for Hurricane Irene.

Station ID	Latitude (°N)	Longitude (°E)		Station ID	Latitude (°N)	Longitude (°E)
CT-FFD-001WL	40.9991	-73.65944		MD-QUA-001WL	38.9715	-76.24839
CT-FFD-002WL	40.99483	-73.65903		MD-SOM-030WL	38.20375	-75.69992
CT-FFD-003WL	41.09979	-73.41568		MD-SOM-031WL	37.97794	-75.863
CT-FFD-006WL	41.1231	-73.36998		MD-SOM-032WL	38.16997	-75.94308
NY-NAS-001WL	40.87791	-73.53057		MD-TAL-002WL	38.71978	-76.33258
NY-NAS-004WL	40.58275	-73.64068		MD-TAL-003WL	38.83164	-75.91442
NY-NAS-005WL	40.64733	-73.46234		MD-TAL-005WL	38.69381	-76.17406
NY-QUE-001WL	40.76229	-73.85828		MD-WIC-011WL	38.36308	-75.60711
NY-QUE-002WL	40.64533	-73.83638		MD-WOR-013WL	38.07642	-75.57061
NY-RIC-001WL	40.59388	-74.05984		VA-IOW-001WL	37.00536	-76.60017
NY-SUF-011WL	40.90048	-73.35304		VA-NFK-001WL	36.85881	-76.29864
NY-SUF-017WL	40.64316	-73.1575		VA-NOR-002WL	37.28789	-75.92556
NY-SUF-018WL	40.63473	-73.20216		VA-NOR-003WL	37.26492	-76.01628
NY-SUF-019WL	40.65932	-73.26486		VA-VAB-001WL	36.90683	-76.08825
NY-SUF-022WL	40.68523	-73.2799		VA-YOR-001WL	37.17833	-76.39694
DE-KEN-003WL	38.98944	-75.49431		NC-CAM-001WL	36.30053	-76.21797
DE-NEW-001WL	39.30928	-75.60947		NC-CHO-001WL	36.05587	-76.60942
DE-NEW-002WL	39.40531	-75.59861		NC-CRT-001WL	34.68598	-76.53169
DE-NEW-005WL	39.50494	-75.58025		NC-CRT-004WL	35.01903	-76.31474
DE-NEW-006WL	39.57708	-75.60206		NC-CRT-006WL	34.69668	-76.78122

DE-NEW-008WL	39.65197	-75.58756		NC-CRT-007WL	34.69715	-76.68161
DE-SUS-004WL	38.87769	-75.35964		NC-CRV-003WL	34.9381	-76.81044
DE-SUS-006WL	38.77697	-75.31247		NC-CRV-005WL	35.09922	-77.03958
DE-SUS-008WL	38.79022	-75.16364		NC-CUR-002WL	36.37357	-75.83351
DE-SUS-009WL	38.77564	-75.13825		NC-DAR-001WL	35.20791	-75.70284
DE-SUS-010WL	38.69453	-75.08419		NC-DAR-005WL	35.79618	-75.5495
DE-SUS-014WL	38.51367	-75.06253		NC-DAR-008WL	36.22331	-75.77248
DE-SUS-015WL	38.45489	-75.05814		NC-DAR-010WL	35.69831	-75.77044
DE-SUS-030WL	38.70269	-75.16183		NC-DAR-011WL	35.91217	-75.76828
DE-SUS-031WL	38.67178	-75.18594		NC-HYD-001WL	35.39345	-76.32847
DE-SUS-032WL	38.62542	-75.09992		NC-PER-001WL	36.193	-76.45458
DE-SUS-033WL	38.59164	-75.21197		NC-WAS-001WL	35.95884	-76.49151
DE-SUS-034WL	38.5945	-75.28919		NC-BRU-011WL	33.8937	-78.03347
DE-SUS-036WL	38.55647	-75.20306		NC-BRU-012WL	33.88649	-78.43587
DE-SUS-037WL	38.48369	-75.11911		NC-BRU-013WL	33.89244	-78.43788
MD-WOR-016WL	38.38775	-75.1035		NC-BRU-014WL	33.89514	-78.43939
MD-WOR-018WL	38.35664	-75.16053		NC-CRT-007WL	34.69715	-76.68161
MD-WOR-019WL	38.33881	-75.12989		NC-NHA-001WL	34.22772	-77.95404
MD-WOR-020WL	38.33456	-75.09836		NC-NHA-002WL	33.96136	-77.93973
MD-WOR-030WL	38.42411	-75.18769		NC-NHA-004WL	34.05685	-77.88097
NJ-ATL-002WL	39.44861	-74.72694		NC-NHA-005WL	34.18906	-77.81263
NJ-CUM-002WL	39.42917	-75.23694		NC-NHA-006WL	34.21418	-77.78834
MD-DOR-007WL	38.57392	-76.06733		NC-NHA-007WL	34.27499	-77.76071
MD-DOR-010WL	38.48339	-75.82292		NC-NHA-008WL	34.235	-77.77692
MD-DOR-033WL	38.30058	-76.00547		NC-ONS-002WL	34.50276	-77.39646
MD-DOR-034WL	38.46956	-76.29333		NC-PEN-003WL	34.36542	-77.62815

As was done with Ike, CSIPS will be compared to the Irene observation data to show the accuracy of the simulation results as well as the sensitivity of those results to different input parameters. Specifically the sensitivity of the results to the bathymetry and topography dataset, the inclusion of wave effects, the bottom roughness parameterization, and the forecast winds and track of the storm will be examined. These sensitivities will be analyzed across all three domain resolutions and compared to the observations as well as a best available or baseline simulation.

2.2.2 Baseline

The baseline simulations for Hurricane Irene consist of 3 sets of simulations; the large scale simulation in the EC domain, followed by the nearshore simulation in the MA domain, and finally the five high resolution simulations in the coastal domains. In all simulations the elevation dataset consisted primarily of bathymetry and topography from the NGDC Coastal Relief Model, SRTM, and GEBCO data (Figure 2.2-2). The baseline simulation was dynamically coupled to the wave module so that wave effects are accounted for. The wave simulations are much more computationally expensive than is the hydrodynamic component. With this in mind the wave grid mirrored the hydrodynamic grid but with half the resolution for all domains (0.2°,

0.04°, 0.008° for the EC, MA, and NY/DB/CB/OB/WJ domains respectively). The wave model was run in non-stationary mode with a 6 minute timestep and communicated with the hydrodynamic model every hour of simulation. Within the hydrodynamic model the bottom roughness was calculated using the Manning formulation. To determine the values for the spatially varying Manning's N coefficient land use data was obtained from NLCD and converted to a corresponding N value based on the tables in Mattocks and Forbes (2008). For offshore areas where land use data is non-existent, a constant value of 0.02 $s/m^{1/3}$ was used (Figure 2.2-3). All baseline simulations in all domains were performed with a 1 minute timestep. The open boundary conditions for the EC domain were specified in terms of astronomic components which were obtained from the TPXO 7.2 database. A total of 13 harmonic constituents were used along with a constant value (zero phase) to account for the initial water level conditions. The open boundaries were Riemann which simulates a weakly reflective boundary which allows outgoing waves to cross the boundary without being reflected back. The atmospheric forcing was obtained from the NOAA H*wind snapshots (Powell et al. 1998) blended with the National Center for Environmental Prediction (NCEP) North American Regional Reanalysis (NARR) wind fields (Messinger et al. 2006). The NARR winds provide the background upon which the high resolution H*wind snapshot was imbedded. A simple smoothing of the outer extent of the H*wind snapshot with the background wind field was performed to create a blended wind field for the north Atlantic to drive the simulations. Given the coarseness of the NARR winds (~0.3°) and the fact that the core of the hurricane wind field remained offshore for most of the storm, no directional land-masking was performed. The air-sea drag formulation of Zijlema et al. (2012) was found to perform the best and was used in this and all other Irene simulations.

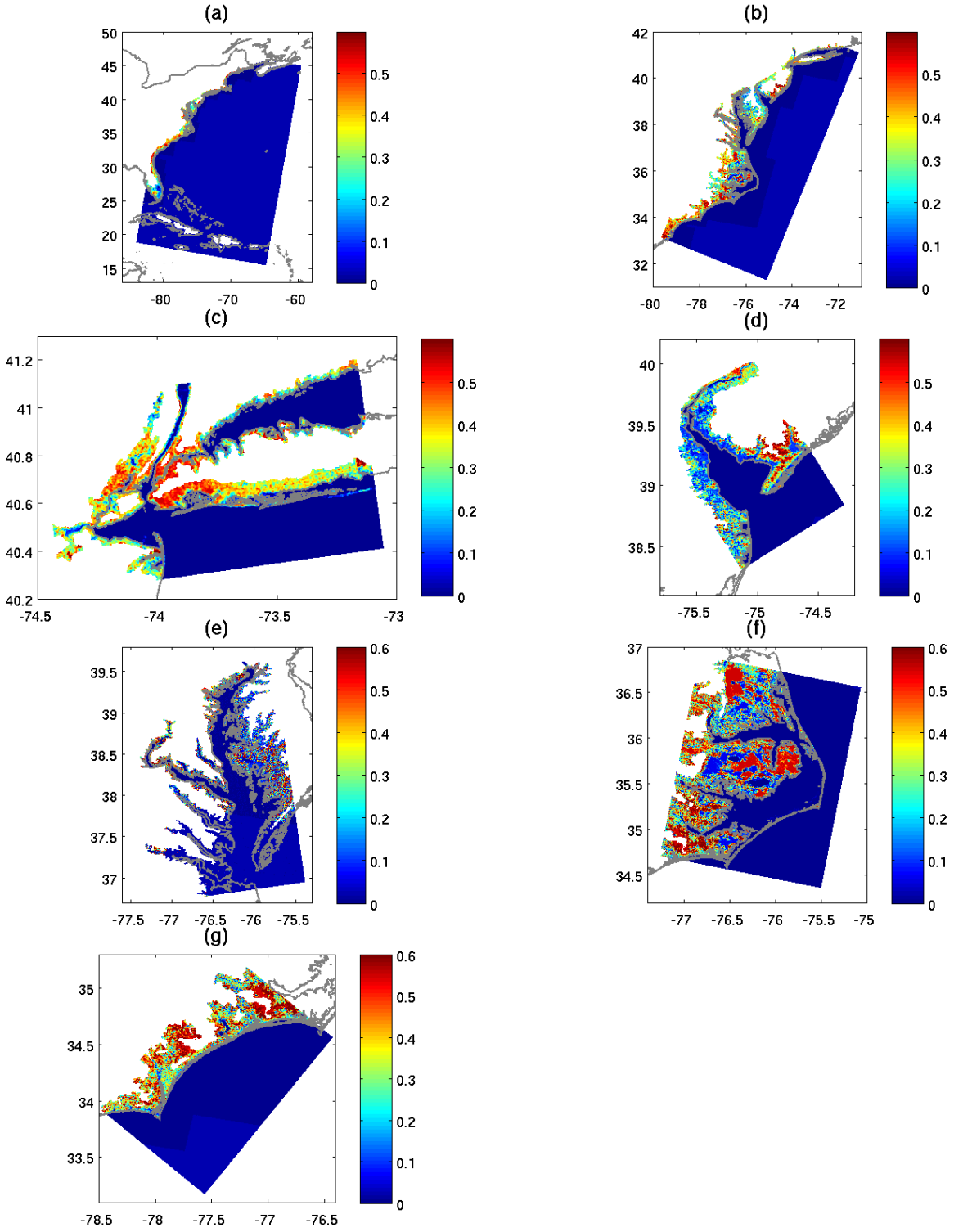

Figure 2.2-3: Variable Manning's N for the 5 domains used in the Irene validation studies (a) EC domain, (b) MA domain, (c) NY domain, (d) DB domain, (e) CB domain, (f) OB domain, and (g) WJ domain.

2.2.3 Wind-Field Comparison

To validate the modeling system, proper forcing is necessary. In storm surge and inundation modeling the primary forcing comes from the hurricane wind field. The blended H*wind/ NARR winds used in the baseline simulation represent the best available winds for re-analysis of Hurricane Irene. Figure 2.2-4 shows the comparison between the modeled wind speed and direction and the observed wind speed and direction at the 24 NDBC buoys listed in Table 2.1-2 with available meteorological data. As with Ike, the simulated wind at these offshore buoys is expected to compare well with the observed data since it is far from the influence of land. The figure demonstrates that the simulated and observed winds and speed compare well throughout the North Atlantic. In general the wind direction matches very closely to the observations and wind speed is good although it does over and under predict at a number of buoys. To get a better quantitative assessment of the agreement between the simulated and modeled winds, we employ the same metrics used for Ike (see section 2.1.3 for details).

As seen qualitatively in Figure 2.2-4, Table 2.2-4 shows that there is very good agreement between the observed and simulated winds at most of the locations. The main outlier is 41001 where the maximum observed wind speed is close to 20 m/s whereas the analysis wind speed has a maximum close to 35 m/s. Smaller, but still significant errors in the maximum wind speed are seen at Buoys 41013 and 41036. However, the bias over the time period considered is under 4 m/s at all buoys and varies from station to station indicating that there is no consistent over or underestimation throughout the domain. For all but four stations, the correlation is greater than 0.75. But for 41001, the absolute and RMS errors are under 3 m/s, and the scatter index is low for most locations. Given that the background winds are very coarse, the agreement between the observations and simulated winds is good. The buoy offshore of Cape Hatteras (41001) likely performs the worst, due to the fact that this buoy is right in line with the strongest winds of Irene as it makes landfall along the NC coast, and the blending between the high resolution H*wind and the coarse resolution NARR wind field stretches the strongest winds to far away from the hurricane center producing the higher than expected wind speeds. Similarly buoy 44008 which is also over predicted lies in a region near where the H*wind snapshot and NARR wind field are blended together. Overall the other stations show good agreement between the simulated and observed winds at the buoys.

Figure 2.2-5 and Table 2.2-5 show the comparison between the simulated and observed winds at the 18 NOS stations located within the coastal zone. These stations are right at the transition from marine exposure to land exposure making it difficult to exactly simulate the observed wind speed but the simulated results show a very good comparison. Only station 8656483 (Beaufort NC) which is located very near the landfall location shows a strong positive bias indicating an over prediction. The peak wind speed here is very highly over predicted and is likely an artifact of the model domain. Although the station lies just to the left of the landfall location, the coarseness of the domain places it directly in line with landfall. So rather than being along the weak side of the storm, the station is placed near the strongest winds leading to the erroneous high values. The Kings Point, NY station also is over predicted. This is likely a case were the

roughness of the terrain has decreased the wind speed however, since this is an outlier and the other stations appear good without the land reduction, no reduction was performed.

The wind field evaluation provides confidence that the core of the hurricane is modeled well and that the forcing is very well simulated offshore and along the coast. The largest outliers are likely a result of the domain resolution and the blending of the two wind fields.

Table 2.2-4: Statistical comparison between observed and simulated winds at NDBC CMAN stations for baseline simulation winds. All speeds in m/s.

Buoy ID	Mean Cond		Bias	Abs. Err	RMS Err	Scat Indx	Linear Regression Estimators				RMSE-SS	No. Obs
	Obs	Sim					Corr (r)	Symm r	Slope (a)	Interc (b)		
41001	10.39	14.02	3.62	3.88	4.22	30.11	0.73	1.42	1.79	-4.56	0.65	96
41004	9.95	9.62	-0.33	1.36	1.67	17.40	0.71	0.98	1.01	-0.44	0.97	95
41008	7.62	5.75	-1.88	2.09	1.87	32.51	0.58	0.74	0.64	0.89	0.75	95
41009	9.37	8.81	-0.56	1.36	1.68	19.04	0.70	0.91	0.69	2.39	0.94	192
41010	11.99	12.64	0.65	1.60	2.04	16.15	0.65	1.01	0.76	3.56	0.95	191
41012	9.37	8.81	-0.57	1.69	1.90	21.55	0.67	0.93	0.78	1.46	0.94	96
41013	10.44	11.72	1.28	2.00	2.71	23.11	0.74	1.15	1.21	-0.90	0.88	96
41036	10.18	11.28	1.10	1.81	2.69	23.85	0.71	1.12	1.15	-0.39	0.89	186
41043	3.93	4.91	0.98	1.01	0.74	15.04	0.58	1.16	0.77	1.88	0.75	96
41046	5.79	8.33	2.54	2.87	2.15	25.85	0.65	1.39	1.17	1.57	0.56	95
41047	11.09	11.66	0.56	0.83	0.98	8.43	0.81	1.05	1.06	-0.09	0.95	94
41048	9.61	9.67	0.06	1.21	1.50	15.52	0.60	0.99	0.67	3.27	0.99	96
44005	6.34	6.88	0.54	1.04	1.11	16.14	0.53	1.06	1.01	0.50	0.91	96
44007	5.63	6.09	0.46	1.16	1.34	21.92	0.59	1.03	0.92	0.89	0.92	96
44008	5.76	9.47	3.70	3.70	1.48	15.59	0.57	1.38	1.03	3.54	0.36	96
44009	9.14	8.70	-0.44	1.54	2.02	23.23	0.65	0.96	1.00	-0.41	0.95	94
44013	6.23	6.68	0.45	1.24	1.52	22.79	0.53	1.09	1.13	-0.33	0.93	96
44014	9.75	10.98	1.23	1.76	1.89	17.18	0.68	1.12	1.10	0.23	0.87	96
44018	6.29	8.30	2.01	2.13	1.70	20.47	0.55	1.30	1.24	0.51	0.68	96
44039	8.45	8.12	-0.33	1.55	1.83	22.59	0.59	0.97	1.00	-0.29	0.96	249
44042	8.73	7.85	-0.88	1.58	2.00	25.53	0.71	0.91	0.95	-0.46	0.90	460
44043	7.77	6.46	-1.31	1.87	1.94	30.06	0.67	0.81	0.76	0.54	0.83	484
44058	9.20	8.31	-0.89	1.21	1.46	17.52	0.71	0.92	0.99	-0.83	0.90	460
44060	7.62	8.45	0.83	1.42	1.52	18.02	0.66	1.08	1.01	0.75	0.89	175
44065	8.58	7.16	-1.42	1.84	1.85	25.88	0.67	0.85	0.88	-0.38	0.83	96

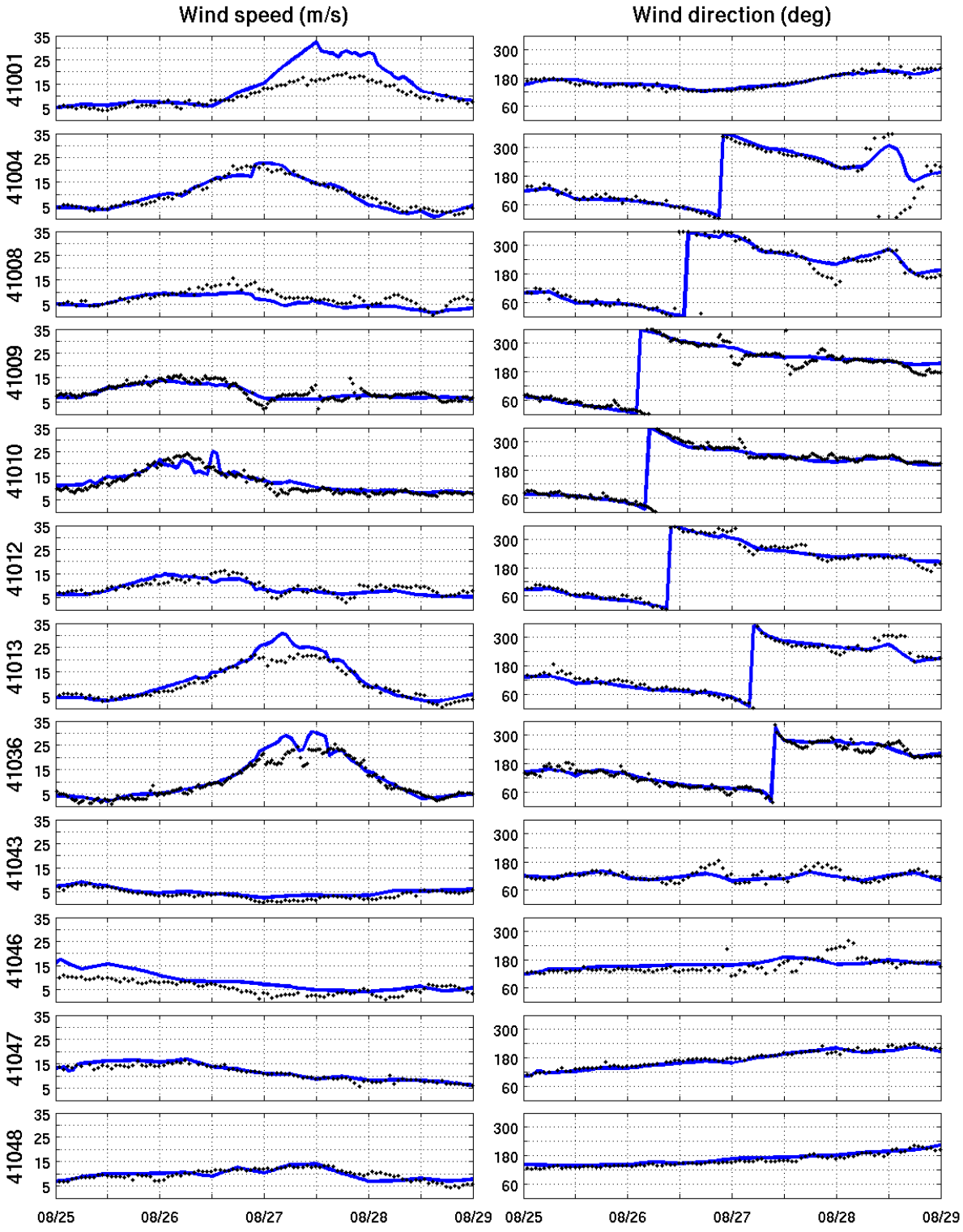
Wind speed (m/s)
Wind direction (deg)
41001
41004
41008
41009
41010
41012
41013
41036
41043
41046
41047
41048
35
25
15
5
300
180
60
08/25
08/26
08/27
08/28
08/29

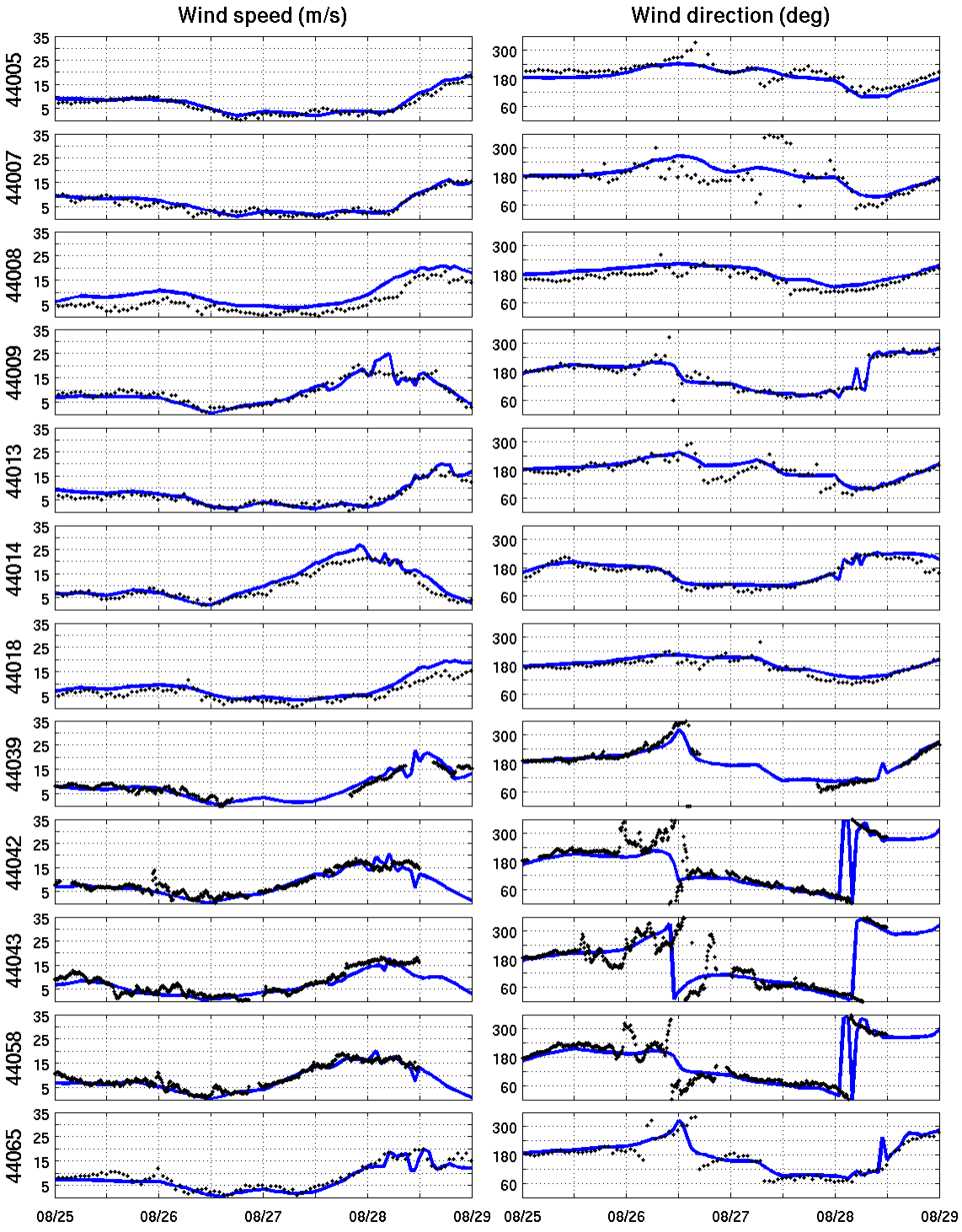

Figure 2.2-4: Comparison between the baseline (Run 000) wind speed and direction and the observed wind speed and direction at 24 NDBC CMAN stations. The Buoy IDs are labeled along the y-axis of the left panel.

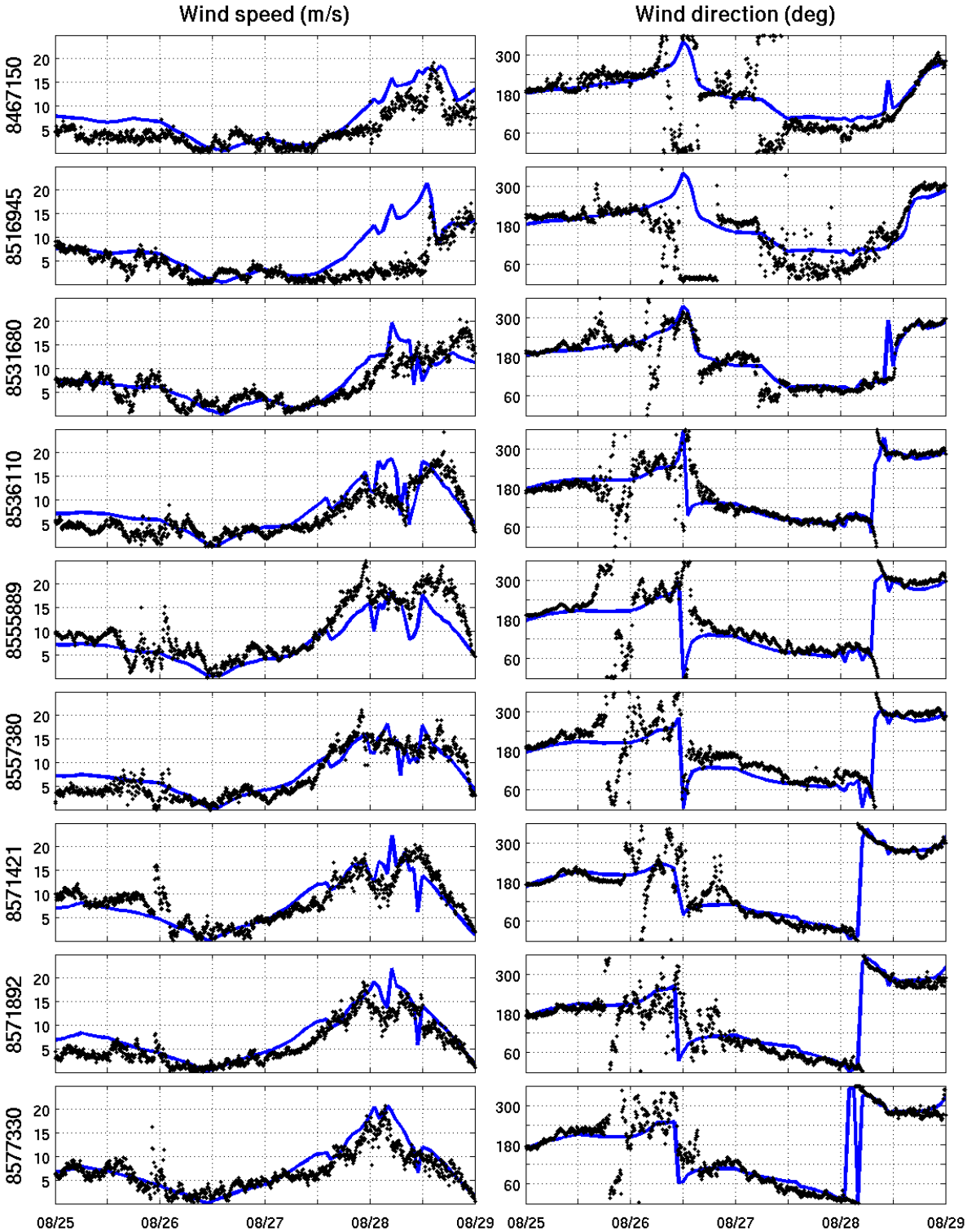
Wind speed (m/s)
Wind direction (deg)
8467150
8516945
8531680
8536110
8555889
8557380
8571421
8571892
8577330
20
15
10
5
300
180
60
08/25
08/26
08/27
08/28
08/29

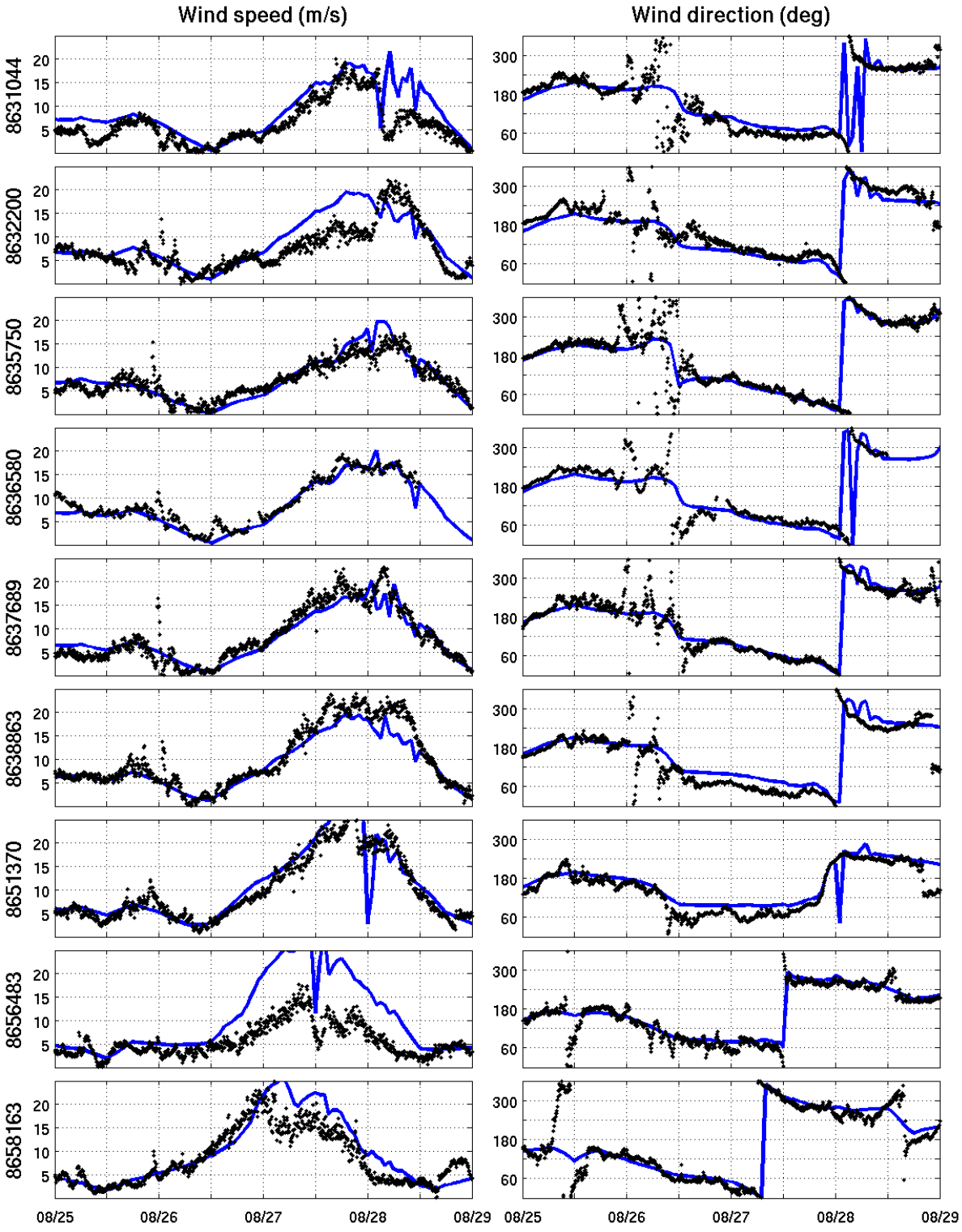

Figure 2.2-5: Comparison between the baseline (Run 000) wind speed and direction and the observed wind speed and direction at 18 NOS stations.

Table 2.2-5: Statistical comparison between observed and simulated winds at NOS stations for baseline simulation winds. All speeds in m/s.

NOS ID	Mean Cond		Bias	Abs. Err	RMS Err	Scat Indx	Linear Regression Estimators				RMSE -SS	No. Obs
	Obs	Sim					Corr (r)	Symm r	Slope (a)	Interc (b)		
8467150	4.73	7.06	2.33	2.69	2.39	33.86	0.54	1.40	1.23	1.25	0.51	950
8516945	4.23	6.95	2.72	3.20	4.31	62.02	0.43	1.27	0.71	3.94	0.36	955
8531680	6.51	6.64	0.13	2.00	2.63	39.57	0.66	0.95	0.81	1.36	0.98	961
8536110	6.45	7.64	1.18	2.47	2.85	37.39	0.59	1.06	0.80	2.46	0.82	953
8555889	10.02	7.54	-2.48	2.85	2.77	36.72	0.67	0.73	0.67	0.83	0.75	960
8557380	7.36	7.72	0.36	2.07	2.49	32.19	0.70	0.94	0.73	2.33	0.95	907
8571421	8.45	7.84	-0.61	2.25	2.96	37.73	0.63	0.91	0.84	0.76	0.93	961
8571892	6.03	7.70	1.67	2.13	2.15	27.90	0.62	1.18	1.00	1.65	0.72	958
8577330	6.75	7.51	0.75	1.83	2.33	31.07	0.53	1.13	1.17	-0.41	0.89	961
8631044	6.17	8.66	2.48	2.77	2.96	34.21	0.57	1.25	0.95	2.77	0.60	955
8632200	7.40	8.74	1.35	2.79	3.45	39.42	0.66	1.09	0.86	2.42	0.82	959
8635750	7.37	7.51	0.14	1.57	2.05	27.35	0.63	1.04	1.13	-0.80	0.98	958
8636580	9.20	8.31	-0.89	1.21	1.46	17.52	0.71	0.92	0.99	-0.83	0.90	460
8637689	8.42	7.99	-0.44	1.69	2.20	27.57	0.68	0.89	0.78	1.40	0.95	957
8638863	9.95	8.66	-1.29	1.70	2.11	24.32	0.69	0.84	0.77	1.01	0.87	945
8651370	10.06	10.60	0.54	1.93	2.83	26.73	0.60	1.04	1.00	0.53	0.95	960
8656483	5.60	10.48	4.88	5.16	5.09	48.53	0.60	1.91	2.00	-0.74	0.13	960
8658163	8.45	9.49	1.04	2.54	3.33	35.05	0.68	1.12	1.11	0.08	0.88	961

2.2.4 Water Level and Inundation Comparison

Hurricane Irene brought storm surge and inundation all along the east coast. While the largest values were in the Pamlico Sound region of North Carolina values in excess of 1 m were found in Chesapeake Bay, over 1.5 m in Delaware Bay, and well over 2 meters near New York and Connecticut. The extent of the inundation was limited to the near coastal regions. In contrast to Ike, the varying terrain of the eastern seaboard features helped to limit the landward extent of the flooding. A total of 77 High Water Marks (HWMs) were used for examination of the inundation. The HWMs tended to be less than 3 meters throughout the region. To assess the accuracy of CSIPS in simulating water levels and inundation in this region for a weaker storm hydrograph and HWM analysis were performed.

Figure 2.2-6 shows a hydrograph comparison between the observations at the 18 NOS stations and the simulated results in each of the three layers of domains. Overall there is good agreement between the observations and the modeled results, especially the final nest. As mentioned the elevation along this region is more rapidly changing than in the Gulf of Mexico. This is evidenced by the noticeable change in many stations between different resolutions of the domains. For example The Battery, NY, Cambridge, MD and Wilmington NC all show that the coarse resolution nest does not accurately represent the conditions at the observation station. In Wilmington, both the EC and MA domains poorly represent the water levels, although the high resolution domain does capture it well. There are two stations, Wachapreague, VA and The Battery, NY where the depth of the high resolution domain is off, but it still does a good job in

catching the peak. To show the difference the domain resolution makes in capturing the peak, Figure 2.2-7 shows the peak water level at the 18 NOS stations versus the simulated peak level (note that station 8631044 stops recording so the simulated peak is the level at the time that the observations stop). Table 2.2-6 shows statistics for the simulated and peak water levels at both the NOS stations and the USGS stations. The first thing to stand out is the outlier in the EC domain (NOS station). This is The Battery, where the EC domain depicts a land cell with elevation of about 4.5 m. This cell never gets flooded and keeps this elevation throughout. Except for that outlier which skews the data for the EC domain, there is a consistent improvement with each nest. The MA and NY/DB/CB/OB/WJ domains show high correlation, small negative bias, RMSE of about 20 cm given peak water levels up to 3 m, low scatter index percent and MAPEs under 15%. The scatter and the errors are larger for the USGS stations primarily due to the stations being located close to shore or on land, where the accuracy of the elevation data set is less compared to the bathymetry. The actual simulated and observed peak values are shown in Table 2.2-7 to get a better idea of the magnitude of the surge and of the statistics.

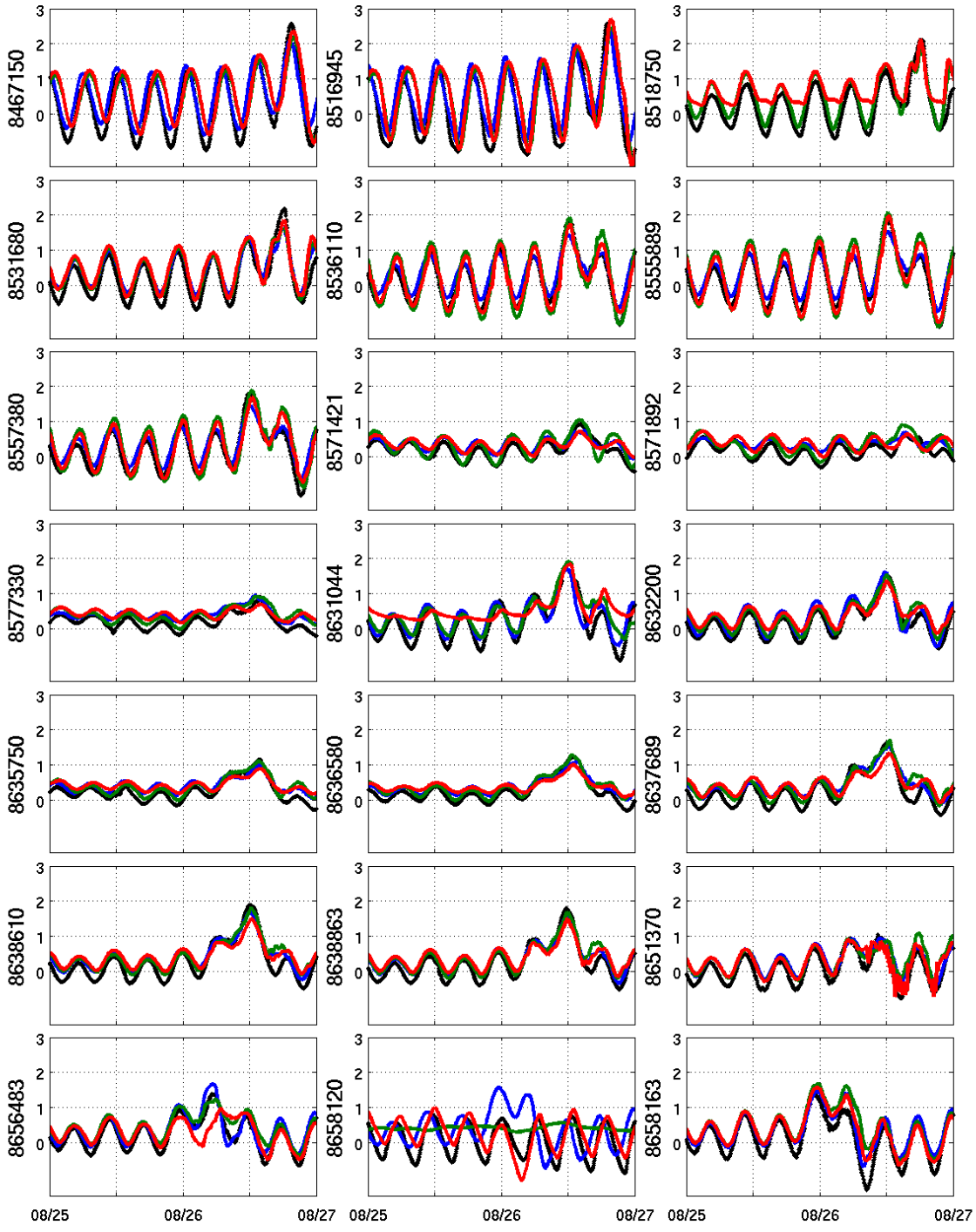

Figure 2.2-6: Hydrograph comparison between NOS stations and baseline simulation runs for different domains.

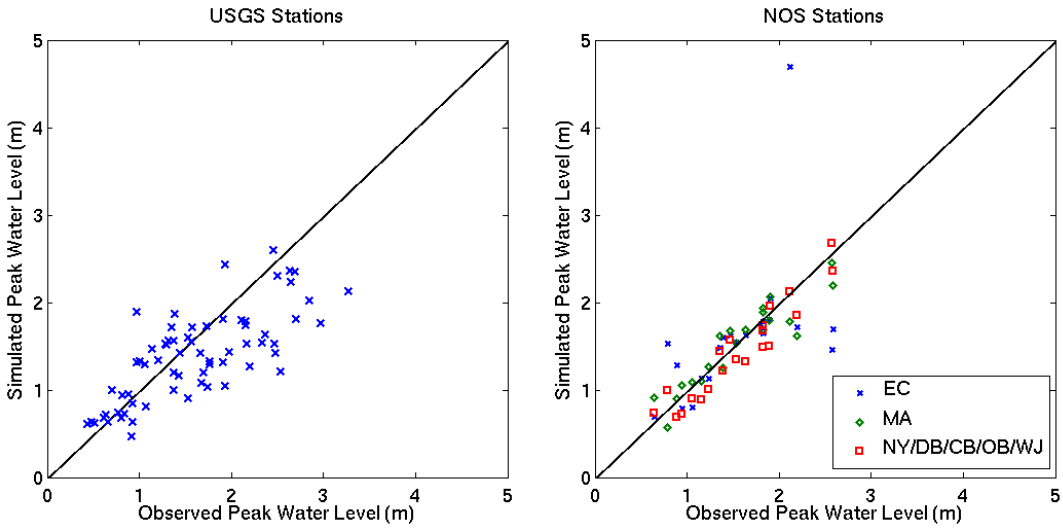

Figure 2.2-7: Simulated versus observed peak water levels at the 92 USGS stations for the high-resolution grids and at the 21 NOS stations for each of the 3 grid resolutions.

Table 2.2-6: Statistics for the peak water level at the NOS stations and at the USGS stations.

	EC	EC (w/o outlier)	MA	NY/DB/CB/OB/WJ	
	NOS	NOS	NOS	NOS	USGS
Corr r	0.25	0.47	0.85	0.90	0.56
Bias (m)	0.05	-0.07	-0.03	-0.12	-.21
RMSE (m)	0.31	0.28	0.23	0.19	.49
Scatter Index	18.91	19.13	14.93	12.96	35.13
MAPE	23.09	18.11	11.15	13.29	24.16

Table 2.2-7: Peak water levels at the 21 NOS stations as observed and simulated.

	Obs	EC	MA	NY/DB/CB/OB/WJ
8467150	2.58	1.70	2.19	2.36
8516945	2.57	1.47	2.45	2.68
8518750	2.11	4.70	1.78	2.12
8531680	2.19	1.72	1.62	1.85
8536110	1.82	1.65	1.93	1.74
8555889	1.90	2.05	2.07	1.96
8557380	1.82	1.78	1.89	1.68
8571421	0.94	0.79	1.05	0.72
8571892	0.64	0.70	0.91	0.73
8577330	0.89	1.29	0.90	0.69
8631044	1.36	1.49	1.62	1.44
8632200	1.54	1.55	1.54	1.35

8635750	1.15	1.13	1.10	0.89
8636580	1.23	1.14	1.27	1.01
8637689	1.63	1.63	1.69	1.32
8638610	1.89	1.81	1.79	1.50
8638863	1.82	1.71	1.69	1.49
8651370	1.05	0.81	1.09	0.90
8656483	1.39	1.61	1.25	1.22
8658120	0.79	1.54	0.57	0.99
8658163	1.47	1.63	1.68	1.57

Not only is capturing the peak important, but capturing the timing of the peak can be just as essential for mitigation and response planning. For weaker storms especially, the timing of the storm with respect to the tidal phase becomes crucial. If the model predictions of the high tide coincides with the arrival of the maximum storm surge, the impact of the storm surge can be exaggerated. Conversely, if model predictions of low-tide coincides with the maximum storm surge, the impact of the storm with respect to surge and inundation is minimized. Table 2.2-8 shows the lag in hours (negative lag indicates that the simulated peak occurs prior to the observed peak) of the peak water level. The lag varies across stations and domains, but in general the simulated peak occurs slightly after the observed peak. There are a few large outliers, particularly Duck, NC, Wilmington, NC, and Wrightsville Beach, NC. In Duck, there is no strong peak, but rather two peaks that are just centimeters off in maximum elevation. By simulating the first peak to a slightly greater elevation than the next peak which occurs roughly a tidal cycle later, the numbers get skewed. In Wilmington it is likely a resolution issue with the WJ domain capturing the timing within an hour, but the EC and MA domains are way off. Likewise the resolution of the EC domain causes the erroneous value in Wrightsville Beach. The overall mean absolute error shows that the peak is nearly always captured within an hour of occurrence excluding the outliers discussed here. Evaluation of the extent of the inundation in the region is very difficult since no published qualitative or quantitative estimates have been found.

Table 2.2-8: Mean absolute error of the time lag (in hrs.) between the simulated and observed peak water level (negative lag indicates simulated peak occurs prior to observed).

NOS Stations	EC	MA	NY/DB/CB/OB/WJ	Mean Abs. Error
8467150	0.2	0.7	0.7	0.53
8516945	3.0	1.3	1.5	1.93
8518750	N/A	-0.2	-0.3	0.25
8531680	-0.3	-0.4	-0.1	0.27
8536110	0.5	0.4	0.7	0.53
8555889	0.6	0.4	0.6	0.53
8557380	0.5	0.7	0.9	0.70
8571421	-0.7	0.1	-0.2	0.33
8571892	1.4	-1.1	1.4	1.3

8577330	1.2	-1.7	0.1	1.0
8631044	0.0	0.0	0.0	0.0
8632200	-0.3	0.4	0.4	0.37
8635750	-0.2	-0.5	0.2	0.30
8636580	-0.9	-0.2	0.2	0.43
8637689	-1.2	0.9	1.0	1.03
8638610	-0.9	0.6	0.8	0.77
8638863	-0.2	0.4	0.4	0.33
8651370	-10.0	12.0	-10.7	10.9
8656483	0.1	1.6	1.4	1.03
8658120	21.6	46.6	0.7	22.97
8658163	11.4	1.5	1.4	4.77
Mean Abs. Error	2.76	3.41	1.15	

Figure 2.2-8 shows the spatial extents of the inundation as simulated in the MA domain (a), the NY domain (b), the DB domain (c), the CB domain (d), the OB domain (e) and the WJ domain (f). The highest values are located in Pamlico Sound, which has been confirmed by various reports (NHC 2012, NOAA 2012, USGS 2012). The peak observed values there are around 2.75 m, which corresponds well with the simulated results. High values also show up along the shores of Delaware Bay which seem to be supported by estimates at the mouth of the Bay and well up the Bay where the tidal contribution is quite large. The inundation in Chesapeake Bay is greatest along the Delmarva Peninsula where the flooding was reported to rival Hurricane Isabel in 2003 (NHC 2012). The NY area also experiences considerable inundation along southern Long Island and the extreme coastal areas of Connecticut. Very little inundation is found to the left of the storm near landfall in the WJ domain due to the core of the storm remaining well to the east.

To get a quantitative estimate of the inundation height, a HWM comparison is presented in Figure 2.2-9 along with the statistics in Table 2.2-9. The statistics show the importance of resolution in capturing inundation. There is a steady improvement in most metrics as the domain resolution becomes higher. For the NY/DB/CB/OB/WJ domains the MAPE is just over 13% the simulated and observed HWMs are well correlated with a slight negative bias and low RMSE and scatter index. The RMSE and MAPE increases quite a bit for the coarser resolution domains. This again emphasizes that the ability of the model to accurately capture the elevation of the underlying terrain is critical to producing accurate results.

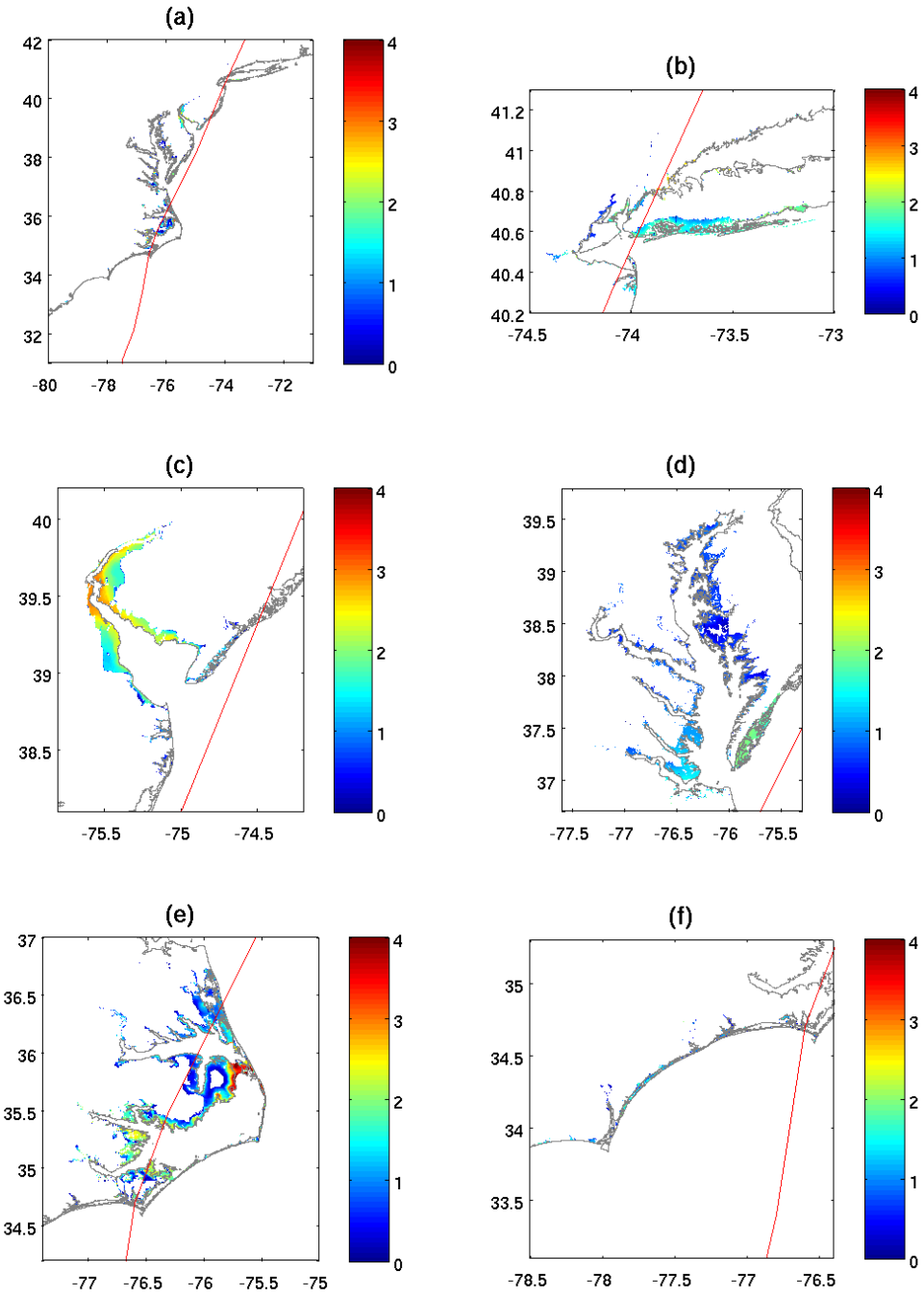

Figure 2.2-8: Simulated envelope of high water for baseline simulations for (a) MA domain, (b) NY domain, (c) DB domain, (d) CB domain, (e) OB domain, and (f) WJ domain.

Overall the baseline simulation results show that CSIPS is capable of producing water level results with high accuracy in the baseline simulations. The hydrographs produced by the model show that the peak and timing of the peak is modeled well in comparison with the observations, especially at the highest resolution. The HWM analysis shows that there is improvement in the inundation results in each layer of nesting. Ideally, given the widely changing nature of the topography, the domain would feature resolution below 100 m to produce inundation estimates. However the 0.004° domain appears adequate to get estimates less than 15% error.

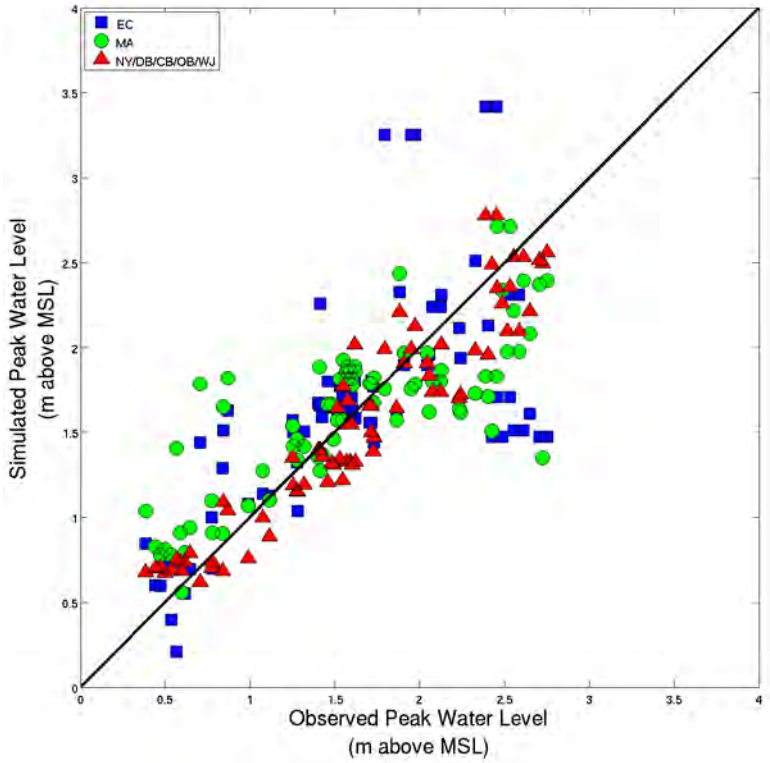

Figure 2.2-9: HWM comparison for baseline simulations of Hurricane Irene.

Table 2.2-9: Statistics from HWM analysis for Hurricane Irene.

	EC	MA	NY/DB/CB/OB/WJ
Corr r	0.42	0.61	0.90
Bias (m)	0.03	0.02	-0.12
RMSE (m)	0.44	0.38	0.19
Scatter Index	26.95	23.57	12.96
MAPE	25.35	26.28	13.29

2.2.5 Wave Comparison

In addition to water level results, CSIPS provides estimates of the wave height, period, and direction among other things. By dynamically coupling the wave and hydrodynamic simulations the influence of the waves on water levels is passed to the hydrodynamic model for use in water level calculations. Due to the coarseness of the grid, where the grid size is several times the wave length, we used the Dingemans et al. (1987) formulation as mentioned in Section 2.1.5 rather

than the radiation stress form. Likewise, the changing water surface is passed to the wave model allowing calculation of waves in areas that would not normally be flooded in a static simulation.

The wave simulation is much more computationally expensive than the hydrodynamic simulation. To save some of this cost the waves are run on grids with half the resolution of the hydrodynamic grid. The wave height, period and direction results of the EC baseline simulation are shown in Figure 2.2-10 and the statistics for the wave heights in Table 2.2-10 and wave periods in Table 2.2-11. The agreement looks good with a few exceptions. Stations 41001, 44014, and 44039 all have positive biases greater than 1 m indicating an over prediction. Buoy 41001 was previously discussed for the high winds, so high wave heights follow along with that. The Virginia Beach buoy (44014) and the Central Long Island Sound Buoy (44039) can be explained by examining the data. Buoy 44039 shows only intermittent pieces of data and misses the peak entirely. The Virginia Beach Buoy is located offshore in some of the highest waves experienced during the storm. A bias of 1 m in a region experiencing 7 m waves, while non-negligible, is within acceptable error. The other metrics also show errors that are larger than those of the other locations. These errors are partly the result of errors in representing the physics of wave generation in the presence of high winds in the SWAN model. The proximity of the buoy to the strongest winds of the hurricane may also lead to some errors due to incorrect wind forcing. Besides those stations the 27 other stations show very good agreement between the observed and simulated significant wave height. The wave period is also modeled fairly well. The same stations with problems in either the wind or wave height have similar errors in the wave period, but the majority of the stations perform very well with high RMS skill scores. With

the exception of the few stations noted, CSIPS accurately predicts the wave characteristics throughout the region.

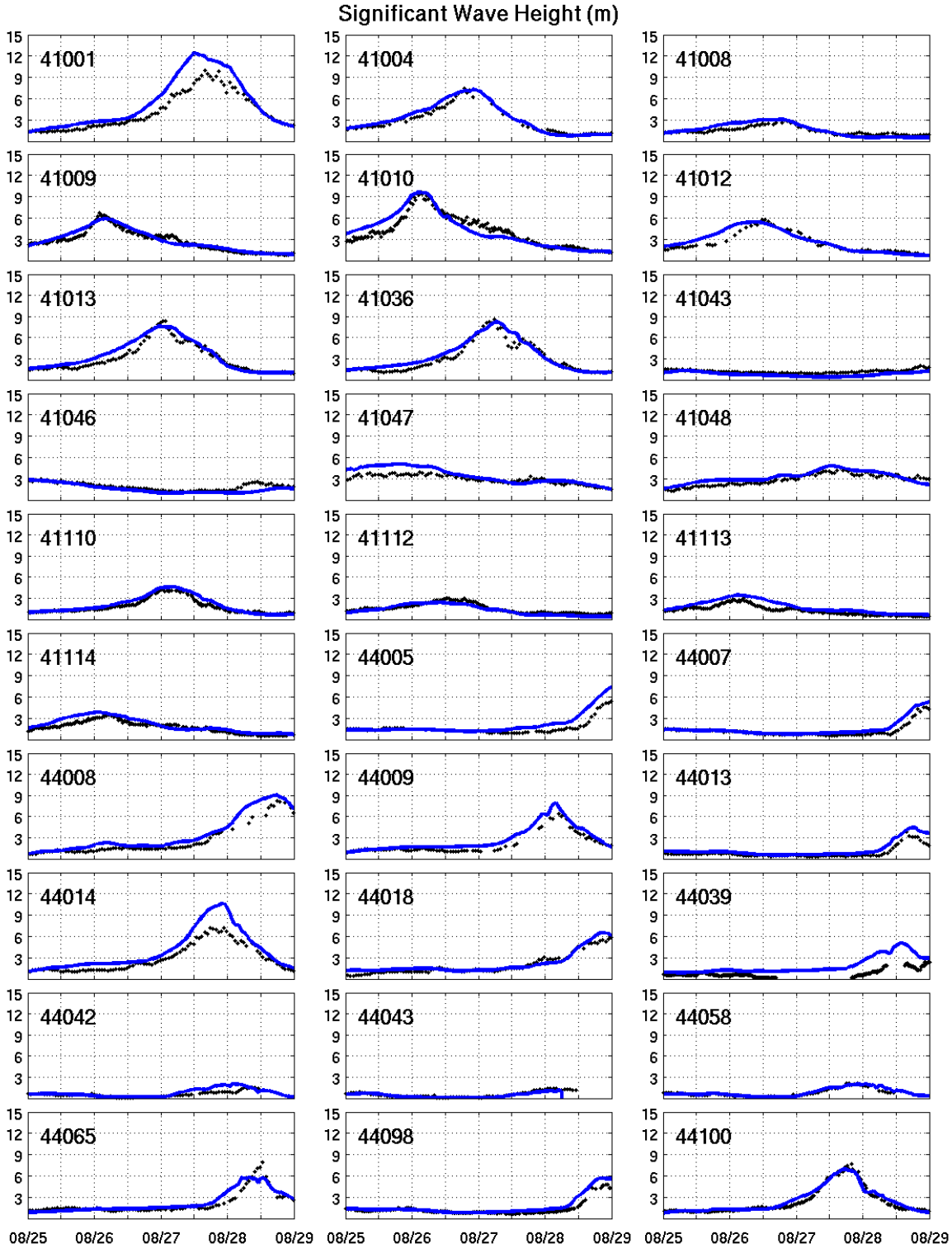

Figure 2.2-10: Wave height (in m) comparison between Baseline EC simulation (blue line) and NDBC CMAN stations (black dots).

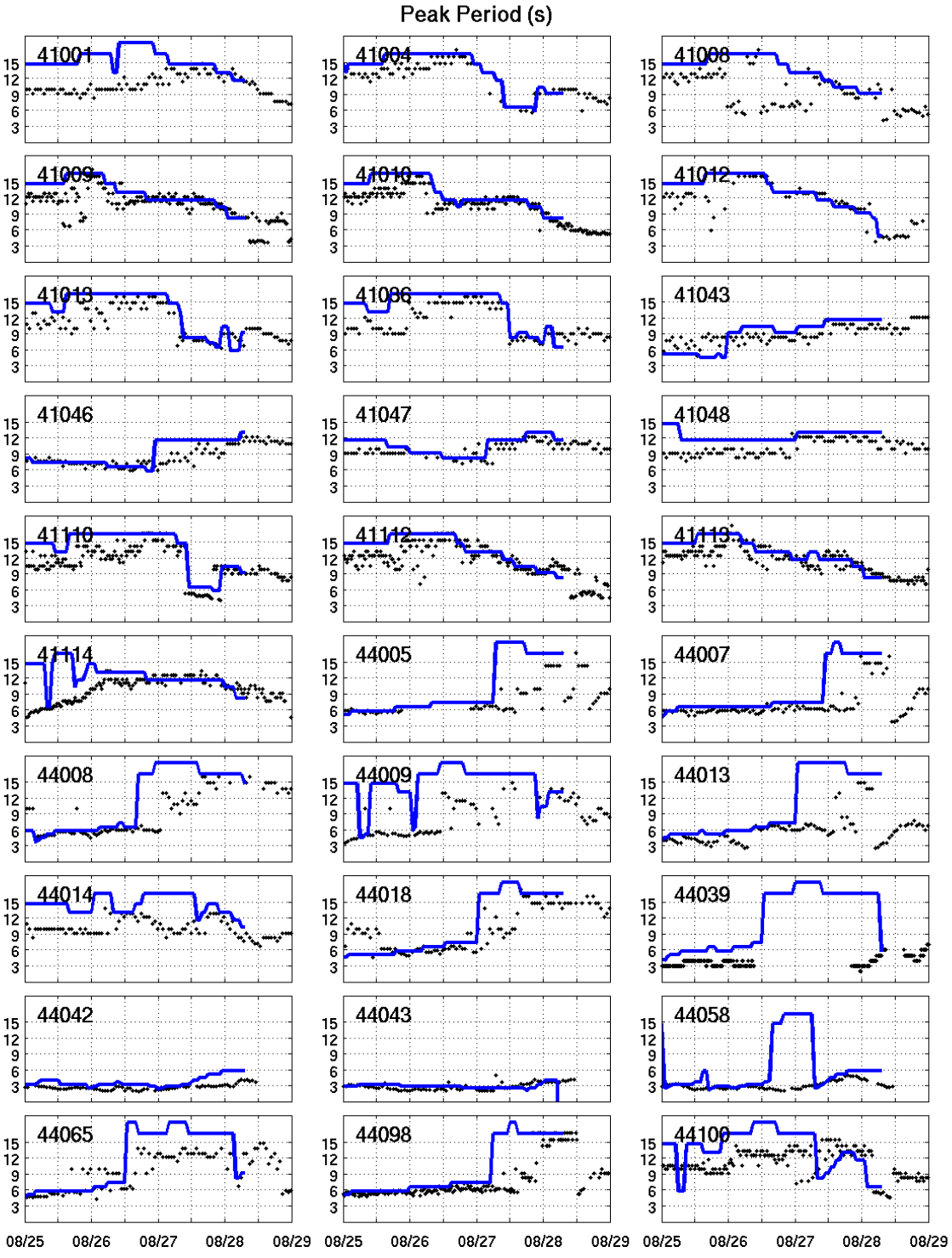

Figure 2.2-11: Peak wave period (secs) comparison between Baseline EC simulation (blue line) and NDBC CMAN stations (black dots).

Table 2.2-10: Statistical comparison between observed and simulated wave height at NDBC CMAN stations for baseline simulation. All heights in m.

Buoy ID	Mean Cond		Bias	Abs. Err	RMS Err	Scat Indx	Linear Regression Estimators				RMSE -SS	No. Obs
	Obs	Sim					Corr (r)	Symm r	Slope (a)	Interc (b)		
41001	4.16	5.35	1.19	1.21	1.19	22.27	0.70	1.30	1.34	-0.22	0.71	95
41004	2.81	3.00	0.19	0.37	0.43	14.23	0.63	1.08	1.11	-0.13	0.93	76
41008	1.45	1.59	0.13	0.37	0.43	26.91	0.69	1.14	1.47	-0.55	0.91	91
41009	2.76	2.87	0.11	0.33	0.43	14.88	0.63	1.02	0.96	0.21	0.96	192
41010	4.07	4.14	0.07	0.73	0.94	22.74	0.58	1.01	1.01	0.03	0.98	187
41012	2.39	2.52	0.13	0.43	0.55	21.99	0.60	1.03	0.98	0.18	0.95	69
41013	3.07	3.41	0.34	0.55	0.61	17.91	0.64	1.09	1.03	0.25	0.89	95
41036	3.11	3.33	0.22	0.56	0.65	19.53	0.63	1.04	0.97	0.32	0.93	94
41043	1.20	0.77	-0.43	0.43	0.17	21.60	0.66	0.66	0.95	-0.36	0.64	96
41046	1.90	1.56	-0.34	0.35	0.32	20.59	0.62	0.83	0.95	-0.24	0.82	95
41047	2.93	3.40	0.47	0.59	0.60	17.73	0.72	1.18	1.54	-1.11	0.84	94
41048	2.87	3.22	0.35	0.48	0.40	12.35	0.65	1.10	0.87	0.72	0.88	95
41110	1.87	2.11	0.24	0.31	0.32	15.14	0.61	1.13	1.15	-0.05	0.87	172
41112	1.52	1.34	-0.18	0.25	0.25	18.91	0.75	0.89	0.90	-0.02	0.88	192
41113	1.29	1.77	0.48	0.48	0.31	17.77	0.65	1.35	1.24	0.18	0.63	183
41114	1.76	2.12	0.36	0.45	0.41	19.12	0.69	1.19	1.11	0.17	0.80	172
44005	1.69	2.29	0.60	0.70	0.72	31.57	0.38	1.36	1.38	-0.03	0.64	70
44007	1.21	1.46	0.26	0.29	0.39	26.51	0.33	1.20	1.18	0.04	0.79	96
44008	2.37	2.94	0.57	0.58	0.47	16.12	0.47	1.18	1.10	0.34	0.76	83
44009	2.06	2.52	0.47	0.50	0.44	17.54	0.47	1.20	1.14	0.19	0.77	78
44013	0.82	1.22	0.40	0.40	0.37	30.54	0.39	1.43	1.36	0.11	0.51	95
44014	2.93	4.05	1.12	1.13	1.04	25.66	0.62	1.40	1.44	-0.18	0.62	96
44018	1.88	2.05	0.18	0.35	0.41	19.91	0.44	1.07	1.03	0.12	0.91	93
44039	0.79	1.82	1.02	1.02	0.81	44.58	0.51	2.08	1.63	0.52	0.29	249
44042	0.56	0.76	0.21	0.27	0.37	48.51	0.65	1.36	1.32	0.03	0.63	78
44043	0.56	0.44	-0.12	0.15	0.14	32.06	0.69	0.79	0.79	0.00	0.79	81
44058	0.76	0.81	0.05	0.14	0.19	23.77	0.61	1.06	1.03	0.03	0.93	78
44065	2.11	2.22	0.10	0.42	0.62	27.78	0.47	0.99	0.88	0.35	0.95	93
44098	1.23	1.45	0.22	0.27	0.37	25.50	0.28	1.20	1.26	-0.11	0.83	171
44100	2.34	2.34	0.01	0.32	0.44	18.57	0.51	0.96	0.89	0.26	1.00	172

Table 2.2-11: Statistical comparison between observed and simulated wave period at NDBC CMAN stations for baseline simulation. All periods in seconds.

Buoy ID	Mean Cond		Bias	Abs. Err	RMS Err	Scat Indx	Linear Regression Estimators				RMSE-SS	No. Obs
	Obs	Sim					Corr (r)	Symm r	Slope (a)	Interc (b)		
41001	10.76	13.04	2.28	2.30	1.39	10.67	0.50	1.20	0.69	5.56	0.79	95
41004	11.81	12.39	0.58	1.15	1.31	10.59	0.77	1.05	1.10	-0.55	0.95	76
41008	9.48	11.84	2.37	3.23	3.68	31.05	0.35	1.17	0.43	7.79	0.75	91
41009	10.67	10.81	0.14	1.57	2.14	19.83	0.52	1.01	0.92	1.00	0.99	192
41010	10.55	10.73	0.18	1.00	1.38	12.88	0.67	1.02	1.05	-0.37	0.98	187
41012	10.77	10.89	0.11	1.63	2.37	21.79	0.60	0.98	0.72	3.09	0.99	69
41013	10.98	12.56	1.59	2.01	2.18	17.32	0.75	1.13	0.98	1.84	0.86	95
41036	11.04	12.59	1.55	1.97	2.18	17.32	0.73	1.13	0.90	2.62	0.86	94
41043	8.95	8.61	-0.34	1.06	1.42	16.48	0.51	0.96	0.95	0.14	0.96	96
41046	8.58	8.67	0.09	0.98	1.21	13.98	0.72	1.02	1.21	-1.74	0.99	95
41047	9.77	10.59	0.82	1.13	1.12	10.57	0.51	1.08	0.68	3.98	0.92	94
41048	10.26	11.67	1.41	1.62	1.38	11.83	0.60	1.13	0.84	3.07	0.86	95
41110	11.11	12.58	1.47	2.51	2.74	21.75	0.61	1.11	0.90	2.62	0.87	172
41112	11.37	11.27	-0.09	2.23	3.01	26.66	0.64	0.98	0.82	2.01	0.99	192
41113	11.66	10.50	-1.16	1.74	2.08	19.77	0.63	0.92	1.39	-5.73	0.90	183
41114	9.86	10.14	0.28	2.18	2.98	29.40	0.36	1.00	0.41	6.11	0.97	172
44005	8.32	10.77	2.45	2.53	2.90	26.91	0.65	1.26	1.04	2.15	0.71	70
44007	7.18	9.29	2.11	2.25	3.33	35.85	0.39	1.23	0.85	3.23	0.71	96
44008	8.92	10.37	1.45	2.20	2.84	27.37	0.77	1.12	0.93	2.08	0.84	83
44009	8.27	12.55	4.27	4.41	3.29	26.19	0.41	1.38	0.46	8.74	0.48	78
44013	6.03	9.50	3.47	3.48	3.76	39.53	0.41	1.47	0.94	3.81	0.42	95
44014	10.12	13.26	3.13	3.16	1.67	12.58	0.43	1.29	0.37	9.54	0.69	96
44018	9.94	10.04	0.10	2.19	2.86	28.47	0.75	0.99	0.87	1.38	0.99	93
44039	3.82	9.22	5.40	5.40	4.66	50.56	0.35	2.38	1.91	1.93	0.41	217
44042	2.71	3.84	1.14	1.14	0.68	17.80	0.54	1.42	1.42	0.00	0.58	78
44043	2.88	3.25	0.37	0.57	0.62	19.20	0.47	1.09	0.47	1.90	0.87	80
44058	3.05	5.68	2.63	2.63	3.82	67.17	-0.23	1.71	-0.98	8.67	0.14	78
44065	9.56	10.97	1.41	2.37	2.89	26.36	0.75	1.14	1.09	0.53	0.85	93
44098	7.86	9.49	1.62	2.04	2.95	31.13	0.54	1.14	0.84	2.85	0.79	171
44100	11.03	12.39	1.35	2.60	2.89	23.35	0.40	1.10	0.72	4.45	0.88	172

2.2.6 Sensitivity Studies

To assess the sensitivity of the system to the elevation dataset, bottom roughness, wave coupling, and wind field a number of tests were conducted. To conduct the sensitivity studies only the component being considered was changed with all other parameters being kept the same as the baseline simulation. Due to the large number of simulations and observations available for comparison, only the highest resolution results (NY/DB/CB/OB/WJ domains) will be discussed. These results will be discussed in terms of their accuracy in predicting the peak water level at the

18 NOS stations as was done in Figure 2.2-7 and Table 2.2-6 with any other interesting features of the wave, wind, inundation, or water levels results discussed as warranted.

2.2.7 Bathymetry

The baseline simulations feature an elevation dataset that is primarily composed of high resolution Laser Imaging Detection and Ranging (LIDAR) data in the coastal zone. The Coastal Relief Model dataset is merged with the GEBCO dataset offshore and with SRTM data onshore to fill in where needed. Since this dataset is not available everywhere throughout the world it is important to see how a dataset with global coverage compares. Sensitivity tests using just the GEBCO dataset and the GEBCO dataset combined with SRTM topography data were examined. Figure 2.2-12 shows the percent change between the baseline dataset and the GEBCO only (left panel) and difference between GEBCO and SRTM (right panel) datasets. The first row shows the difference for the full domain. The rest of the rows are zoomed into areas of interest. Most variation is confined to the topography as evidenced by plots. While there are some changes to the coastal bathymetry amongst the datasets, the majority of the change is right along the land-sea interface. This region is where the brunt of the impacts from the storm surge will be felt, so accurate elevation data is needed.

These changes in the elevation dataset are evident in Figure 2.2-13, which shows that the Bridgeport, CT, Kings Point, NY, Cape May, NJ, Cambridge, MD, and Wilmington, NC all have incorrect bathymetry data for the GEBCO dataset. The Battery, NY and Sandy Hook, NJ stations are wrong for the GEBCO + SRTM dataset in addition to all those listed for the GEBCO dataset. The NOS stations are generally placed at the end of a dock or pier within a few hundred meters of the shore. The GEBCO and GEBCO + SRTM resolution is not high enough, which leads to many of these stations being depicted as land. It is important when using the lower resolution elevation datasets to check the monitoring stations. By moving stations a grid cell or two seaward they are placed in elevation conditions more closely resembling the actual station

locations. For the stations where the bathymetry is accurately represented the hydrographs compare well with the observations.

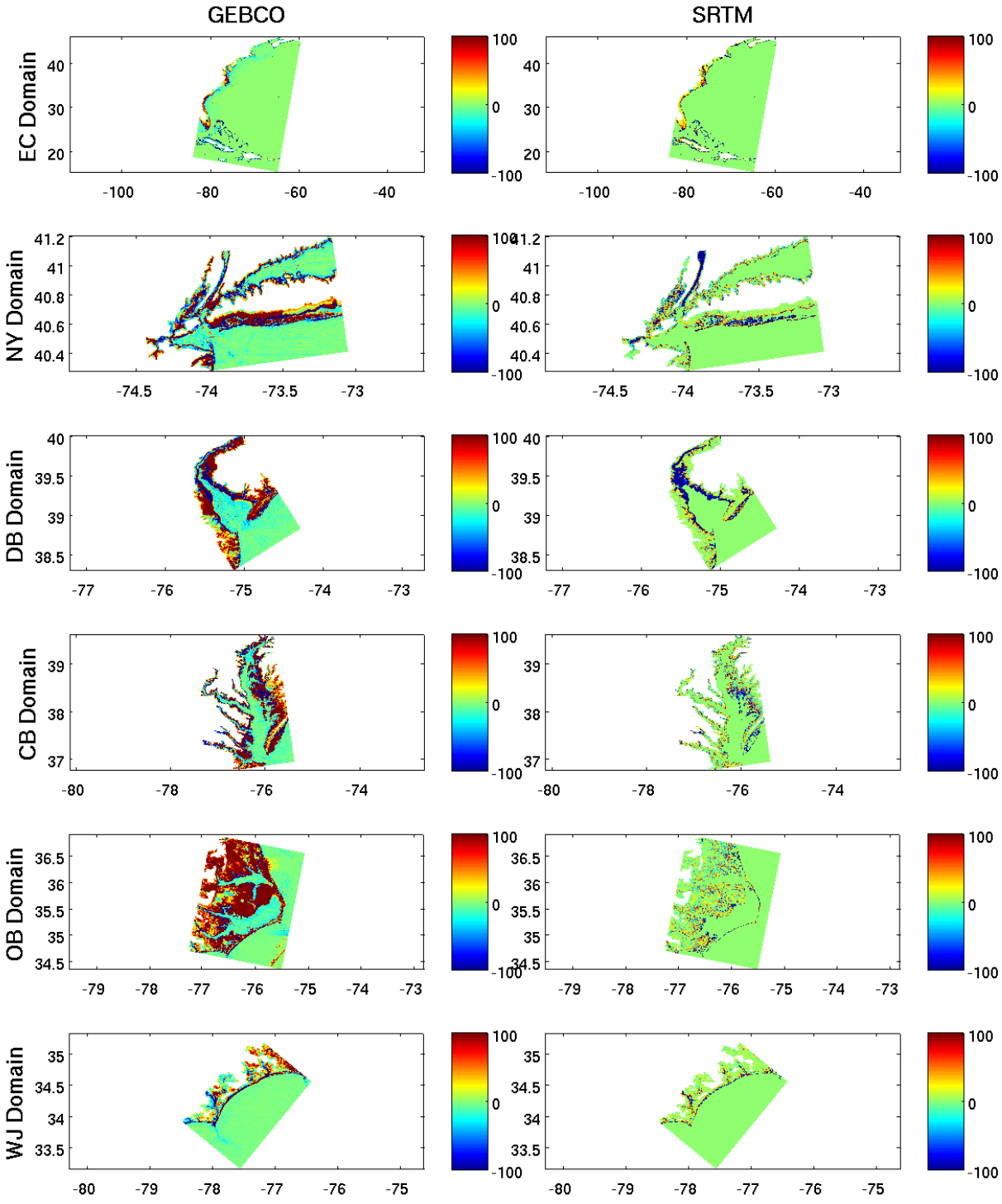

Figure 2.2-12: Percent change in the elevation between the Baseline simulation and GEBCO (left

panel) and between GEBCO and SRTM (right panel) in the EC domain.

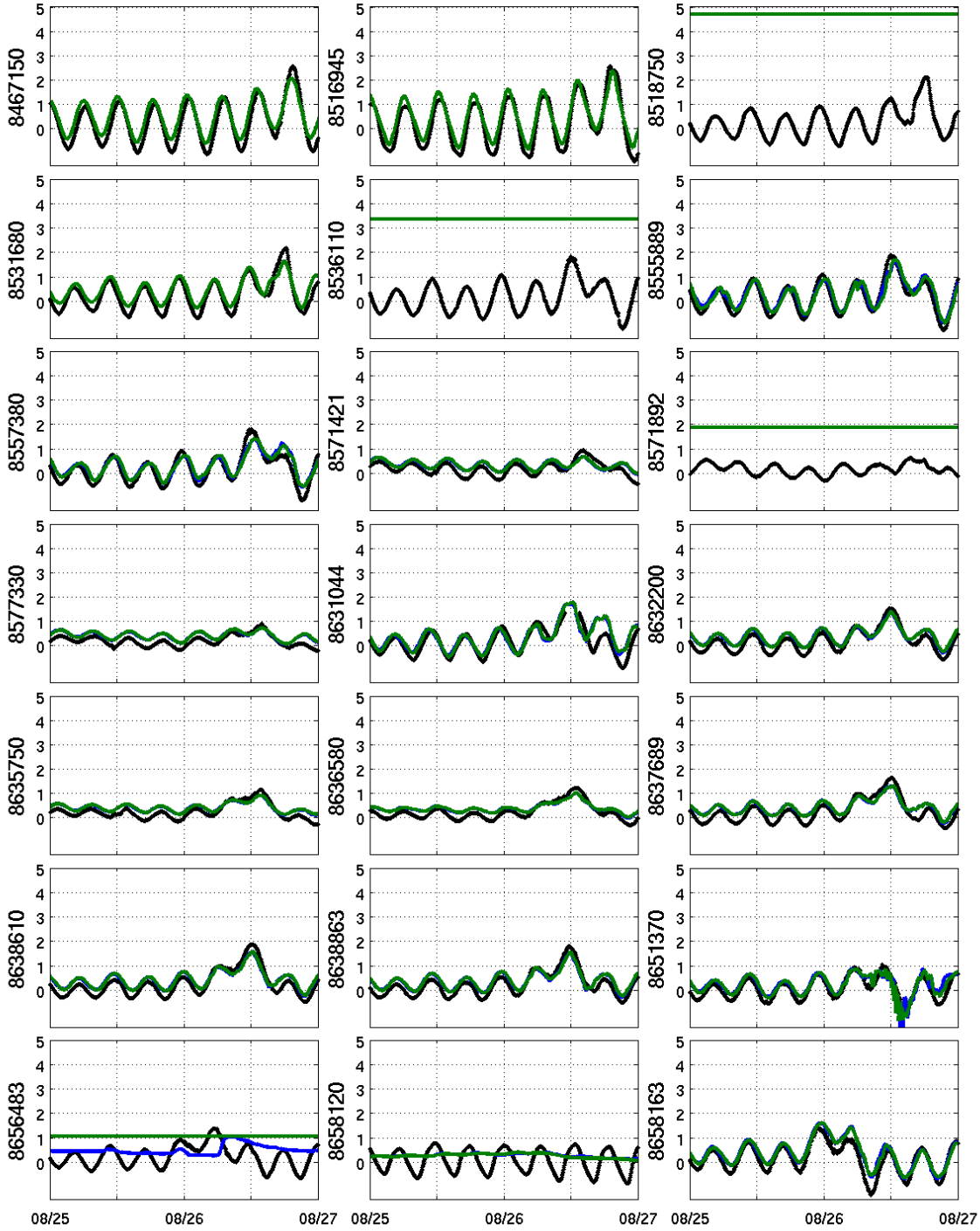

Figure 2.2-13: Hydrographs for 21 NOS Stations for different elevation datasets in the NY/DB/CB/OB/WJ domains (Data as black, GEBCO only as blue line and GEBCO+SRTM as

green line). Where there is no inundation, the water depth is shown at that location (flat lines).

Figure 2.2-14 shows the peak water levels for the NOS stations for the two elevation datasets and the statistics are summarized in Table 2.2-12. The GEBCO only dataset performs slightly better, although neither dataset shows very good results. As was the case with Ike, it is recommended to supplement the GEBCO bathymetry dataset with any available high resolution data for the area of interest.

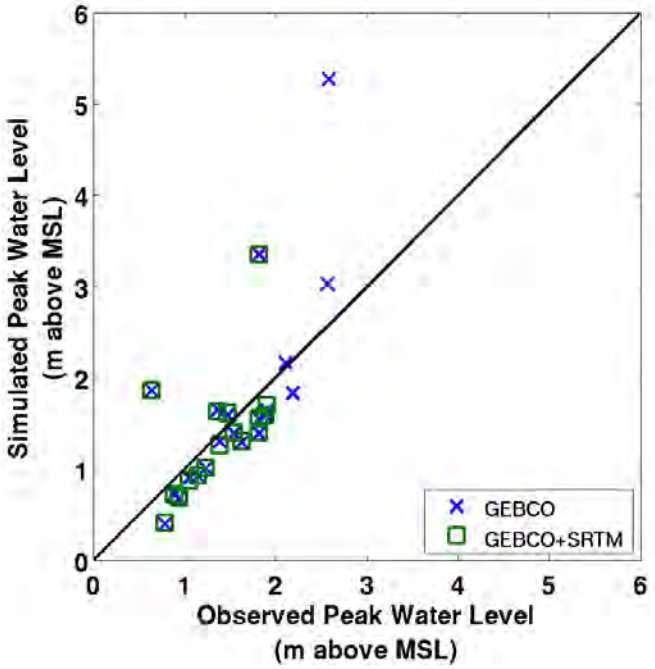

Figure 2.2-14: Simulated versus observed peak water levels at the 21 NOS stations for high resolution simulations with elevation dataset from GEBCO only and GEBCO + SRTM.

Table 2.2-12: Statistics for the peak water level at the NOS stations for the baseline NY/DB/CB/OB/WJ domains and runs with GEBCO bathymetry/topography and GEBCO + SRTM bathymetry and topography in same domains.

	GEBCO	GEBCO + SRTM
Corr r	0.53	0.31
Bias (m)	0.13	0.00
RMSE (m)	0.40	0.35
Scatter Index	23.46	25.41
MAPE	33.26	32.76

2.2.8 Waves

As previously mentioned, the computation of the wave field is a very time consuming process. To evaluate whether it is a necessary process a series of simulations without waves were run and compared to those with waves. Figure 2.2-15 shows the hydrograph comparison for the baseline simulation with waves and the sensitivity study simulation without waves. Figure 2.2-16 and Table 2.2-13 show the peak water level comparison and the statistics. In a sharp contrast to the

results obtained from the Hurricane Ike studies, the importance of wave coupling is negligible. The US east coast features a very sharp drop with a fairly wide continental shelf and steep sloping bathymetry very close to the shore. In this environment wave setup is reduced leading to a lesser importance in the wave simulation. Coupled with that is the fact that this is a much weaker storm with much smaller wave heights close to shore

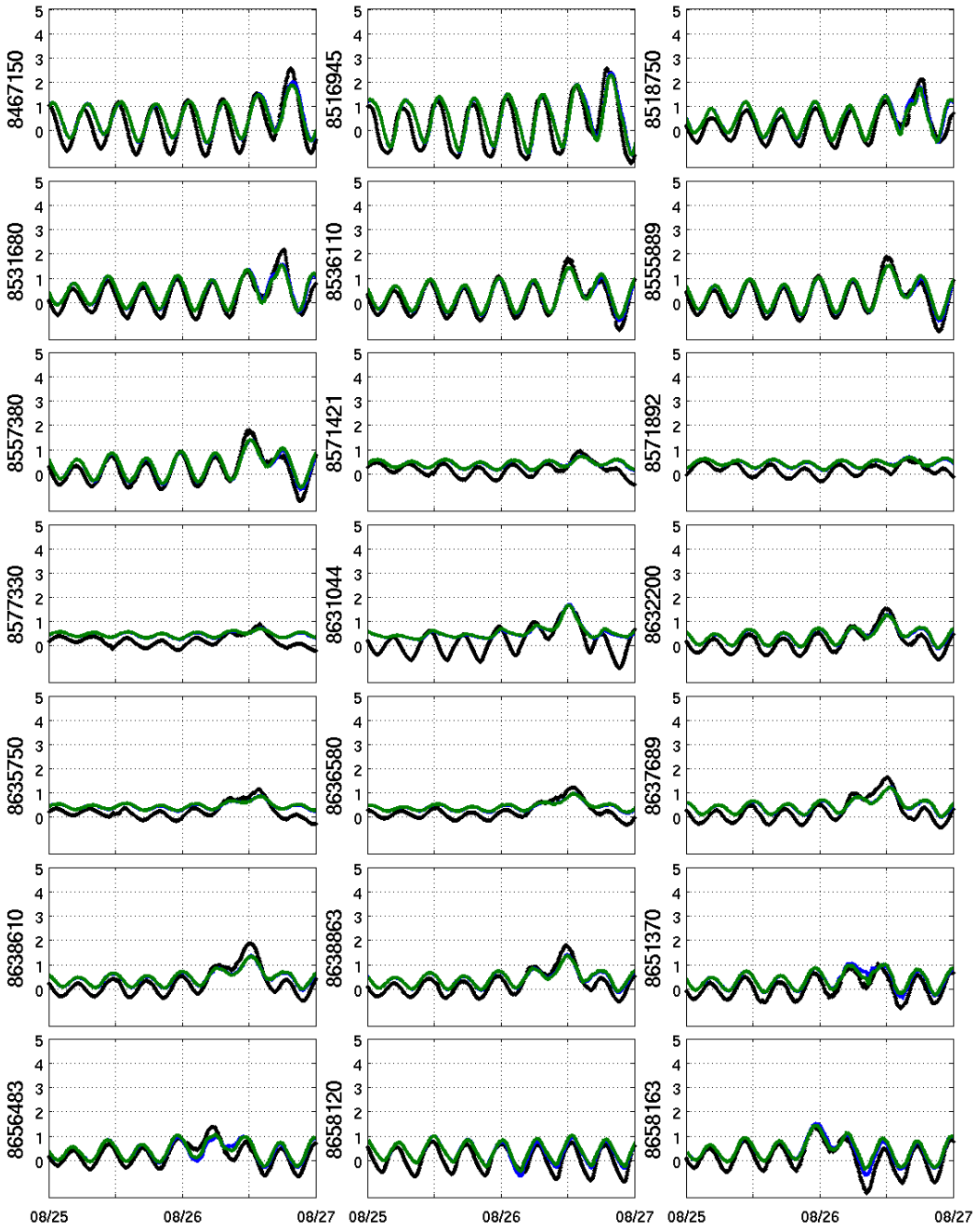

Figure 2.2-15: Hydrograph comparison between simulations with waves and simulations without

waves in the NY/DB/CB/OB/WJ domains.

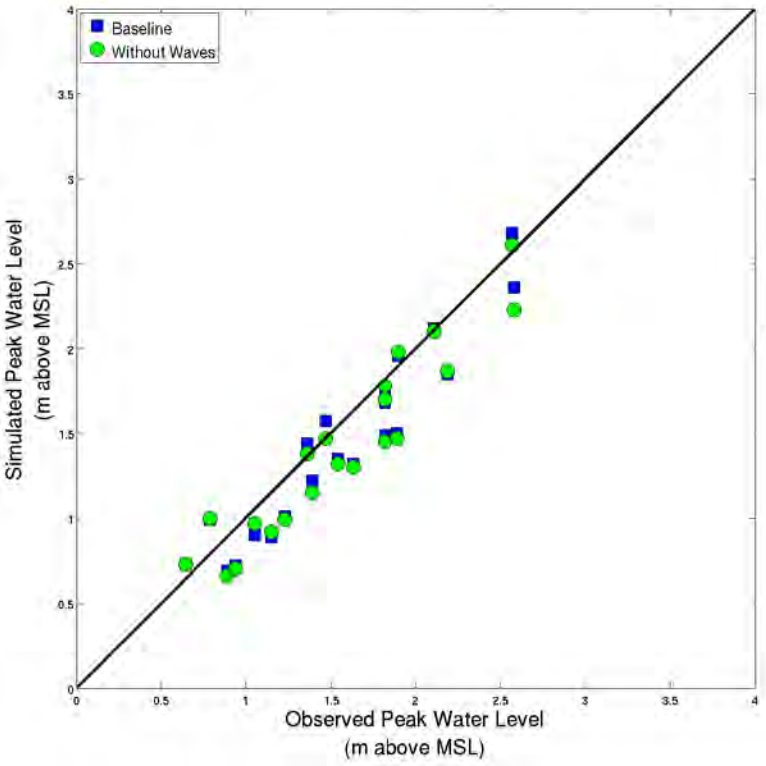

Figure 2.2-16: Simulated versus observed peak water levels at the 21 NOS stations for high resolution simulations of the baseline runs and runs with no waves.

Table 2.2-13: Statistics for the peak water level at the NOS stations for the baseline NY/DB/CB/OB/WJ domains and runs with no waves in same domains.

	Baseline	No Waves
Corr r	0.90	0.90
Bias (m)	-0.12	-0.14
RMSE (m)	0.19	0.19
Scatter Index	12.96	13.71
MAPE	13.29	13.25

2.2.9 Bottom Roughness

The frictional effects of the bottom are depicted using the Manning formulation. Categorical descriptions of Manning's N coefficients exist for various land use classes. Based on this information a spatially varying Manning's N file can be used in CSIPS. However the development of this file can be time consuming and the land use data which is necessary for its development may not be available worldwide. With that in mind three simulations were conducted with a constant Manning's N value (0.02, 0.025, and 0.03 $s/m^{1/3}$). These cover the values that are commonly used in storm surge studies. The value 0.02 $s/m^{1/3}$ was used in the spatially varying case to represent the offshore areas. Once over land the roughness value increases based on the land type. Table 2.2-14 and Figure 2.2-17 show the statistics and plot of the peak water level for the various constant values. Since these stations are located in the nearshore regions where the influence of the increased roughness of the land is not as important,

all three values perform very well. Likely due to the steep bathymetric slope there is little influence in the roughness values on the water level elevation which lead to the very similar values. Table 2.2-15 shows the statistics for the comparison between the simulated and observed inland HWMs. In general the HWMs are much more sensitive to the bottom roughness. However in this case where the values are pretty small and clustered very near the coast the influence is minimal. There is a slight drop-off in nearly all metrics when compared to the spatially varying Manning's N used in the baseline simulation, but it is small. When the hydrographs and HWMs are taken together anyone of the three values could do a comparable job to the spatially varying Manning's N in reproducing the observed water level and inundation.

Table 2.2-14: Statistics for the peak water level at the NOS stations for the baseline NY/DB/CB/OB/WJ domains and runs with constant Manning's N coefficient of 0.02, 0.025, and 0.03 in same domains.

	Baseline	Manning's N 0.02	Manning's N 0.025	Manning's N 0.03
Corr r	0.90	0.88	0.89	0.89
Bias (m)	-0.12	-0.16	-0.17	-0.19
RMSE (m)	0.19	0.21	0.20	0.20
Scatter Index	12.96	14.85	14.70	14.52
MAPE	13.29	14.12	14.73	15.22

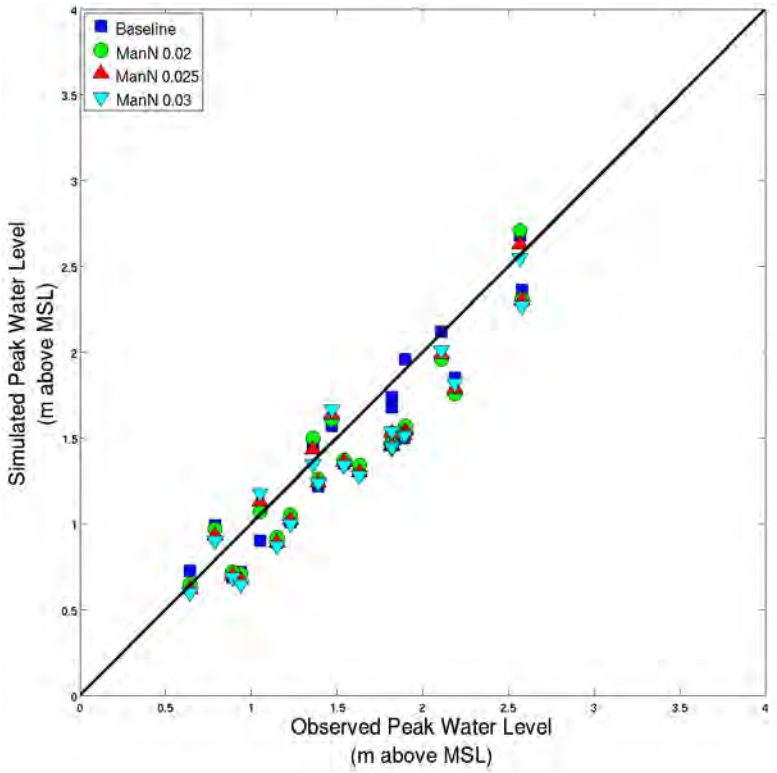

Figure 2.2-17: Simulated versus observed peak water levels at the 21 NOS stations for high resolution simulations of the baseline runs and runs with constant Manning's N coefficients.

Table 2.2-15: Statistics for the HWM comparison for the baseline NY/DB/CB/OB/WJ domains and runs with constant Manning's N coefficient of 0.02, 0.025, and 0.03 in same domains.

	Baseline	Manning's N 0.02	Manning's N 0.025	Manning's N 0.03
Corr r	0.90	0.86	0.87	0.87
Bias (m)	-0.12	-0.05	-0.07	-0.08
RMSE (m)	0.19	0.22	0.22	0.22
Scatter Index	12.96	14.22	13.96	14.33
MAPE	13.29	15.13	14.20	14.11

2.2.10 Forecast Wind

The baseline simulation utilizes the best available hindcast winds and pressure fields. In a forecast environment, these winds are not available so an analytic wind model must be used to generate a snapshot of the hurricane wind field based on the forecast information. CSIPS uses the analytic model of Condon and Veeramony (2014) to generate these snapshots on the Delft3D spiderweb grid. This model uses all available forecast information and multivariate interpolation to produce the hurricane wind field. This includes the radial extent of the 64, 50, and 34 knot winds along with the central pressure deficit, maximum wind speed, ambient pressure, radius to maximum winds, radius of the outermost closed isobar, and eye diameter when available. When the radial extent of the winds is not available, the Holland (1980) model is used to fill in. The spiderweb grid provides a moving snapshot of the hurricane wind field. The main advantage is that the file can be read in quickly and the wind field interpolated throughout the computational domain. This is a much quicker process than reading in the entire wind field from the computational mesh or another equidistant grid. Perhaps the largest drawback to using an analytic wind model is that it is designed to accurately represent the hurricane wind field but does not produce the larger scale atmospheric conditions. This results in no wind forcing outside of the immediate hurricane vortex which can be problematic if large scale atmospheric conditions prior to the storm are anything other than benign.

The CSIPS system is designed to provide forecasts starting 48 hours prior to landfall and continued until landfall. For Irene this is a unique timeframe since it made multiple landfalls as it progressed up the east coast. The initial landfall at Cape Lookout, NC occurred at 1200 UTC on August 27. The sensitivity studies will begin with the forecast closest to 48 hours prior to that, which is forecast 020 issued on August 25 at 0900 UTC. The forecast times, locations and intensity of Irene at the time of the forecast are listed in Table 2.2-16. The analytic model is used to create wind fields beginning with forecast 020 and continuing through forecast 032 which was issued just prior to Irene's final landfall near New York.

Table 2.2-16: Forecast times and storm position and intensity at time of forecast.

Forecast	Date (2011) / Time (UTC)	Storm Latitude	Storm Longitude	Max. Wind Speed knots (m/s)
020	Aug. 25 / 0900	24.6 N	-76.2 E	100 (51)
021	Aug. 25 / 1500	25.9 N	-76.8 E	100 (51)
022	Aug. 25 / 2100	27.0 N	-77.3 E	100 (51)

023	Aug. 26 / 0300	28.3 N	-77.3 E	100 (51)
024	Aug. 26 / 0900	29.3 N	-77.2 E	95 (49)
025	Aug. 26 / 1500	30.7 N	-77.3 E	90 (46)
026	Aug. 26 / 2100	31.7 N	-77.4 E	85 (44)
027	Aug. 27 / 0300	32.6 N	-76.9 E	85 (44)
028	Aug. 27 / 0900	34.1 N	-76.5 E	80 (41)
029	Aug. 27 / 1500	35.2 N	-76.4 E	75 (39)
030	Aug. 27 / 2100	36.2 N	-76.0 E	70 (36)
031	Aug. 28 / 0300	37.3 N	-75.4 E	70 (36)
032	Aug. 28 / 0900	39.2 N	-74.5 E	65 (33)

In addition to testing the sensitivity of the results to using the analytic forecast wind model, and to the variation from forecast to forecast, the variation in the track is also considered. To evaluate how the forecasts compare to the baseline, Figure 2.2 20 shows the peak water level at the 21 NOS stations for the forecast wind fields following the center of the hurricane cone (the actual forecasts as issued by the NHC). The statistics for the comparison are in Table 2.2 17 and show steady improvement as the forecast evolves. There is a big improvement between F021 and F022 as the extent of the intensity increase is reduced and landfall location shifts slightly. Beyond that there are minor adjustments between forecasts. The correlation and scatter index improve as the forecasts are issued indicating more reliable results. The RMSE also increases as the forecasts are issued. The MAPE reaches its lowest value with F029 but remains below 20% for all but the initial forecasts. The bias is interesting as it shifts from an under-prediction to an over-prediction as the forecast evolves. At the same time the forecast wind intensity is actually decreasing. This indicates that the subtle track changes may have a large influence on the storm surge results in order to overcome the decrease in the forecast intensity over time. The analytic model tends to err on the side of caution by outputting one-minute averaged winds which are slightly stronger than the ten-minute average winds produced by the re-analysis fields. This can lead to the positive bias in the results over the slight negative bias in the baseline simulation.

Figure 2.2-18 shows the forecast track for each advisory along with a track along the left extent of the NHC's forecast cone (http://www.nhc.noaa.gov/aboutcone.shtml) and a track along the right extent of the cone. Just like Hurricane Ike, the track for Irene is extremely well forecasted and there is little variation in the center forecast from advisory to advisory. The left track is over land for much of the simulation while the right track is offshore for much of the simulation providing a sharp contrast. While the track is forecasted extremely well, the intensity forecast does vary. Irene begins as a category 3 (100 kt ; 51 m/s) storm for the first day but slowly weakens prior to initial landfall down to a category 1 storm (75 – 80 kt; 39-41 m/s). After the initial landfall Irene weakens further to a very weak category 1 storm (65 kt; 33 m/s). Fortunately for the east coast the intensity of Irene did not follow the initial forecasts. Figure 2.2-19 shows the forecast intensity of Irene over time for each forecast advisory and the post-storm best track. Every advisory had Irene becoming more intense than what actually happened according to the best track. The initial forecast considered (020) had Irene as a strong category 3 borderline

category 4 hurricane on August 26. Subsequent forecasts continued to strengthen Irene even though the strengthening never occurred as forecasted.

To evaluate how the forecasts compare to the baseline, Figure 2.2-20 shows the peak water level at the 21 NOS stations for the forecast wind fields following the center of the hurricane cone (the actual forecasts as issued by the NHC). The statistics for the comparison are in Table 2.2-17 and show steady improvement as the forecast evolves. There is a big improvement between F021 and F022 as the extent of the intensity increase is reduced and landfall location shifts slightly. Beyond that there are minor adjustments between forecasts. The correlation and scatter index improve as the forecasts are issued indicating more reliable results. The RMSE also increases as the forecasts are issued. The MAPE reaches its lowest value with F029 but remains below 20% for all but the initial forecasts. The bias is interesting as it shifts from an under-prediction to an over-prediction as the forecast evolves. At the same time the forecast wind intensity is actually decreasing. This indicates that the subtle track changes may have a large influence on the storm surge results in order to overcome the decrease in the forecast intensity over time. The analytic model tends to err on the side of caution by outputting one-minute averaged winds which are slightly stronger than the ten-minute average winds produced by the re-analysis fields. This can lead to the positive bias in the results over the slight negative bias in the baseline simulation.

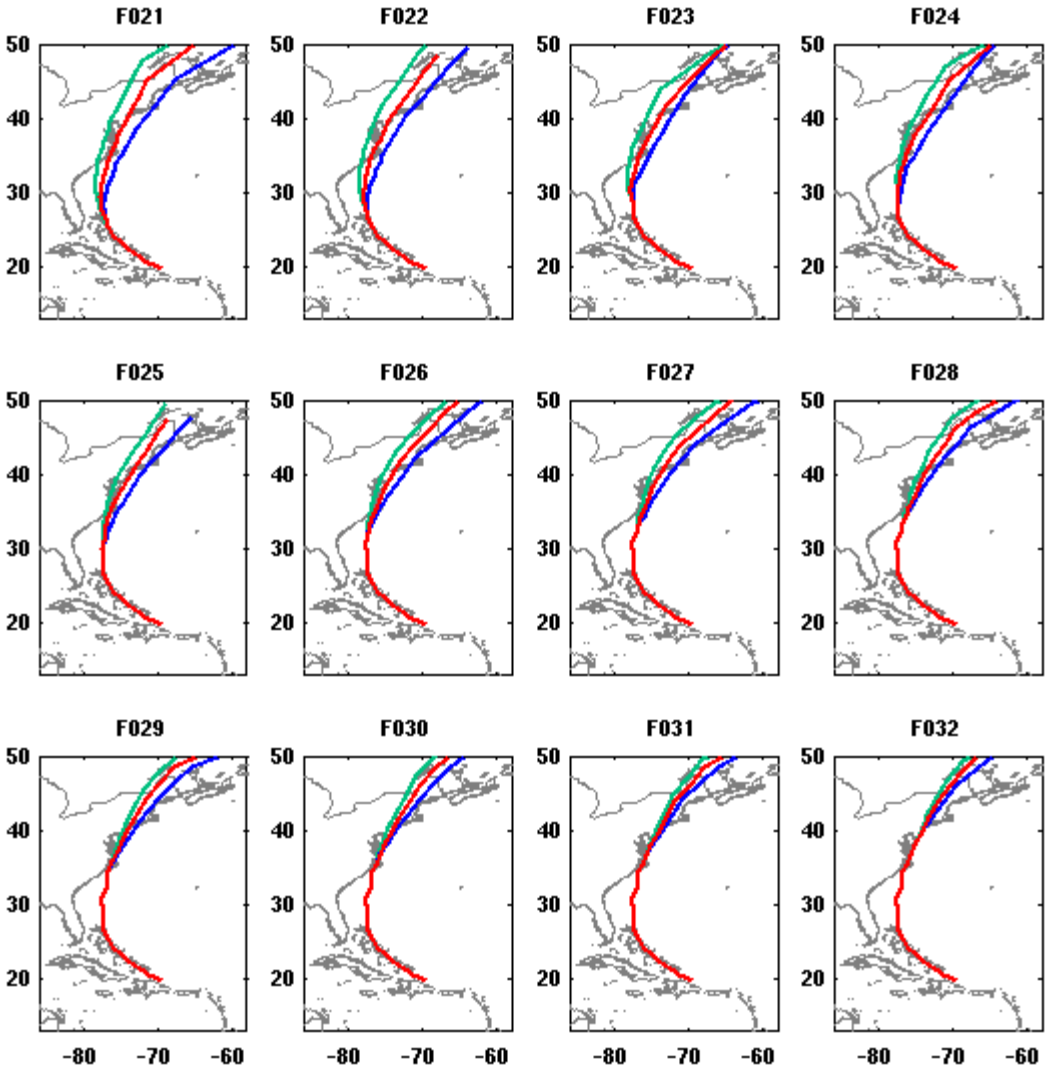

Figure 2.2-18: Forecast tracks for the 020 through 032 forecasts of Hurricane Irene depicting the left side of the NHC cone, right side and center.

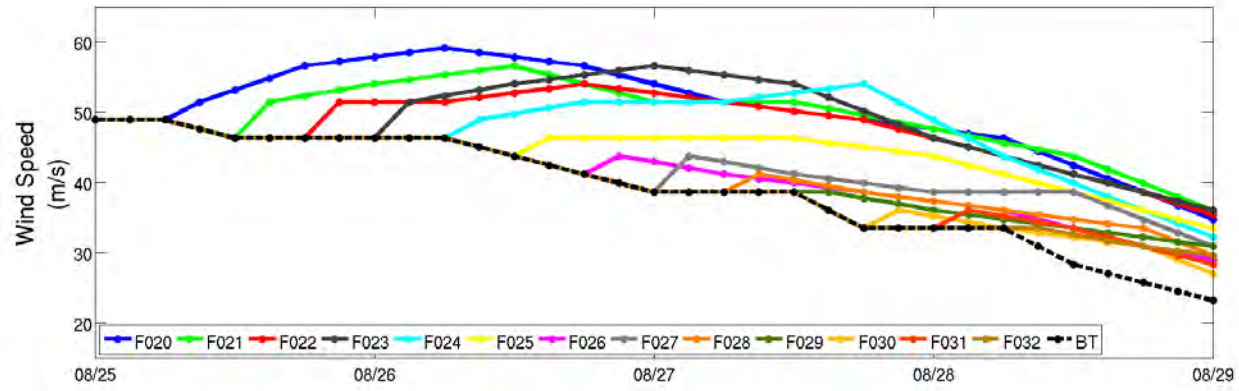

Figure 2.2-19: Changes in the forecast intensity of hurricane Irene for each forecast.

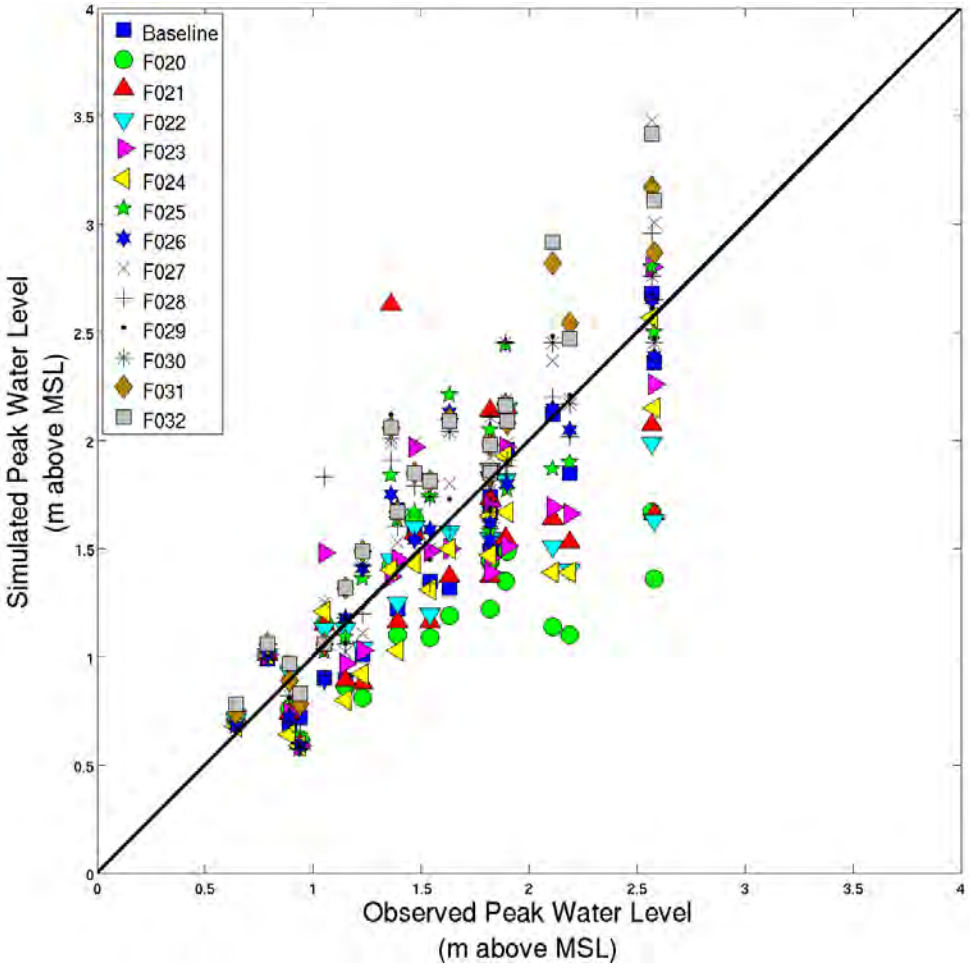

Figure 2.2-20: Peak water level at 21 NOS stations for center forecast runs.

Table 2.2-17: Statistics for the peak water level at the NOS stations for the baseline NY/DB/CB/OB/WJ domains and runs with analytic wind model and different forecasts.

	Baseline	F020	F021	F022	F023	F024	F025	F026	F027	F028	F029	F030	F031	F032
Corr r	0.90	0.48	0.43	0.64	0.74	0.78	0.80	0.85	0.88	0.80	0.84	0.84	0.91	0.91

Bias (m)	-0.12	-0.39	-0.15	-0.16	-0.09	-0.22	0.06	0.03	0.15	0.06	0.07	0.14	0.26	0.29
RMSE (m)	0.19	0.47	0.39	0.35	0.31	0.28	0.28	0.24	0.21	0.24	0.22	0.24	0.18	0.18
Scatter Index	12.96	40.46	27.55	25.10	20.89	20.91	16.67	14.91	12.46	14.86	13.39	14.18	9.71	9.70
MAPE	13.29	26.42	23.75	14.99	17.26	17.81	15.81	13.27	15.89	15.07	12.38	15.16	17.48	18.98

Table 2.2-18 and Figure 2.2-21 show the statistics and comparison between the baseline winds and the best track winds. Both are highly correlated with low RMSE, scatter index and MAPE. The biggest difference is the positive bias in the analytical winds and the negative bias in the re-analysis winds. The very good agreement between the simulated and observed peaks for the analytic wind model gives confidence in its continued use.

Table 2.2-18: Statistics for the peak water level at the NOS stations for the baseline NY/DB/CB/OB/WJ domains and runs with analytic wind model for best track.

	Baseline	Best Track
Corr r	0.90	0.88
Bias (m)	-0.12	0.20
RMSE (m)	0.19	0.20
Scatter Index	12.96	11.33
MAPE	13.29	15.74

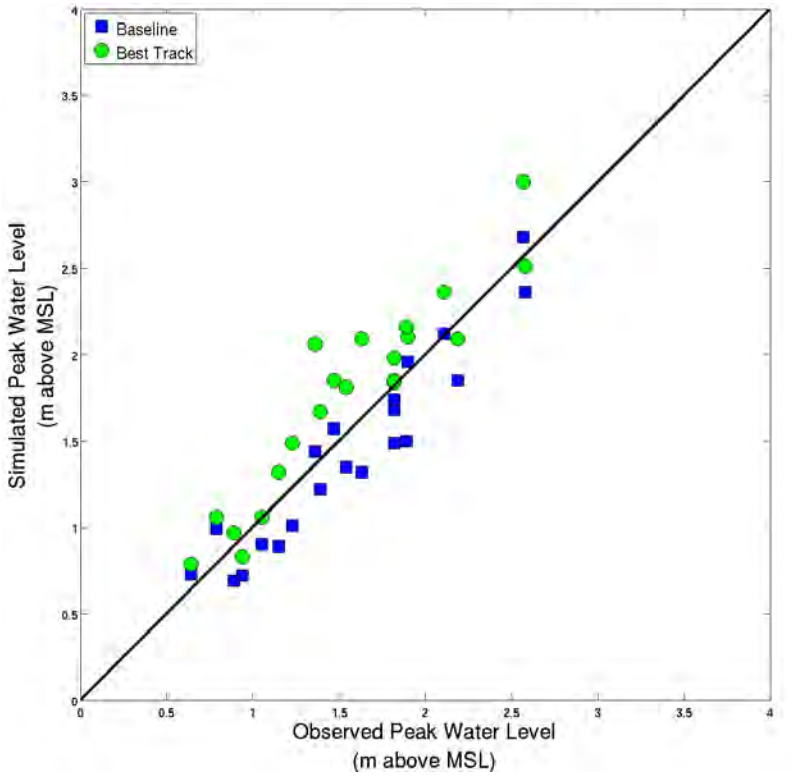

Figure 2.2-21: Peak water level at 21 NOS stations for the baseline simulation and the analytic winds from the best track.

With too many simulations and results to present in a plot, Table 2.2-19 shows the statistics for each forecast advisory run using the track along the center, left, and right of the forecast cone. For the later forecasts there is little variation since the cone is very narrow. However the earlier forecasts show much greater variation. In these simulations the left track, which is mostly over land, produces large errors. The right track which is much further out to sea is closer to the center track but tends to underestimate since the storm is much further from the shore. Between F029 and F030 the right simulation shows much improvement and begins to closely resemble the center simulation. This corresponds with a slight westward shift in the track and a decrease in the forecast intensity. From F031 on the tracks are very close to one another, yielding similar results.

Table 2.2-19: Statistics for the peak water level at the NOS stations for the baseline NY/DB/CB/OB/WJ domains and runs with analytic wind model for each forecast and the corresponding Center, Left, and Right track.

F020	Center	Left	Right	F021	Center	Left	Right
Corr r	0.48	0.21	0.36	Corr r	0.43	0.00	0.50
Bias (m)	-0.39	0.18	-0.37	Bias (m)	-0.15	-0.20	-0.31
RMSE (m)	0.47	0.37	0.48	RMSE (m)	0.39	0.62	0.42
Scatter Index	40.46	21.19	40.52	Scatter Index	27.55	45.96	33.63
MAPE	26.42	58.29	32.37	MAPE	23.75	41.80	27.94

F022	Center	Left	Right	F023	Center	Left	Right
Corr r	0.64	0.01	0.61	Corr r	0.74	0.01	0.52
Bias (m)	-0.16	-0.10	-0.22	Bias (m)	-0.09	0.03	-0.20
RMSE (m)	0.35	0.61	0.38	RMSE (m)	0.31	0.62	0.43
Scatter Index	25.10	41.52	28.11	Scatter Index	20.89	38.87	31.35
MAPE	14.99	45.46	25.33	MAPE	17.26	49.07	27.33
F024	Center	Left	Right	F025	Center	Left	Right
Corr r	0.78	0.00	0.32	Corr r	0.80	0.08	0.39
Bias (m)	-0.22	-0.10	-0.29	Bias (m)	0.06	0.16	-0.11
RMSE (m)	0.28	0.63	0.52	RMSE (m)	0.28	0.59	0.49
Scatter Index	20.91	42.88	40.86	Scatter Index	16.97	34.19	33.64
MAPE	17.81	38.99	31.87	MAPE	15.81	38.96	28.59
F026	Center	Left	Right	F027	Center	Left	Right
Corr r	0.85	0.13	0.52	Corr r	0.88	0.42	0.60
Bias (m)	0.03	0.09	-0.18	Bias (m)	0.15	0.12	0.04
RMSE (m)	0.24	0.56	0.39	RMSE (m)	0.21	0.45	0.38
Scatter Index	14.91	34.16	28.48	Scatter Index	12.46	26.45	23.65
MAPE	13.27	34.02	24.56	MAPE	15.89	25.71	25.61
F028	Center	Left	Right	F029	Center	Left	Right
Corr r	0.80	0.49	0.61	Corr r	0.84	0.54	0.68
Bias (m)	0.06	0.00	-0.08	Bias (m)	0.07	0.12	0.03
RMSE (m)	0.24	0.40	0.38	RMSE (m)	0.22	0.34	0.33
Scatter Index	14.86	25.75	25.50	Scatter Index	13.39	20.36	20.89
MAPE	15.07	20.30	22.07	MAPE	12.38	19.74	18.62
F030	Center	Left	Right	F031	Center	Left	Right
Corr r	0.84	0.74	0.83	Corr r	0.91	0.84	0.90
Bias (m)	0.14	0.18	0.11	Bias (m)	0.26	0.27	0.27
RMSE (m)	0.24	0.30	0.25	RMSE (m)	0.18	0.20	0.19
Scatter Index	14.18	17.35	14.73	Scatter Index	9.71	11.06	10.34
MAPE	15.16	18.37	14.62	MAPE	17.48	18.96	17.86

F032	Center	Left	Right
Corr r	0.91	0.90	0.91
Bias (m)	0.29	0.28	0.30
RMSE (m)	0.18	0.19	0.18
Scatter Index	9.70	10.17	9.91
MAPE	18.98	18.59	19.27

2.2.11 Conclusions

Validation of the CSIPS for hindcast simulations of Hurricane Irene along with sensitivity studies has been presented. The baseline simulations show very good agreement between the

simulated and observed peak water levels at a number NOAA tide gauges along the East Coast. There is some variation in the results depending on domain resolution, but the end product of the high resolution domains shows great agreement with observations. The high resolution domains also do a good job predicting the inundation when compared to HWMs. When the input wind field is good, the wave results compare very well with the buoy observations in all domains.

Similar to the studies of Hurricane Ike presented earlier, sensitivity studies examining the influence of the bathymetry, wave coupling, bottom roughness, wind field, and track were conducted. Overall there is sensitivity to each component, but the results from this storm in this basin were not nearly as sensitive as those for Hurricane Ike in the Gulf of Mexico. The results are most sensitive to the elevation dataset. Whenever possible a high resolution coastal dataset should be used. When this data is not available careful consideration of the desired output must be taken. A coarse dataset like GEBCO performs admirably offshore but not so well when trying to capture processes very near to shore, especially in the coarse domain. The coarseness often leads to placing cells that should have a negative elevation (wet cells) on land with a positive elevation leading to errors in the output. The influence of the wave coupling and use of a constant bottom roughness coefficient were much milder than the elevation influence. These two components had little impact on the simulation results. The wind on the other hand is a key component. Accurate forecasts and representations of the wind field are essential. The Condon and Veeramony (2014) model performed very well when given good input (the Best Track). Slight adjustments in the forecast track can change the simulation results dramatically. With this in mind it is recommended that multiple forecast tracks be generated and simulated to provide a range of expectations and to better prepare for the worst case scenario.

2.3 Super Typhoon Pongsona

For an evaluation of CSIPS in predicting surge and inundation world-wide, the system was used to evaluate the impacts to Guam due to Super Typhoon Pongsona. Pongsona impacted Guam on December 8, 2002 as an intense Super Typhoon. It was one of the most devastating typhoons to ever impact the island (NOAA 2003a). Winds on the island reached 64 m/s and barometric pressure readings were as low as 935 mb. Impacts included more than $700 million in damages and at least one death.

The storm originated east of Pohnpei on December 2, 2002 and began moving westward (NOAA 2003b). It passed just north of Pohnpei on December 5, 2002 and was upgraded to a typhoon on December 6, 2002 and headed toward the Marhsall Islands. Pongsona eventually made a turn to the north with the center of its eye passing within 20 km of Guam. The island was immersed in the southwestern semicircle of the storm, experiencing heavy rainfall and high winds. After passing over Guam the storm moved on a northwestward course, hitting Rota before re-curving to the northeast and weakening. The major impacts to Guam were from wind and rain, but a NOS tide gauge on the western side of the island did record a storm surge.

To simulate the surge and inundation two domains were used. For this study a large scale domain similar to that used in the Ike and Irene studies featuring 0.1° spacing was not used. Due to the small size of the area of interest and the absence of a continental shelf or any other gentle sloping bathymetric features a 0.02° domain and a 0.004° domain were used. The 0.02° domain features 160,801 cells (401 x 401) and covers 142° E to 150° E and 10° N to 18° N centered around Guam (Figure 2.3-1). The simulation runs from 00:00 UTC on December 5, 2002 through 00:00 UTC December 11, 2002. The finer domain features 90,601 cells (301 x 301) covering from 144.25° E to 145.45° E and 12.75° N to 13.95° N and was run from 00:00 UTC on December 6, 2002 until 00:00 UTC on December 11. Pongsona enters the 0.02° domain around 18:00 UTC on December 6, 2002 and the fine domain around 03:00 UTC on December 8, 2002 exiting that domain around 09:00 UTC on the same day and the 0.02° domain at 12:00 UTC on December 9. The bathymetry and topography are plotted in Figure 2.3-2 along with the track of Pongsona and the location of the observations. The bathymetry and topography is derived from the GEBCO elevation dataset. The Apra Harbor, Guam NOS water level gauge (Station 1630000) is the only water level gauge available. This gauge is located on the western side of the island and is sheltered from the brunt of the storm. NOS does offer tidal predictions in Pago Bay on the

eastern side of the island for the time period of interest as well (depicted as an orange triangle in Figure 2.3-2(b)).

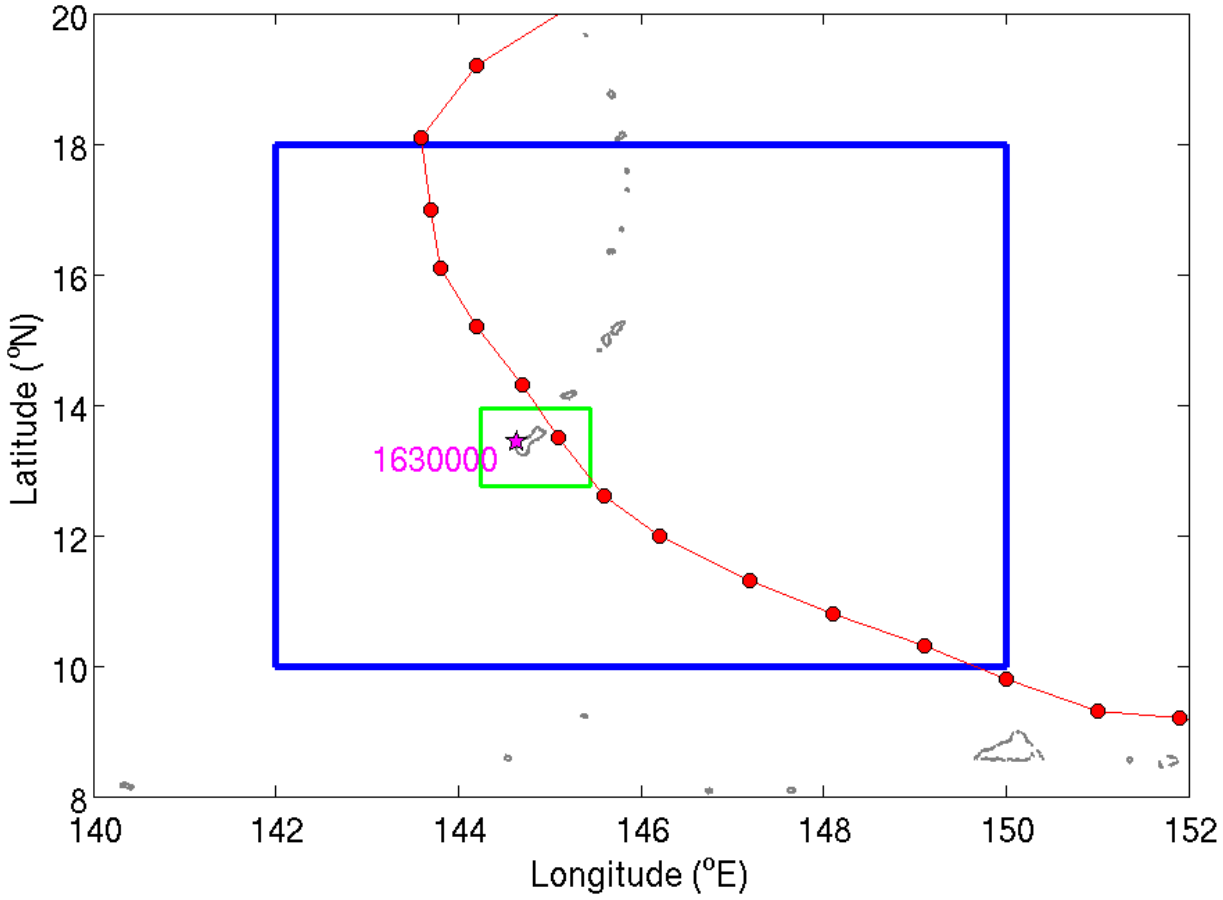

Figure 2.3-1: Domains for Typhoon Pongsona storm surge study. 0.02° domain in blue and 0.004° domain in green along with NOS station 1630000 and the typhoon track.

(a)

(b)

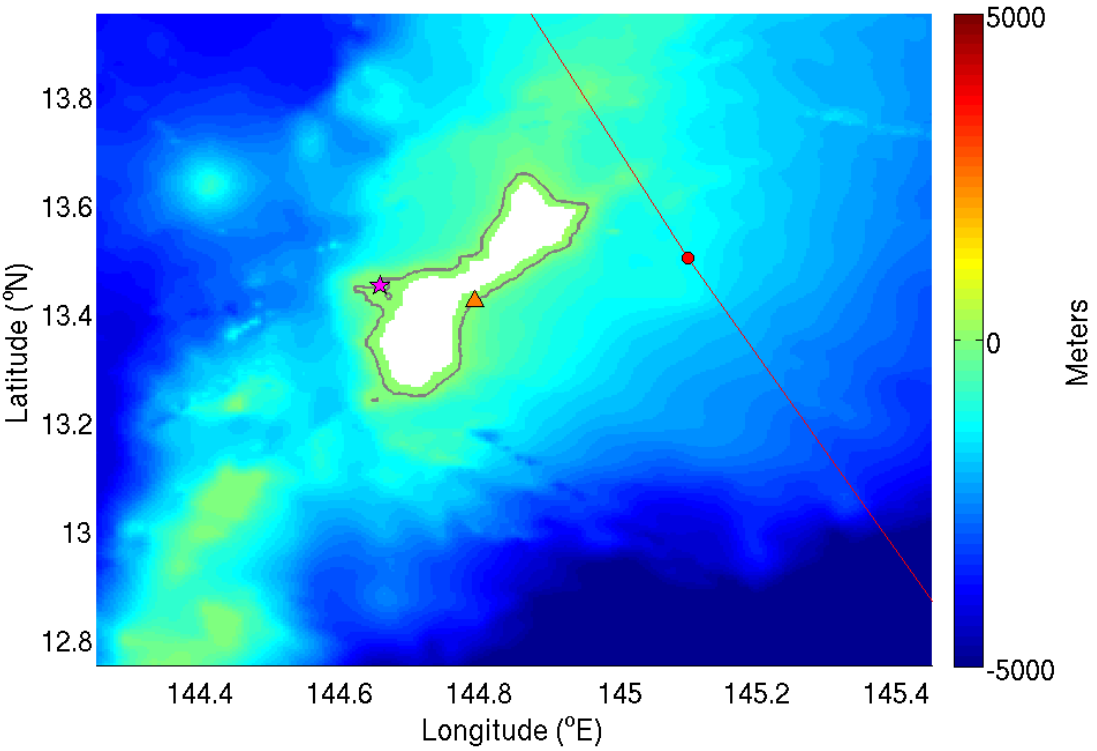

Figure 2.3-2: Bathymetry and topography of the 0.02° (a) and 0.004° (b) domains used in Pongsona studies Purple star indicates NOS water level station 1630000, orange triangle in (b) indicates location of NOS predicted tides station 1631428.

For this study CSIPS is run with no calibration. The setup involves using the GEBCO dataset for elevation data, the Condon and Veeramony (2014) wind model, the air-sea drag coefficient of Zijlema et al. (2012), a constant Manning's N coefficient of 0.02 over water, and 0.075 over land and wave coupling. The simulated results are compared to the NOS water level station in Apra Harbor in Figure 2.3-3. The gauge measured a peak surge of 0.59 m which was half a meter greater than the predicted level of 0.08 m. The observed and predicted water levels at the NOS tide gauge as well as the CSIPS simulated values are shown in the plot and statistics are presented in Table 2.3-1. Notice that the peak surge occurs during ebb tide, likely saving Guam from further flooding. CSIPS over predicts the water level by about 10 cm and misses the timing of the peak by under 2 hours. There is a slight positive bias to the simulated results and the 1.8 hour error in the timing of the peak appears to be at least partly due to a consistent phase shift in the simulated tides with simulated highs and lows occurring an hour or so after observations. Although the Pago Bay water level station (1631428) did not record water level at the time of the event, tidal predictions are available. Figure 2.3-4 shows the predicted value compared to the CSIPS simulated value. Again there appears to be a persistent phase shift between the simulated peak tides and the predicted levels of about one hour. CSIPS predicts a peak water level of 0.83 m which is about 70 cm above the expected water level according to the predictions. Figure 2.3-5 shows a spatial distribution of the peak water levels in and around Guam. The highest water level is confined to the small coastal bays and right along the typhoon path. The tidal signal is also

shown in the peak water levels with the passing of the storm by the north coast of Guam coinciding with a local minimum in the tides.

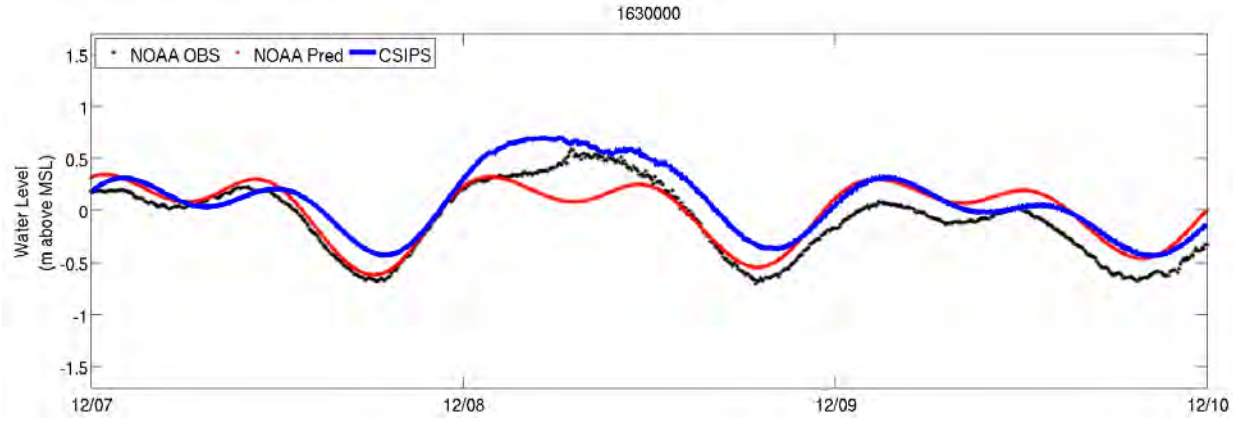

Figure 2.3-3: Observed, predicted, and simulated water levels at Apra Harbor, Guam during Typhoon Pongsona.

Table 2.3-1: Statistics of the hydrograph analysis for Apra Harbor Guam during Typhoon Pongsona.

	NOS ID	1630000
Mean Condition	**Observed (m)**	0.13
	Simulated (m)	0.28
	Bias (m)	0.15
	Absolute Error (m)	0.16
	RMS Error (m)	0.11
	Scatter Index	40.74
Linear Regression Estimators	**Correlation Coef (r)**	0.66
	Symmetric (r)	1.28
	Slope (a)	0.92
	Intercept (b)	0.16
	RMSE-SS	0.61
	Observed Peak (m)	0.59
	Simulated Peak (m)	0.69
	Peak Percent Error	17.63
	Error in Peak Timing (hr)	-1.80
	Number of Observations	454

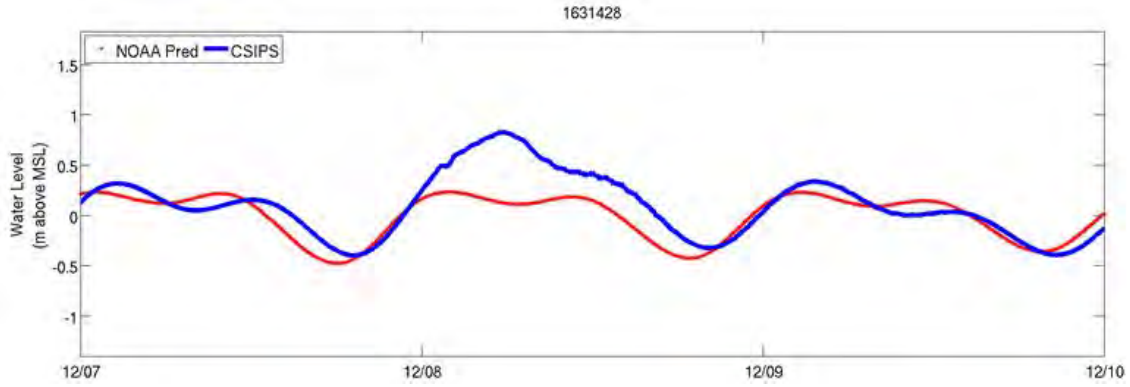

Figure 2.3-4: CSIPS simulated water level at Pago Bay, Guam during December 2002, compared to NOS predicted water level.

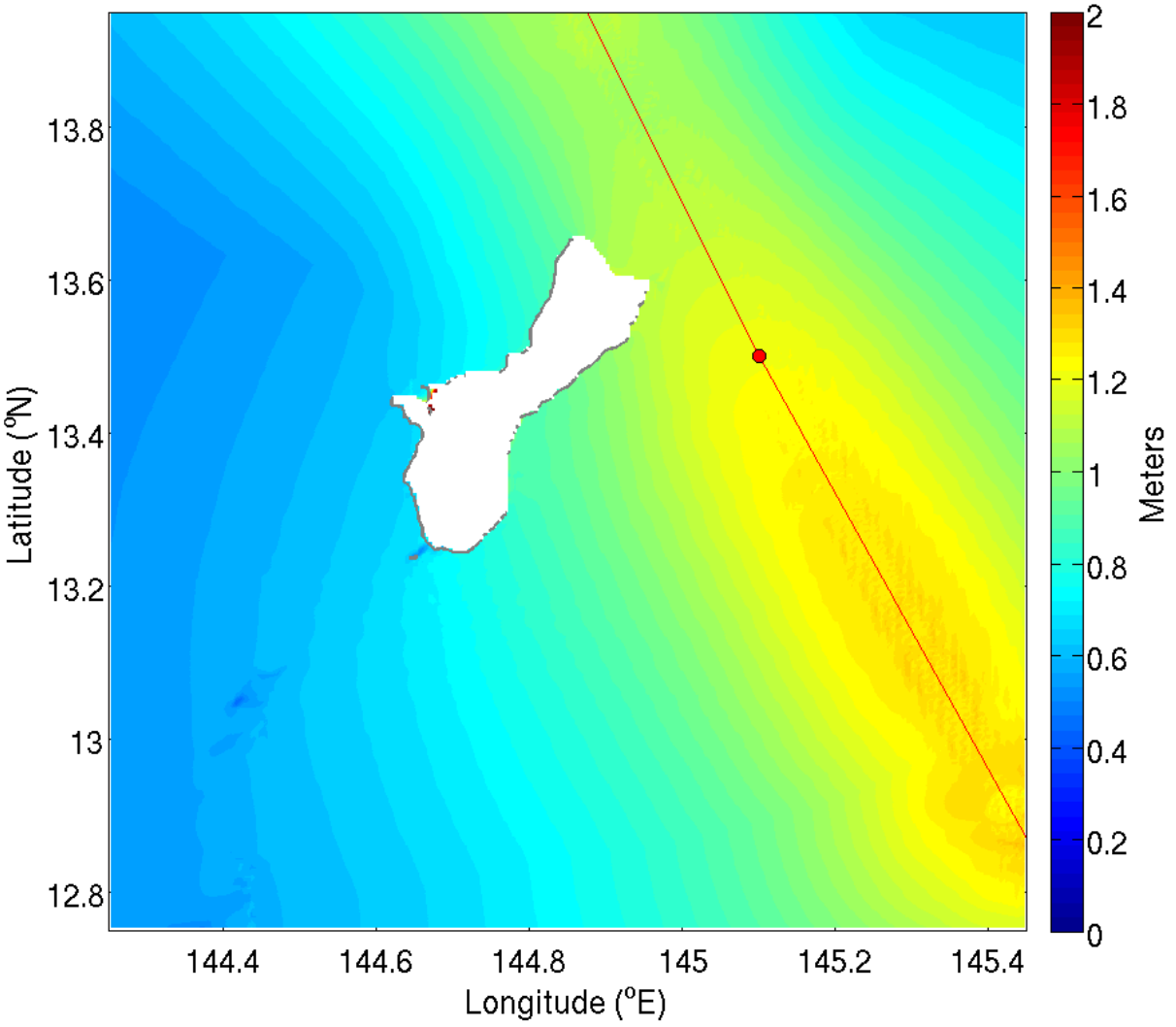

Figure 2.3-5: Maximum water levels around Guam throughout the passage of Typhoon Pongsona.

2.3.1 Summary

CSIPS was used to predict the storm surge and inundation from Typhoon Pongsona which impacted the island of Guam in early December 2002. The storm surge impact was minimal and measured 0.59 m at NOS station 1630000. CSIPS predicts the peak water level reasonably well at this station using the 'most likely' setup that was previously applied to Hurricanes Ike and Irene. There is a persistent bias in the timing of the surge and in the water level. The simulations tend to predict high and low tides up to an hour after when they actually occur. This could likely be resolved by better calibration of the tidal signal, but this is not reasonable in a tight forecast window. With no calibration CSIPS does well at predicting the peak water level elevation within 18% of the recorded value and in predicting the timing of the peak within 2 hours of the actual peak.

3 OPERATIONAL IMPLEMENTATION

After review of the sensitivity studies for Hurricanes Ike and Irene, a general guidance was developed given the constraints of the forecast environment. In the absence of high resolution bathymetry and topography data, the GEBCO dataset should be used. Wave coupling should be included and the bottom roughness Manning's N coefficient will have a constant value of 0.02 in the absence of land use data. After review of the wind fields, the drag coefficient formulation of Zijlema et al. (2012) is adopted.

Following these recommendations a "most likely" simulation for each forecast was carried out. These follow the above guidance along with the official NHC forecast track for forecast 40 -48 (Ike) and 20 – 32 (Irene). These results represent what would likely be obtained in a forecast environment in the absence of higher quality data.

3.1 Most Likely Forecast Run – Hurricane Ike

Figure 3.1-1 and Table 3.1-1 show the peak water level at the 7 NOS stations and the corresponding statistics. As was the case in the sensitivity studies, there is a noticeable improvement as the forecasts progress and the final MAPE is under 15%. In all cases there is a negative bias. Although the bias does diminish with progressing forecasts, it is still present at the last forecast. The RMSE is high throughout the forecast although it does improve. With peak elevations of up to 4 m, an RMSE of 0.49 m is not too high, but could be improved with better data as in the baseline simulation. The hydrographs in Figure 3.1-2 show the simulated versus observed water levels at the 7 NOS stations for the final forecast (044). From these plots part of the reason for the poorer results in capturing the peak water level becomes obvious. Both stations 8768094 and 8770570 have poorly represented bathymetry. They are both located in dry cells that only become flooded as the hurricane comes near. The tidal signal is not felt at either station. In fact the GEBCO bathymetry does not resolve Calcasieu Lake at all, leading to little chance of an accurate representation of the water levels at station 8768094. To highlight the discrepancy in the simulated and actual bathymetry and topography Table 3.1-2 shows the NOAA reported depths at the recording stations and the depths in the model. Those two stations have negative

depths (negative depths means they are on land or positive elevation) where the others are more representative of the actual station locations. This highlights the need for good elevation data.

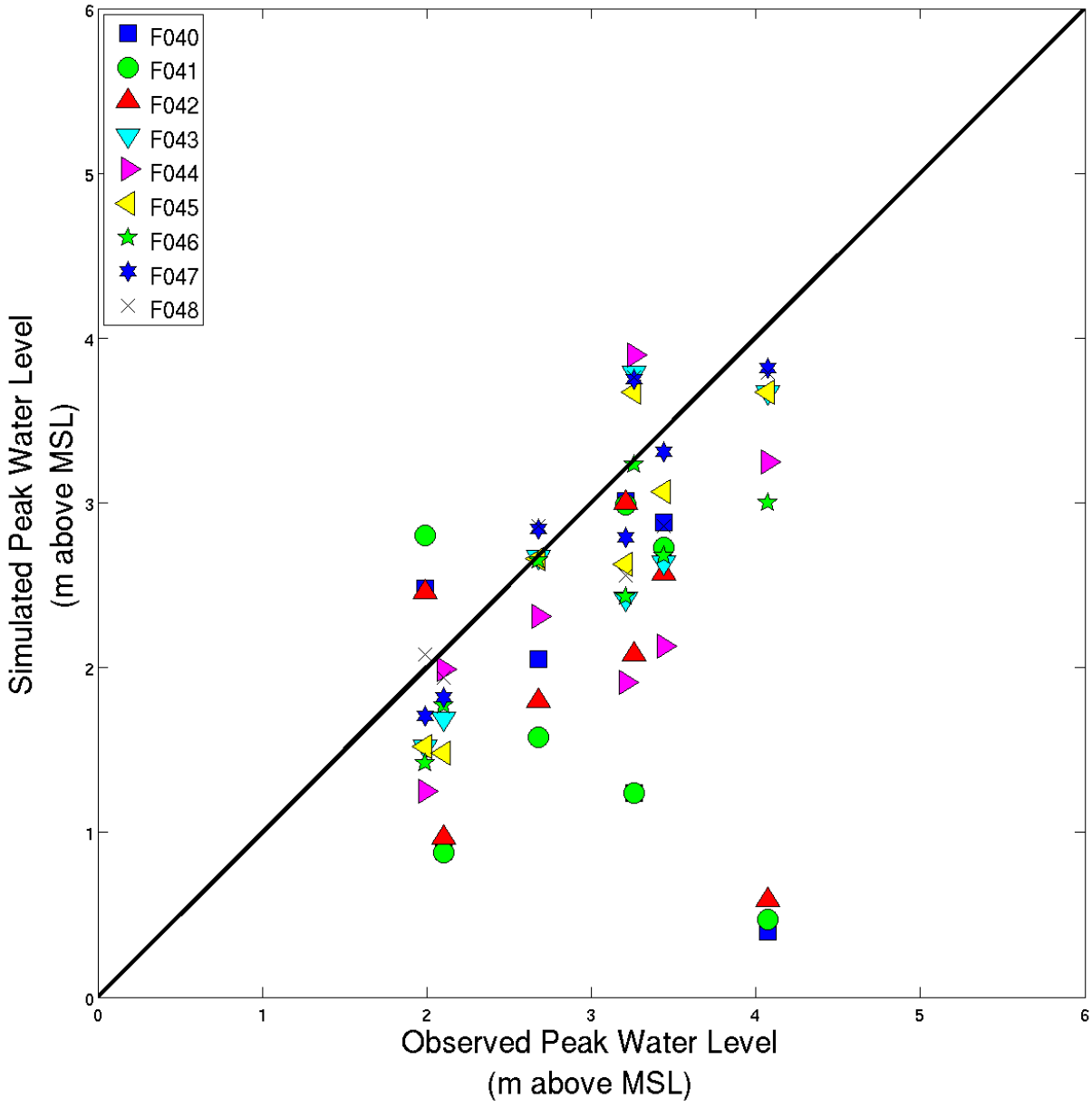

Figure 3.1-1: Peak water level results at 7 NOS stations for most likely Hurricane Ike runs .

Table 3.1-1: Peak water level results at 7 NOS stations for Hurricane Ike most likely forecast runs.

	F040	F041	F042	F043	F044	F045	F046	F047	F048
Corr r	0.03	0.05	0.02	0.72	0.43	0.84	0.72	0.86	0.71
Bias	-1.11	-1.15	-1.04	-0.34	-0.57	-0.29	-0.51	-0.10	-0.13
RMSE	0.88	0.88	0.91	0.49	0.69	0.36	0.48	0.33	0.49
Scatter Index	47.81	48.53	47.09	18.66	28.69	13.46	19.73	11.54	17.45

MAPE	40.06	45.39	37.69	16.78	24.94	15.02	17.01	10.20	11.17

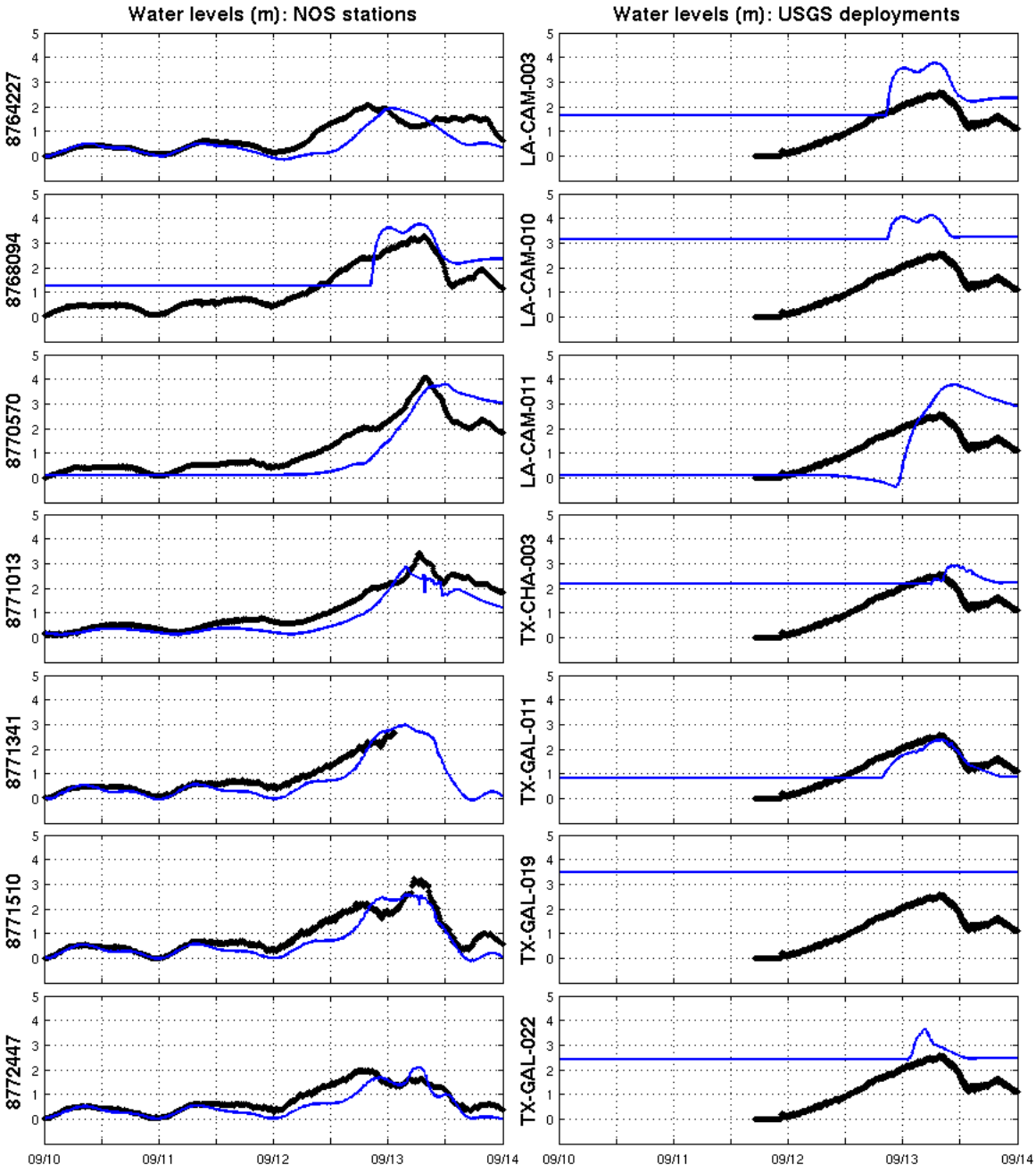

Figure 3.1-2: Hydrographs for forecast 044 for Hurricane Ike with observations in black and simulated results in blue.

Table 3.1-2: GEBCO and published depth (m, MSL) of the 7 NOS stations.

Station ID	Location	Station Depth (m, MSL)	Simulated Depth (m, MSL)
8764227	Armeda Pass, LA	7.42	1.01
8768094	Calcasieu Pass, LA	8.55	-1.24
8770570	Sabine Pass North, TX	1.34	-0.17
8771013	Eagle Point, TX	1.47	1.68
8771341*	Galveston Bay North Jetty, TX	3.07	5.71
8771510	Galveston Pleasure Pier, TX	1.40	3.96
8772447	USCG Freeport, TX	8.72	5.41

Figure 3.1-2 also shows the agreement between the timing of the simulated and observed peaks. The timing appears close for all stations. For the stations on the ends of the domain (8764227 and 8772447) the simulated peak occurs a few hours after the observed. But for the stations located closer to the landfall location and in the area of the peak surge the timing is within an hour or two.

The inundation extent can be estimated both quantitatively (Figure 3.1-3 and Table 3.1-3) and qualitatively (Figure 3.1-4). The HWM analysis in Figure 3.1-3 shows that the simulated results are somewhat scattered. This is shown in the correlation coefficient in Table 3.1-3. There is improvement with the nesting as expected. The MAPE is high for all levels but does drop from nearly 36% in the coarse grid to just under 23% in the high resolution domains although the RMSE remains virtually unchanged. In comparison to the published estimates of inundation extent, the simulated results miss much of the inundation southwest of Galveston Bay and along the Bolivar Peninsula. It does a better job of capturing the inundation in and around Sabine Lake and the Texas/Louisiana border. The underestimation of the inundation along the Bolivar Peninsula is likely due to the misrepresentation of the elevation there. An examination of the hydrograph at Galveston Pleasure Pier shows an underestimate of the peak of over half a meter. The same wind field, with the baseline bathymetry and spatially varying Manning's N coefficient produced a simulated inundation within 20 cm of the observed peak. Since this station is at the end of pier and the influence of the spatially varying Manning's N is small, the bathymetry can

be attributed with the discrepancy. The other trouble area is around Calcasieu Lake, which was discussed earlier. Since the Lake is not resolved, errors in the inundation are high around it.

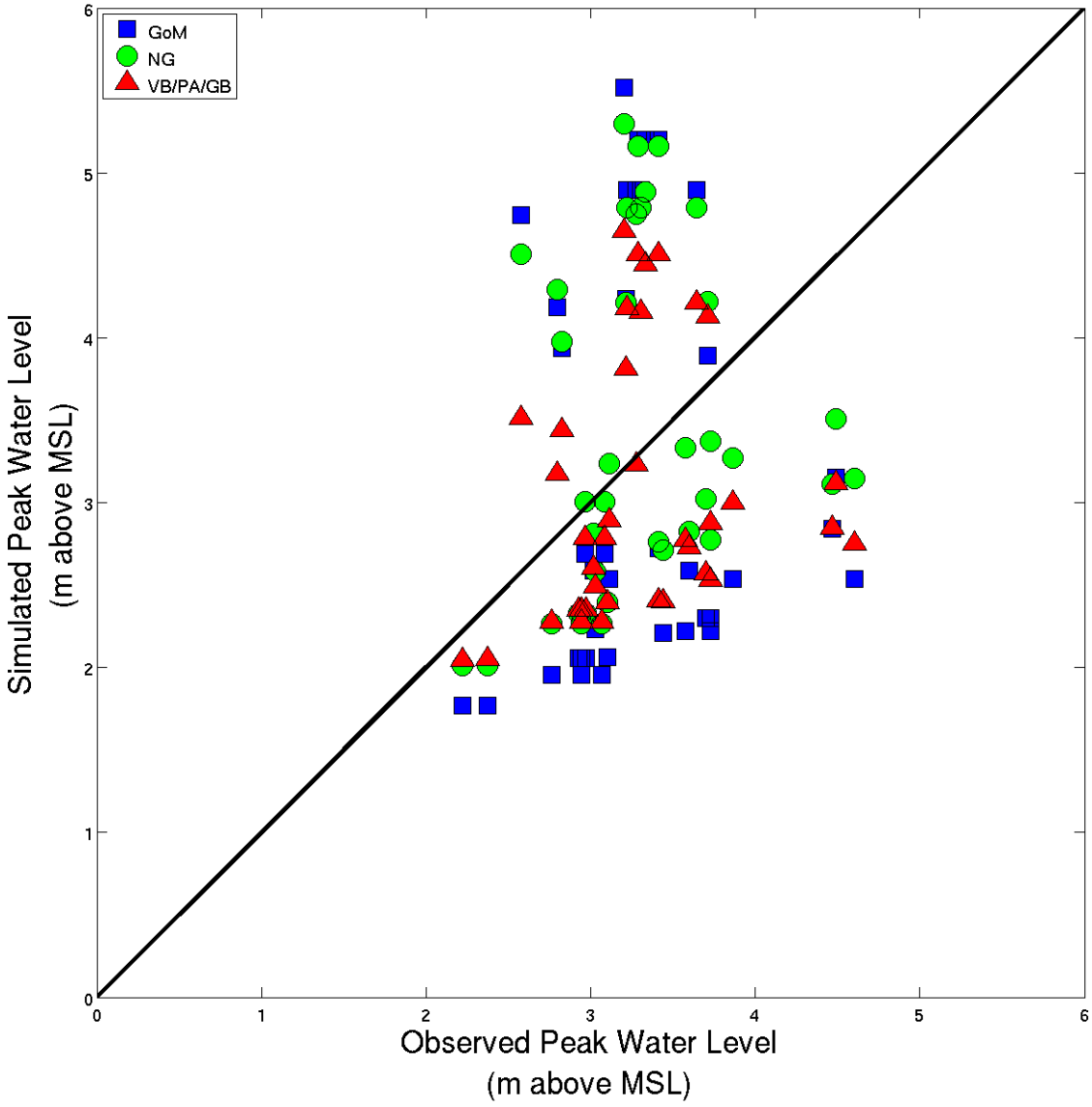

Figure 3.1-3: HWM analysis for 044 forecast run for each nest of Hurricane Ike simulation.

Table 3.1-3: Statistics for HWM analysis of Hurricane Ike forecast 044 run.

	GoM	NG	VB/PA/GB
Corr r	0.01	0.04	0.04
Bias	-0.14	0.12	-0.24
RMSE	0.48	0.47	0.47
Scatter Index	15.34	13.89	15.56
MAPE	35.96	27.18	22.82

Hurricane Ike Inundation Depth

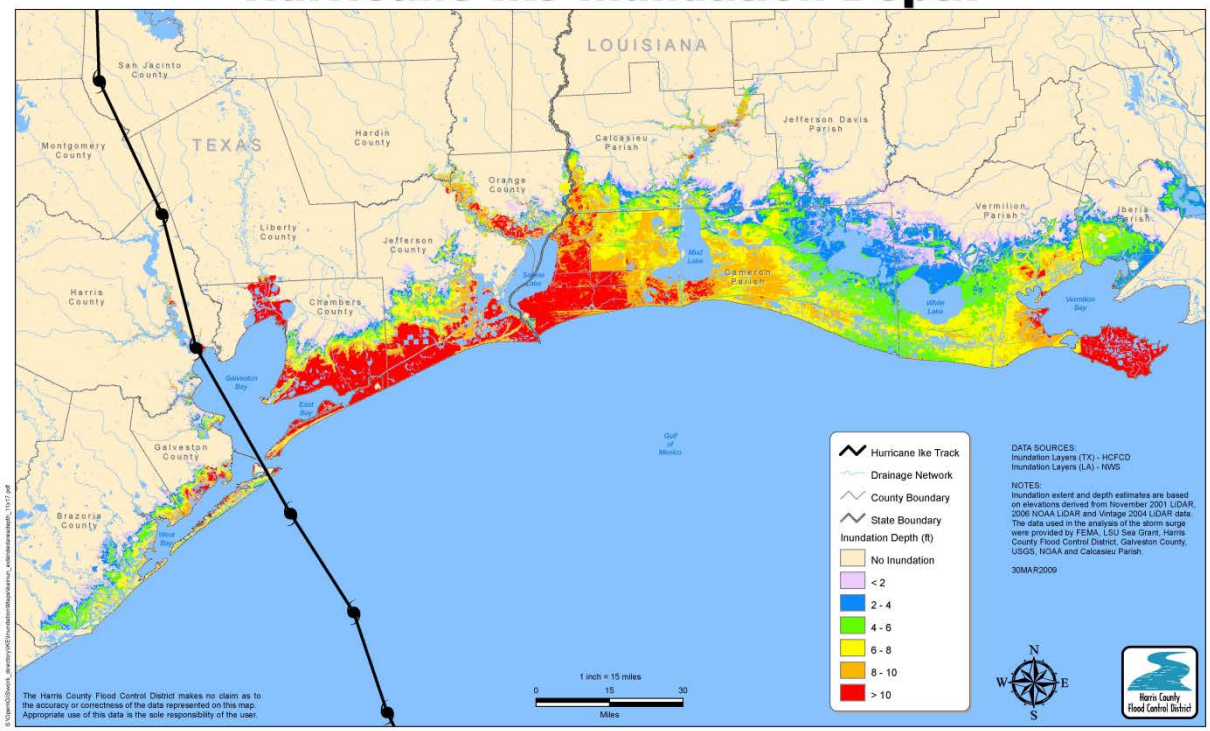

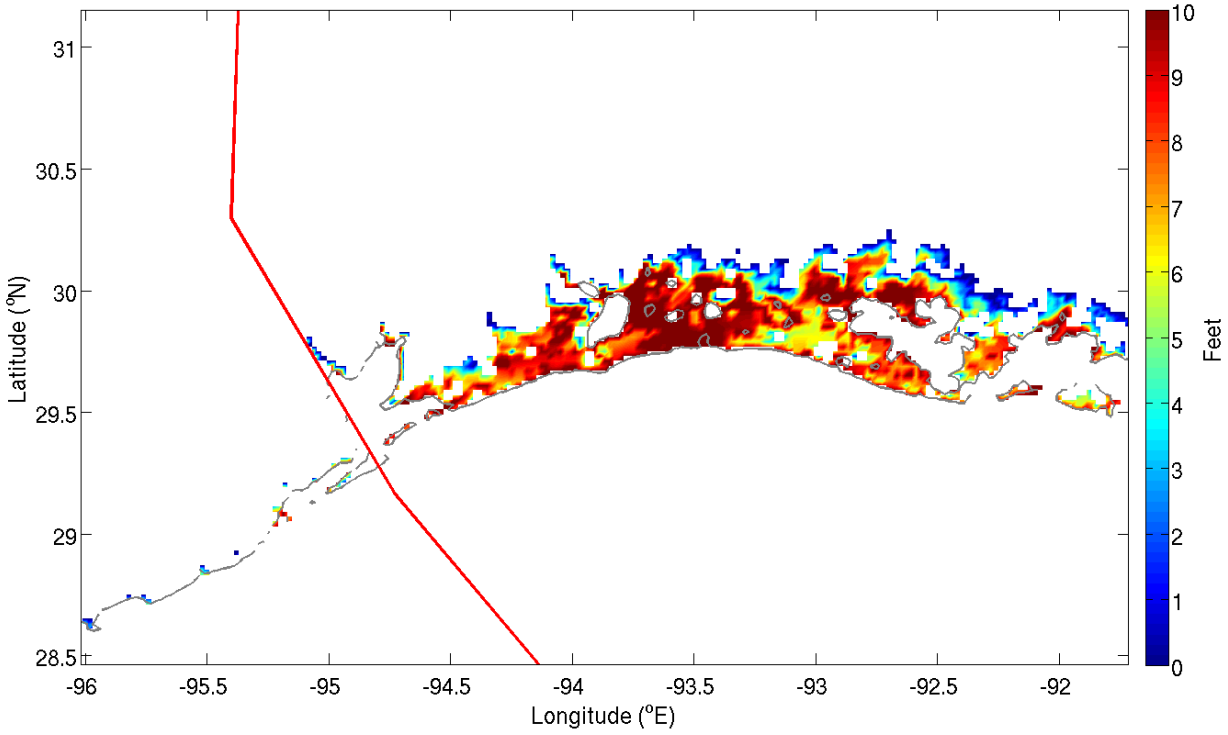

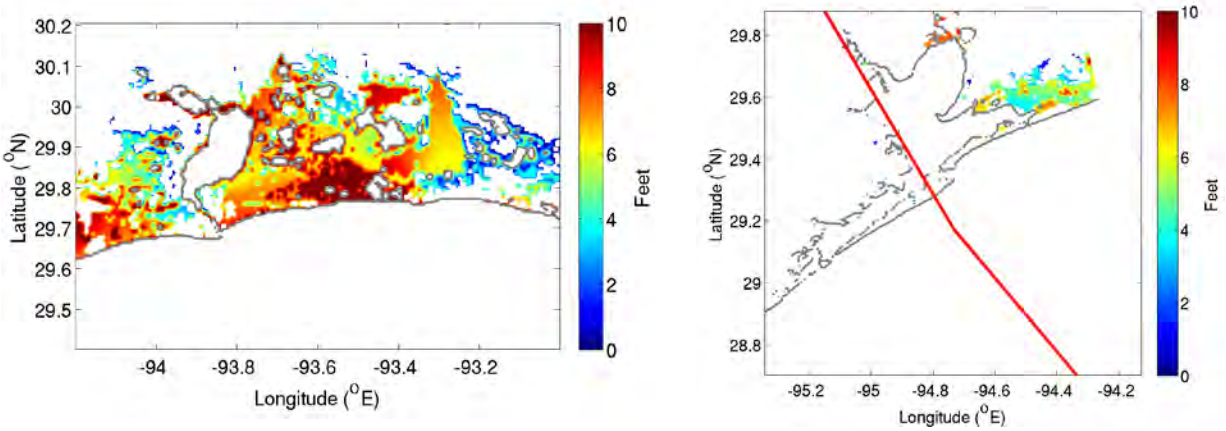

Figure 3.1-4: Estimated observed inundation extent compared with simulated extents for forecast 044.

3.2 Most Likely Forecast Run – Hurricane Irene

The thirteen forecasts runs for Hurricane Irene were also run using the most likely inputs. Figure 3.2-1 shows the peak water levels at the 21 NOS stations for each forecast run. The statistics for these runs are summarized in Table 3.2-1. For all of the runs the observed and simulated water levels are correlated and in general become more strongly correlated as the forecasts progress. The bias in the simulations also improves as the simulations progress from a negative value of half a meter to a small positive value of six centimeters. The RMSE improves as well but is around 0.3 m for all the simulations with a little variation in either direction. The scatter index percent decreases as the forecasts progress and the MAPE also decreases. The final forecast features a mean absolute percent error of just over 16% for the NOS stations. By examining the hydrographs in Figure 3.2-2, it is seen that the Wilmington, NC station is well off but most other stations are fairly well represented. The reason for Wilmington being so far off is the bathymetry in the area. The recording station is located up a channel in a region that is not well resolved in the GEBCO dataset. With the exception of this station there is good agreement between the

simulated and observed results both in terms of capturing the height and timing of the peak surge.

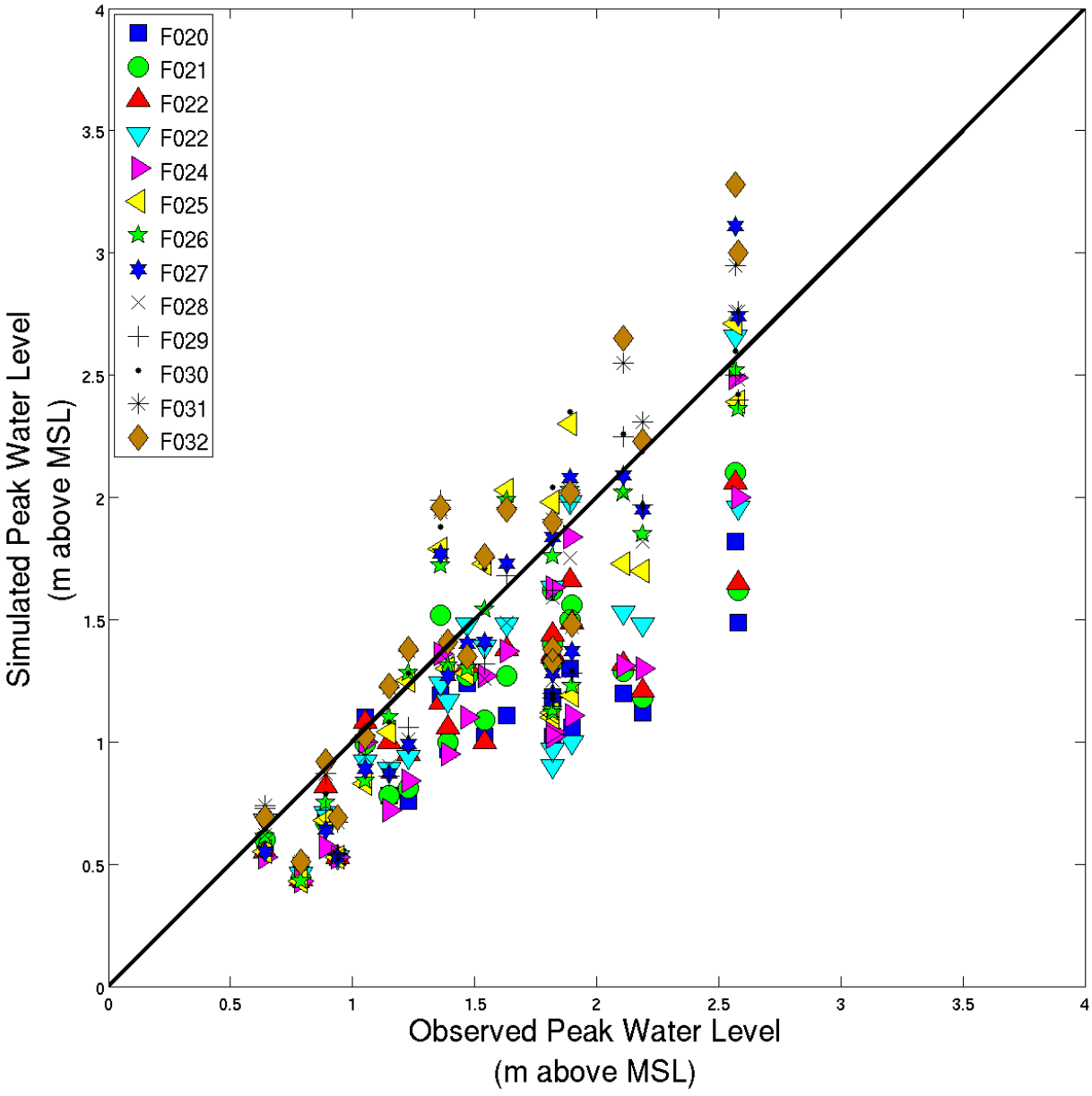

Figure 3.2-1: Peak water level results at 21 NOS stations for most likely Hurricane Irene runs.

Table 3.2-1: Peak water level results at 21 NOS stations for Hurricane Irene most likely forecast runs.

	F020	F021	F022	F023	F024	F025	F026	F027	F028	F029	F030	F031	F032
Corr r	0.74	0.75	0.79	0.68	0.75	0.70	0.76	0.84	0.81	0.77	0.73	0.82	0.82
Bias	-0.53	-0.39	-0.38	-0.32	-0.40	-0.15	-0.16	-0.12	-0.20	-0.15	-0.06	0.03	0.06
RMSE	0.30	0.24	026	0.35	0.30	0.33	0.30	0.22	0.21	0.27	0.32	0.24	0.25

Scatter Index	29.60	20.59	22.17	28.25	26.07	23.58	21.72	15.75	15.63	18.98	21.67	15.07	15.33
MAPE	32.45	25.51	23.43	22.00	26.29	21.24	16.98	18.11	18.59	17.73	17.09	15.38	16.13

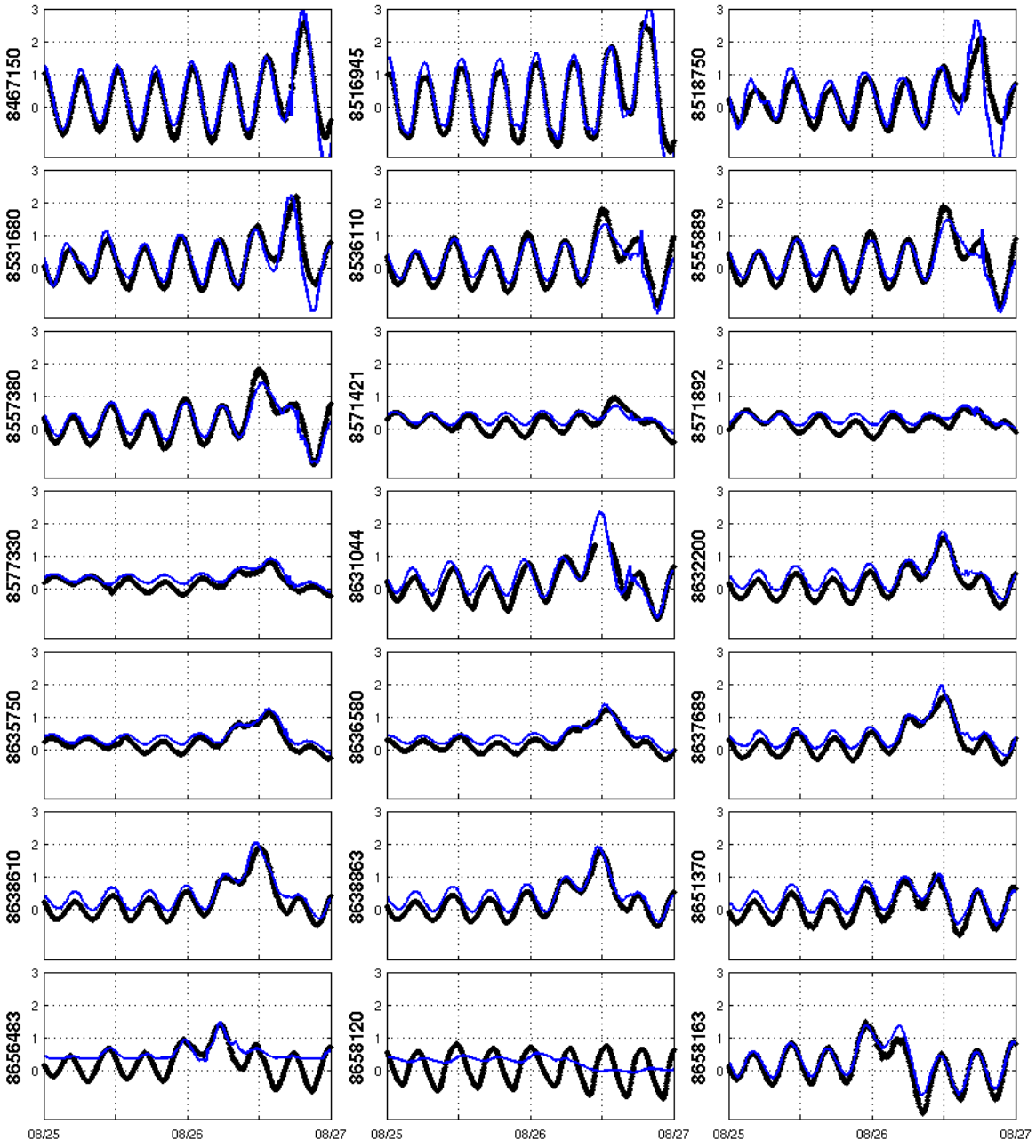

Figure 3.2-2: Hydrographs for forecast 048 for Hurricane Irene with observations in black and simulated results in blue.

The inundation results using the most likely setup were not as good as the water level results. The maximum water levels are shown in Figure 3.2-3 and the HWM analysis in Figure 3.2-5 with the statistics presented in Table 3.2-2. However, the inundation levels shown Figure 3.2-4 shows very little flooded areas. This is due to the coarseness of the bathymetry and topography dataset and the generation of the plot. The HWM analysis shows improvement with each layer of nesting but still a MAPE of 27.5% for the finest resolution. Ignoring the water cells and only plotting inundation depth over land generates the inundation plot. Due to the misrepresentation in the elevation dataset, many of the cells are water cells even though they likely should be land cells. By removing them based on the incorrect bathymetry, they do not show up in the

inundation extent plots. However the value of the water level is used in the HWM analysis leading to results that are reasonable, if a little overestimated.

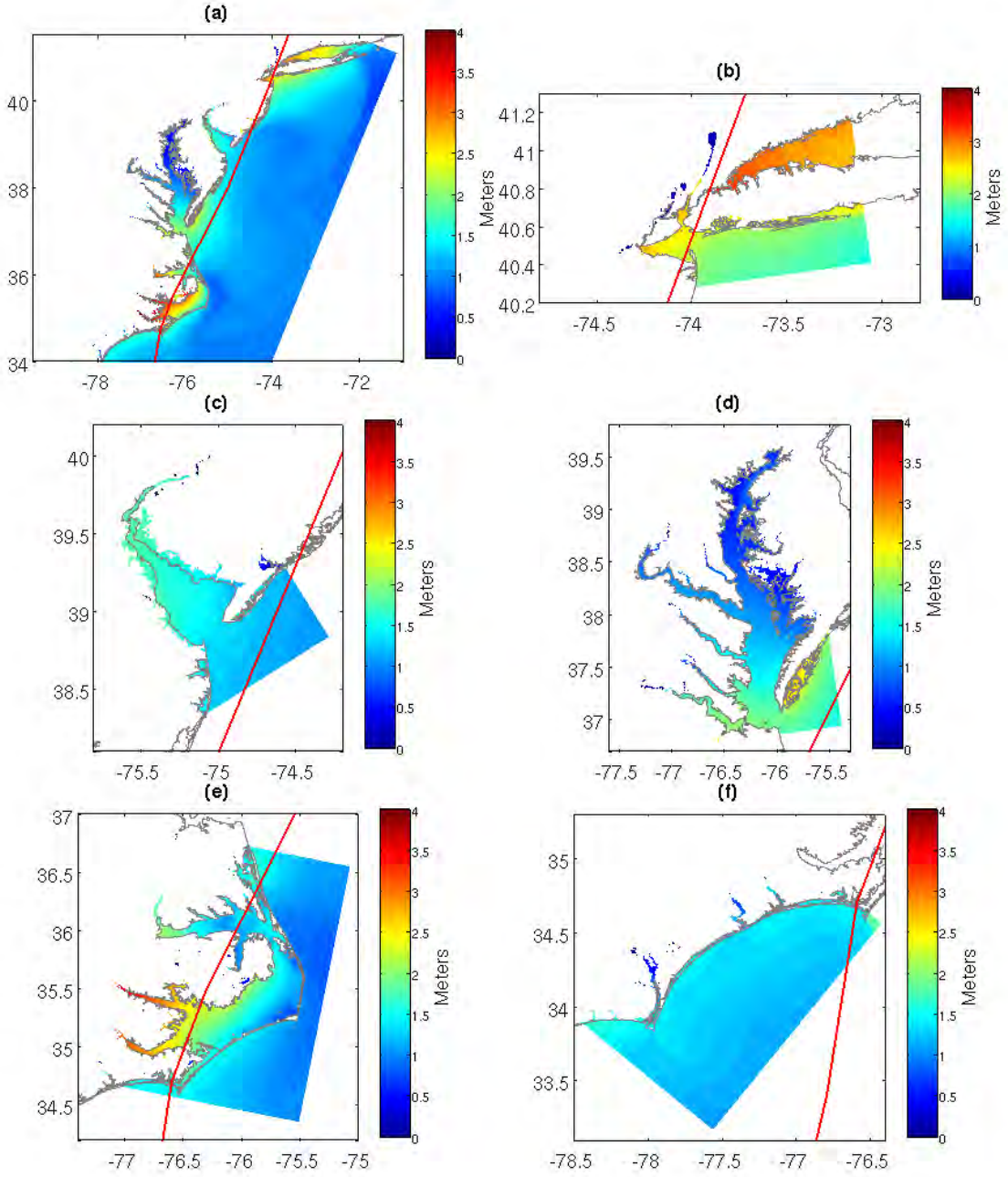

Figure 3.2-3: Simulated maximum water level extents for Hurricane Irene forecast 032 runs for the MA (a), NY (b), DB (c), CB (d), OB (e), and WJ (f) domains

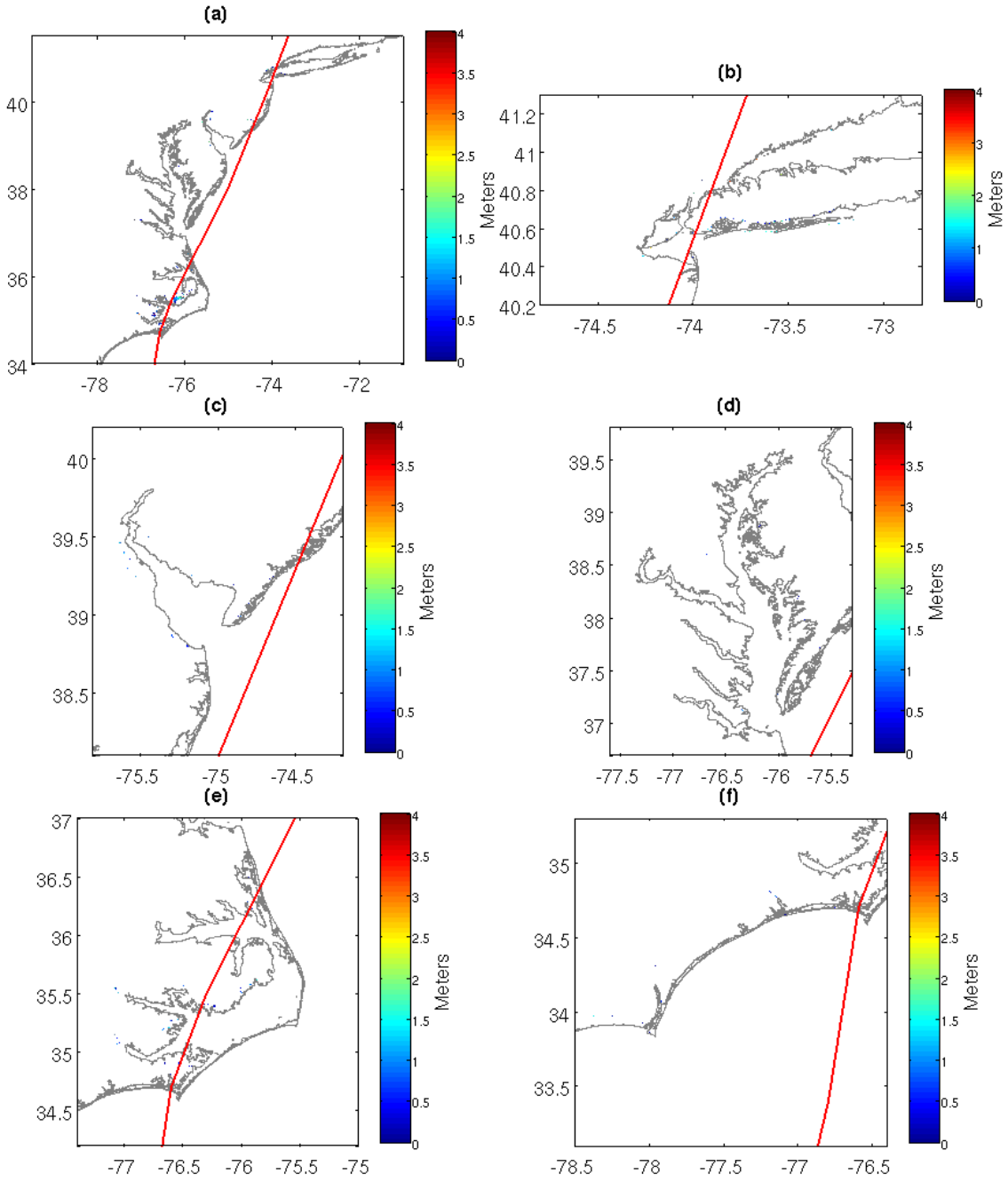

Figure 3.2-4: Simulated inundation extents for Hurricane Irene forecast 032 runs for the MA (a), NY (b), DB (c), CB (d), OB (e), and WJ (f) domains

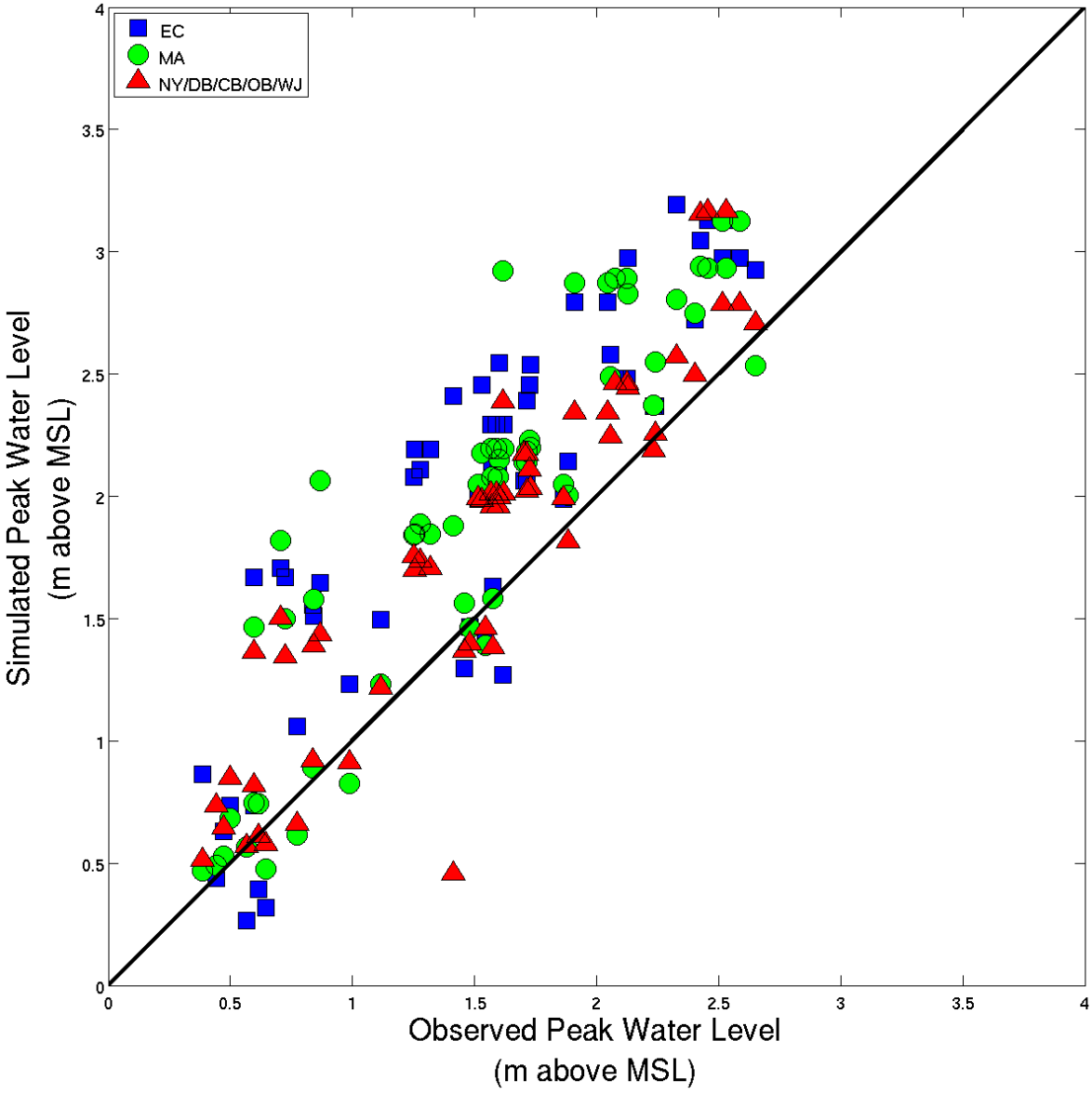

Figure 3.2-5: Simulated versus observed HWMs for Hurricane Irene forecast 032 run.

Table 3.2-2: Statistics for HWM analysis of Hurricane Irene forecast 032 run.

	EC	MA	NY/DB/CB/OB/WJ
Corr r	0.77	0.81	0.83
Bias	0.47	0.42	0.27
RMSE	0.33	0.26	0.25
Scatter Index	16.63	13.67	14.30
MAPE	42.64	34.10	27.46

3.3 Summary - Most Likely Forecast Run Results

The most likely forecast runs highlight both the strengths and weaknesses of CSIPS. In general it does a very good job in capturing the water level elevation in the coastal regions. This is limited by the bathymetry and topography dataset, but for coastal locations it tends to do well. For inundation, CSIPS becomes much more sensitive to the elevation dataset and the bottom roughness. By combining the constant bottom roughness value with the coarse elevation dataset, the inundation results are not as good as those obtained in the sensitivity studies where only one of these components was adjusted. To maximize the accuracy of CSIPS in predicting both surge and inundation, the best available input data should be used.

4 CONCLUSIONS

Validation of the CSIPS using the FLOW and WAVE components of the Delft3D modeling suite was performed for Hurricanes Ike and Irene and Typhoon Pongsona. Sensitivity studies are also presented for Hurricanes Ike and Irene. For Hurricane Ike, three nested domains were used, with the outermost domain having a resolution of 0.1 degrees covering the entire Gulf of Mexico, a second nest having a resolution on 0.02 degrees covering the northwest Gulf of Mexico and the five high resolution local nests having a resolution of 0.004 degrees covering areas of interest. Baseline simulations were performed using the best available bathymetry, re-analyzed and blended winds from OceanWeather, Inc. and bottom roughness using land-use data, and the model results show very good agreement between the simulated and observed peak water levels at the NOAA tide gauges for all three domain resolutions. The coarsest domain does a very good job in capturing the water level at these coastal stations. However, the higher resolution domains much accurately predict the inundation. For Hurricane Irene, the number of nests and the resolutions of the domains are the same, except now the domains cover the western Atlantic Ocean. Once again the baseline simulations show very good agreement between the simulated and observed peak water levels at a number NOAA tide gauges along the East Coast. There is some variation in the results depending on domain resolution, but the end product of the high-resolution domains shows great agreement with observations. The high-resolution domains also do a good job predicting the inundation when compared to HWMs. When the input wind field is good, the wave results compare very well with the buoy observations in all domains.

In a forecast environment, many of the inputs used in the hindcast study either will not be available or may be impractical to implement. To determine the importance of these inputs, sensitivity studies examining the influence of the bathymetry, wave coupling, bottom roughness, wind field, and track were conducted. The overall conclusion is that the results are sensitive to each of the components, but to different degrees.

For Hurricane Ike, bathymetry and topography datasets show a lot of variation from one set to the next. When the recording stations are properly placed, the variation was slight. However, many of the stations that should have been located in wet grid cells were not in the lower resolution elevation datasets. Adjacent cells were wet and the operator would have to adjust the station locations accordingly to get accurate results. In the context of surge and inundation forecasting, this implies that the model resolution needs to be adjusted to account for the accuracy of the available bathymetry data.

Wave coupling was found to be essential to accurately capture the peak of the storm surge. However, including waves does increase the computational time substantially since wave computations take up close to 90% of the overall computation time. Bottom roughness had little influence on the coastal water levels, but did have a large influence on the inundation results. The spatially varying Manning's N coefficient used in the baseline simulation only varied over land. As a result the use of a constant Manning's N coefficient produced similar results in the nearshore water levels, but very different results in the inundation. For this test a constant value of 0.02 performed the best but that is likely subject to the land-use characteristics of the location. Like the other variables the results are sensitive to the forecast wind field. As the forecast evolves the results get better as expected. The later forecasts that more closely resemble the best

track do a nice job of capturing the peak water levels. By adjusting the track of the storm left or right of the actual forecast, the simulated water levels can change dramatically illustrating how sensitive storm surge is to the hurricane track.

For Hurricane Irene, overall the results were not nearly as sensitive as those for Hurricane Ike in the Gulf of Mexico. The results are most sensitive to the elevation dataset. Whenever possible a high-resolution coastal dataset should be used. When this data is not available careful consideration of the desired output must be taken. A coarse dataset like GEBCO performs admirably offshore but not so well when trying to capture processes very near to shore, especially in the coarse domain. The coarseness often leads to placing cells that should have a negative elevation (wet cells) on land with a positive elevation leading to errors in the output.

The influence of the wave coupling and use of a constant bottom roughness coefficient were much milder than the elevation influence. These two components had little impact on the simulation results. The wind on the other hand is a key component. Accurate forecasts and representations of the wind field are essential. The Condon and Veeramony (2014) wind model (which has been incorporated into the CSIPS toolbox) performed very well when given good input (the Best Track). Slight adjustments in the forecast track can change the simulation results dramatically. With this in mind it is recommended that multiple forecast tracks be generated and simulated to provide a range of expectations and to better prepare for the worst-case scenario.

For Typhoon Pongsona, there was not much data available, however the area (Guam) is of considerable interest to the US Navy. CSIPS was used to predict the storm surge and inundation from Typhoon Pongsona which impacted the island of Guam in early December 2002. The storm surge impact was minimal and measured 0.59 m at NOS station 1630000. Due to the lack of much data, the model setup used was the “most likely” setup previously applied to Hurricanes Ike and Irene and CSIPS predicts the peak water level reasonably well at the NOS station. There is a persistent bias in the timing of the surge and in the water level. The simulations tend to predict high and low tides up to an hour after when they actually occur. This could likely be resolved by better calibration of the tidal signal, but this is not reasonable in a tight forecast window. With no calibration CSIPS does well at predicting the peak water level elevation within 18% of the recorded value and in predicting the timing of the peak within 2 hours of the actual peak.

The most likely forecast runs highlight both the strengths and weaknesses of CSIPS. In general it does a very good job in capturing the water level elevation in the coastal regions. This is limited by the bathymetry and topography dataset, but for coastal locations it tends to do well. For inundation, CSIPS becomes much more sensitive to the elevation dataset and the bottom roughness. By combining the constant bottom roughness value with the coarse elevation dataset, the inundation results are not as good as those obtained in the sensitivity studies where only one of these components was adjusted. To maximize the accuracy of CSIPS in predicting both surge and inundation, the best available input data should be used.

5 ACKNOWLEDGEMENTS

This work was sponsored by ONR and SPAWAR PMW-120 under the project: Coastal Surge and Inundation Prediction System.

6 TECHNICAL REFERENCES

Aerts, J. C. J. H., and W. J. W. Botzen, 2012. Hurricane Irene: a wake-up call for New York City. *Natural Hazards and Earth System Sciences,* 12, 1837-1840.

Bender C., J. McKee Smith, A. Kennedy, and R. Jensen, 2013. STWAVE simulation of Hurricane Ike: Model results and comparison to data. *Coastal Engineering*, 73, 58-70.

Booij, N., R. Ris and L. Holthuijsen, 1999. A third-generation wave model for coastal regions, Part I, Model description and validation. *Journal of Geophysical Research 104* (C4): 7649–7666.

Clinch, A. S., E. R. Russ, R. C. Oliver, H. Mitasova, and M. F. Overton, 2012. Hurricane Irene and Pea Island Breach: Pre-storm site characterization and storm surge estimation using geospatial technologies. *Shore and Beach.* 80(2), 1-10.

Coch, N. K., 2012. Hurricane flood protection in NYC – Now is not the time for multiple surge barriers. Discussion of: Hill, D., 2012. The lessons of Katrina, learned and unlearned. *Journal of Coastal Research*, 28(2), 324-331., *Journal of Coastal Research*, 28(5), 1313-1315.

Condon, A., and J. Veeramony, 2014. Wind effects on storm surge and inundation modeling, *Natural Hazards*, (Submitted).

Dingemans, M.W., Radder, A.C. and de Vriend, H.J., 1987. Computation of the driving forces of wave-induced currents. *Coastal Eng.*, 11: 539-563.

East, J. W., M. J. Turco, and R. R. Mason, 2008. Monitoring inland storm surge and flooding from Hurricane Ike in Texas and Louisiana, September 2008, *U.S. Geological Survey Open File Report*, 2008-1365.

Ebersole, B. A., J. J. Westerink, D. T. Resio, and R. G. Dean, 2007. Performance evaluation of the New Orleans and Southeast Louisiana hurricane protection system, Vol. IV – The Storm. *Final Report of the Interagency Performance Evaluation Task Force. U.S. Army Corps of Engineers, Washington*.

Egbert, G. D. and S. Y. Erofeeva, 2002. Efficient inverse modeling of barotropic ocean tides, *Journal of Atmospheric and Oceanic Technology*, 19(2), 183-204, doi:10.1175/1520-0426(2002)019<0183:EIMOBO>2.0.CO;2

FEMA, 2009. Hurricane Ike in Texas and Louisiana: Building performance observations, recommendations, and technical guidance. *Mitigation Assessment Team Report FEMA P-757* 458 pp.

Holland, G. J., 1980. An analytic model of wind and pressure profiles in hurricanes. *Mon. Wea. Rev.*, 108, 1212-1218.

Holthuijsen, L. H., M. D. Powell, and J. D. Pietrzak, 2012. Wind and waves in extreme hurricanes. *J. Geophys. Res.* 117: C09003. Doi: 10.1029/2012JC007983.

Holthuijsen, L., N. Booij and R. Ris, 1993. A spectral wave model for the coastal zone. In *Proceedings of 2nd International Symposium on Ocean Wave Measurement and Analysis, New Orleans*, pages 630–641.

Hope, M. E., J. J. Westerink, A. B. Kennedy, P. C. Kerr, J. C. Dietrich, C. Dawson, C. J. Bender, J. M. Smith, R. E. Jensen, M. Zijlema, L. H. Holthuijsen, R. A. Luettich Jr., M. D. Powell, V. J. Cardone, A. T. Cox, H. Pourtaheri, H. J. Roberts, J. H. Atkinson, S. Tanaka, H. J. Westerink, L. G. Westerink, 2013. Hindcast and validation of Hurricane Ike (2008) waves, forerunner, and storm surge, *J. Geophys. Res. Oceans*, 118, 4424–4460, doi:10.1002/jgrc.20314.

Hsu, Y.L., J.D. Dykes, R.A. Allard and D. W. Wang, 2008. Validation Test Report for Delft3D, *NRL memorandum report, NRL/MR/7320-08-9079*, 47 pp.

Hsu, Y.L., J.M. Kaihatu, J.D. Dykes and R.A. Allard, 2006. Evaluation of Delft3D performance in nearshore flows, *NRL memorandum report, NRL/MR/7320-06-8984*, 24 pp.

Ingram, C. A. and C. M. Greenfield, 2011. An analysis of U.S. Navy humanitarian assistance and disaster relief operations, *Naval Postgraduate School Acquisition Research Sponsored Report.*

Kennedy, A. B., U. Gravois, B. C. Zachry, J. J. Westerink, M. E. Hope, J. C. Dietrich, M. D. Powell, A. T. Cox, R. A. Luettich, and R. G. Dean, 2011a. Origin of the Hurricane Ike forerunner surge. *Geophysical Research Letters*, 38, L08608, doi:10.1029/2011GL047090.

Kennedy, A. B., S. Rogers, A. Sallenger, U. Gravois, B. Zachry, M. Dosa, and F. Zarama, 2011b. Building destruction form waves and surge on the Bolivar Peninsula during Hurricane Ike. *Journal of Waterway, Port, Coastal, and Ocean Engineering- ASCE*, 137(3), 132-141.

Kerr, P. C., et al., 2013. U.S. IOOS coastal and ocean modeling testbed: Inter-model evaluation of tides, waves, and hurricane surge in the Gulf of Mexico, *J. Geophys. Res. Oceans*, 118, 5129–5172, doi:10.1002/jgrc.20376.

Lester, M., 2012. Study of residential damages in coastal North Carolina from Hurricane Irene. *Forensic Engineering*. 783-792. doi: 10:1061/9780784412640.083

R.A. Luettich Jr, J.J. Westerink, N.W. Scheffner, 1992. ADCIRC: an advanced three-dimensional circulation model for shelves coasts and estuaries, Report 1: theory and methodology of ADCIRD-2DDI and ADCIRC-3DL, *Dredging Research Program Technical Report DRP-92-6, U.S. Army Engineers Waterways Experiment Station, Vicksburg, MS.*

Mattocks, C. and C. Forbes, 2008. A real time, event triggered storm surge forecasting system for the state of North Carolina. *Ocean Modelling*, 25, 95 -119.

Mesinger, F., and Coauthors, 2006. North American Regional Reanalysis. *Bulletin of the American Meteorological Society*, 87, 343-360.

National Hurricane Center (NHC), 2010. Tropical cyclone report, Hurricane Ike (AL092008) 1-14 September 2008. January 2009; updated May 2010.

National Hurricane Center (NHC), 2011. Tropical cyclone report, Hurricane Irene (AL092011) 21-28 August 2011. December 2011; updated April 2012.

National Oceanic and Atmospheric Administration (NOAA), 2012. Service Assessment, Hurricane Irene, August 21-30, 2011.

National Oceanic and Atmospheric Administration (NOAA), 2003a. Super Typhoon Pongsona, December 8, 2002. Service Assessment. April 2003

National Oceanic and Atmospheric Administration (NOAA), 2003b. NOAA/NWS meteorological assessment for Typhoon Pongsona in: Pohnpei State, FSM; Chuuk State, FSM; Guam; and Rota, CNMI. April 2003.

Oliver-Smith, A., 2009. Sea level rise and the vulnerability of coastal peoples: Responding to the local challenges of global climate change in teh 21st century, Interdisciplinary Security Connnections Publication Series of UNU-EHS, vol. 7, p. 56.

Peng, M., L. Xie and L. J. Pietrafesa, 2004. A numerical study of storm surge and inundation in the Croatan-Albermarle-Pamlico estuary system, Estuarine, Coastal and Shelf Science, vol. 59, pp. 121 - 137.

Posey, P. G., R. A. Allard, R. H. Preller and G. M. Dawson, 2008. Validation of the global relocatable tide / surge model PC-Tides, Journal of Atmospheric and Oceanic. Technology, vol. 25, pp. 755-775.

Powell, M. D., S. H. Houston, L. R. Amat, and N Morisseau-Leroy, 1998. The HRD real-time hurricane wind analysis system. *J. Wind Engineer. and Indust. Aerodyn.* 77&78, 53-64

Rego, J. L., and C. Li, 2010. Storm surge propagation in Galveston Bay during Hurricane Ike. *Journal of Marine Systems*, 82, 265-279.

Ris, R., N. Booij and L. Holthuijsen, 1999. A third-generation wave model for coastal regions, Part II: Verification, *Journal of Geophysical Research* 104 (C4): 7649–7666.

Sheng, Y. P., V. Alymov and V. A. Paramygin, 2010a. Simulation of storm surge, wave, currents, and inundation in the Outer Banks and Chesapeake Bay during Hurricane Isabel in 2003: The importance of waves, *Journal of Geophysical Research - Oceans*, vol. 115, no. C04008, pp. 1-27.

Sheng, Y. P., Y. Zhang and V. A. Paramygin, 2010b. Simulation of storm surge, wave, and coastal inundation in the Northeaster Gulf of Mexico during Hurricane Ivan in 2004, *Ocean Modelling*, vol. 35, pp. 314 - 331.

Small, C. and R. J. Nicholls, 2003. A global analysis of human settlement in coastal zones, *J. Coastal Research*, vol. 19, no. 3, pp. 584-599,.

Stelling, G. S., 1996. A non-hydrostatic flow model in cartesian coordinates, Technical note Z0901-10, WL | Delft Hydraulics, The Netherlands.

United States Geological Survey (USGS), 2012. Monitoring inland storm tide and flooding from hurricane Irene along the Atlantic coast of the United States, August 2011. Open File Report 2012-1022. 34 pp.

Wang, H. V., J. Cho, J. Shen and Y. Wang, 2005. What has been learned about storm surge dynamics for Hurricane Isabel model simulations, in Hurricane Isabel in Perspective Conference, Baltimore, MD.

Weisberg, R. H. and L. Zheng, 2008. Hurricane storm surge simulations comparing three-dimensional with two-dimensional formulations based on an Ivan-like storm in Tampa Bay, Florida, *Journal of Geophysical Research*, vol. 113, no. C12001.

Westerink, J. J., R. A. Luettich, A. M. Baptista and N. W. Scheffner, 1992. Tide and storm surge predictions using a finite element model, *Journal of Hydraulic Engineering*, vol. 118, pp. 1373 - 1390.

Westerink, J. J., R. A. Luettich, J. C. Feyen, J. H. Atkinson, C. Dawson, H. J. Roberts, M. D. Powell, J. P. Dunion, E. J. Kubtatko, and H. Pourtaheri, 2008. A basin to channel scale unstructured grid hurricane storm surge model applied to Southern Louisiana. *Mon. Wea. Rev.* 136, 833-864.

Xie, L., H. Liu and M. Peng, 2008. The effect of wave-current interactions on the storm surge and inundation in Charleston Harbor during Hurricane Hugo 1989, *Ocean Modelling*, vol. 20, pp. 252 - 269.

Xie, L., L. J. Pietrafesa and M. Peng, 2004. Incorporation of a mass-conserving inundation scheme into a three-dimensional storm surge model, *Coastal Research*, vol. 20, pp. 1209 – 1223.

Zhang, Y., A. M. Baptista and E. P. Meyers, 2004. A cross-scale model for 3D baroclinic circulation in estuary-plume-shelf system: I. Formulation and skill assessment, *Continental Shelf Research*, vol. 24, pp. 2187 - 2214.

Zijlema, M., G. Ph.. van Vledder, and L. H. Holthuijsen, 2012. Bottom friction and wind drag for wave models. *Coastal Engineering*, 65, 19-26.

7 ACRONYMS AND ABBREVIATIONS

Acronym	Description
2D	2 Dimensional
3D	3 Dimensional
ADCIRC	ADvanced CIRCulation model for oceanic, coastal and estuarine waters
ASCII	American Standard Code for Information Interchange, set of digital codes used as a standard format in the transfer of text
CB	Chesapeake Bay domain
CH3D –SSMS	Curvilinear-grid Hydrodynamics 3D Storm Surge Modeling System
CMAN	Coastal-Marine Automated Network
CMEPS	Coastal Marine Environmental Prediction System
CSIPS	Coastal Surge and Inundation Prediction System
DB	Delaware Bay domain
DDB	Delft DashBoard
Delft3D	Fully integrated suite of models for 2D and 2D computations for coastal, river and estuarine areas developed by Delft Hydraulics
Delft3D–FLOW (FLOW)	Module of Delft3D that can simulate hydrodynamic flows
Delft3D–WAVE (WAVE)	Module of Delft3D that can simulate waves

Acronym	Description
Delft3D-SED	Module of Delft3D that can simulate sediment transport
Delft3D-WAQ	Module of Delft3D that can simulate water quality
EC	East Coast (US) domain
ELCIRC	Eulerian-Lagrangian CIRCulation, an unstructured-grid model designed for the effective simulation of 3D baroclinic circulation across river-to-ocean scales
EOHW	Envelope Of High Water
FEMA	Federal Emergency Management Agency
FL	FLorida
GB	Galveston Bay domain
GEBCO	General Bathymetric Chart of the Oceans
GoM	Gulf of Mexico domain
GUI	Graphical User Interface
HWM	High Water Mark
ID	IDentification
IHO	International Hydrographic Office
IPET	Interagency Performance Evaluation Taskforce
JTWC	Joint Typhoon Warning Center
LA	Lousiana
LECZ	Low Elevation Coastal Zone
LIDAR	Laser Imaging Detection and Ranging system
MA	Mid-Atlantic domain
MAPE	Mean Absolute Percent Error
MATLAB	MATrix LABoratory, a numerical computing environment and fourth-generation programming language.

Acronym	Description
MDF	Master Definition FLOW
MDW	Master Definition WAVE
MSL	Mean Sea Level
MSW	Mean Surface Wind
NAVOCEANO	Naval Oceanographic Office
NARR	North American Regional Reanalysis
NCEP	National Center for Environmental Prediction
NDBC	National Data Buoy Center
netCDF	network Common Data Form
NG	Northern Gulf (of Mexico) domain
NGDC	National Geophysical Data Center
NHC	National Hurricane Center
NJ	New Jersey
NLCD	National Land Cover Database
NOAA	National Oceanographic and Atmospheric Admistration
NC	North Carolina
NOS	National Ocean Services
NRL	Naval Research Laboratory
NY	New York (City) domain
OB	Outer Banks domain
OFCM	Office of the Federal Coordinator for Meteorology
OWI	OceanWeather Inc.
PA	Port Arthur (along Texas Lousisana border) domain
PCTIDES	A Navy relocatable tide/surge modeling system
POM	Princeton Ocean Model
PR	Puerto Rico
RMS	Root Mean Square
RMSE	Root Mean Square Error
SRTM	Shuttle Radar Topography Mission
SSM/I	Special Sensor Microwave/Imager
SURA	Southeastern Universities Research Association
SWAN	Simulating WAves Nearshore model
TC	Tropical Cyclone
TX	Texas
USGS	United States Geological Survey
USPACOM	US PAcific COMmand
USVI	United States Virgin Islands
UTC	Coordinated Universal Time

Acronym	Description
VB	Vermillion Bay (Lousiana) domain
WJ	Wilmington/Jacksonville domain
X	Longitude
Y	Latitude
Z	Depth/elevation